INAUGURAL – DISSERTATION

zur

Erlangung der Doktorwürde

der

Gesamtfakultät für Mathematik, Ingenieur- und Naturwissenschaften

der

Ruprecht-Karls-Universität
Heidelberg

vorgelegt von:

Dipl. Chem. Baldur Knörr
aus Leimen

Tag der mündlichen Prüfung:

29.4.2025 11:00

Siderite and Dolomite as a possible tool for thermochronological use

Gutachter:

Prof. Dr. Ulrich A. Glasmacher

Prof. Dr. Christina Trautmann

Keywords: swift heavy ion irradiation, fission-track dating, visualization of ion-induced tracks, thermal neutrons, dolomite, siderite, malachite, rhodochrosite, visualization by etching techniques, HCl, H_2SO_4, acetic acid, HNO_3, preparation of dolomite and siderite for ion irradiation, dislocations, annealing of etch pits and dislocations, online Raman measurements, geochemistry of siderite

Abstract

The present study focuses on the visualization and counting of ion-induced linear tracks in dolomite and siderite crystals by using etching and spectroscopic techniques to answer the question whether dolomite (CaMg[CO3]2) and siderite (FeCO3) are usable as fission-track dating archives. Since the uranium content in natural samples can be highly variable, the areal density and distribution of fission tracks created by spontaneous fission of ^{235}U in natural samples might be very variable too. Therefore, to conduct etching experiments, artificial linear tracks had to be generated. These artificial ion tracks were created on natural samples by swift heavy ion irradiation with ^{197}Au (1.10-2.18 GeV, fluence $1*10^6$ ions/cm^2) at the Universal Linear Accelerator (UNILAC), GSI Helmholtzzentrum für Schwerionenforschung, Darmstadt. This method produced artificial ion tracks that were used for the etching experiments described in this study.

Induced fission tracks were created on natural samples by covering them with a uranium source (CN5 glass and zircon) and performing thermal neutron irradiation ($1*10^{15}$-$1*10^{16}$ neutrons/cm^2) at the FRM II reactor in Munich. This method causes fission of ^{235}U, generating fission fragments which induce fission tracks upon hitting the mineral samples. These induced fission tracks can be assumed to be very similar in nature to spontaneous fission tracks occurring on natural samples as a result of their ^{235}U content.

The **primary research objective** was to visualize induced heavy ion tracks on dolomite and siderite, respectively, by using chemical etching techniques, and quantifying them with an optical microscope. For this purpose, the quality of mineral samples was very important; when possible, samples with very smooth surfaces were used, but for siderite in particular where the available samples were too coarse, a preparation method had to be established in order to obtain high-quality, polished surfaces. First, the established mineral etching techniques published in literature were tested for their applicability and ability to visualize induced or natural tracks on the mineral samples. In order to establish the optimal etching recipe, these etching methods had to be slightly modified with regard to the etchant concentration, etching time, and etching temperature, which also involved figuring out methods to conduct etching at elevated temperatures (50-70 °C), safely. Ideally the etching methods should be as safe as possible, with non-toxic etching solutions that are easy to handle

and don't require special safety precautions. For the visualization of ion-induced tracks in dolomite, one suitable etching solution was found: 0.001 mol/l HCl at a temperature of 20 °C, which produces roughly trigonal etch pits after 60-120 minutes of etching. Two etchants proved capable of revealing heavy ion tracks on siderite: 10% HCl at a temperature of 50 °C results in triangular etch pits after 10 minutes of etching, while 10% H_2SO_4 at a temperature of 50 °C produces hexagonal etch pits after an etching time of 30-60 minutes. These etching methods are all optimized for the areal density of tracks that an ion fluence of about $1*10^6$ ions/cm^2 will generate. The observation of different shapes of etch pits on siderite depending on the etchant used matches the descriptions of etching techniques found in literature, including a couple of very old publications, which also showed various etch pit shapes depending on which etchant is used.

After the etching methods for visualizing heavy ion tracks had been established, they were tested on neutron-irradiated samples with induced fission tracks. For both dolomite and siderite, the established etching solutions also proved capable of etching induced fission tracks generated by irradiation with fission fragments of a kinetic energy of about 170 MeV. The results showed that the etching conditions that were used for visualization of heavy ion tracks work basically the same for visualizing induced fission tracks. This means that dolomite and siderite are minerals that can be used as an archive for fission-track dating, as long as they have a sufficiently high uranium content.

For the purpose of conducting these irradiation and etching experiments, it was important to develop suitable preparation methods for mineral samples so they can be used in heavy ion irradiation or thermal neutron irradiation experiments. This was done by establishing a grinding and polishing procedure that results in very smooth mineral surfaces, minimizing the negative effects that a natural crystal topography would otherwise have on the sample's ability to display etched tracks.

The **secondary objective** of this work was to test the thermal stability of induced ion tracks in dolomite and siderite, as well as studying their annealing behaviour. In the case of dolomite, it was found that tracks generated by the heavy ion irradiation method will anneal when the sample is heated to about 500 °C for 100 h, while natural dislocations in the samples will persist at this temperature. Therefore, this method can be used to separate natural dislocations from artificial ion tracks. Siderite, on the other hand, decomposes when exposed to a temperature of 400 °C for 5 h, leaving only a

black powdery residue made up of decomposition products which are expected to either be wüstite (FeO) or graphite (C). Exposing siderite to 300 °C for 4.5 h results in a thin layer of black powder on the surface, and the heavy ion tracks present on the sample could still be etched normally, meaning that in the case of siderite the annealing temperature for ion tracks lies above the decomposition temperature.

Furthermore, online Raman measurements were conducted to study the behaviour of siderite samples during irradiation, observing changes in the sample's structure and possible also in the chemical composition. The results showed that all three siderite bands (180, 282 and 1084 cm^{-1}) decrease in intensity as the fluence of ions is increased, culminating in their complete disappearance at a fluence of about $1*10^{12}$ ions/cm^2. After the experiment was finished, the siderite sample was found to have transformed into the same black residue seen in the annealing experiments, indicating that siderite will also decompose when exposed to high amounts of irradiation.

Zusammenfassung

Die vorliegende Doktorarbeit thematisiert die Visualisierung und Zählung ioneninduzierter Spuren in Dolomit- und Sideritkristallen mittels Ätzung und spektroskopischer Methoden in Bezug auf die Fragestellung, ob Dolomit ($CaMg[CO_3]_2$) und Siderit ($FeCO_3$) als Archiv für Fission-Track Dating nutzbar sind. Da der Urangehalt in natürlichen Proben stark variieren kann, ist die Flächendichte sowie die Verteilung von Spaltspuren aufgrund des natürlichen Zerfalls von ^{235}U möglicherweise auch stark variabel. Daher müssen für die Durchführung von Ätzexperimenten künstliche Spuren geschaffen werden. Zu diesem Zweck wurden Schwerionenspuren erzeugt. Dabei handelt es sich um künstliche Ionenspuren, die durch Bestrahlung natürlicher Proben mit Schwerionen (1.10-2.18 GeV, Fluenz $1*10^6$ Ionen/cm^2) am Universal Linear Accelerator (UNILAC) des GSI Helmholtzzentrums für Schwerionenforschung in Darmstadt geschaffen werden. Mittels dieser Methode wurden künstliche Ionenspuren erzeugt, die für die in dieser Arbeit beschriebenen Ätzexperimente benutzt wurden.

Induzierte Spaltspuren wurden auf natürlichen Proben erzeugt, indem diese mit einer Uranquelle (CN5-Glas und Zirkon) bedeckt und mit thermischen Neutronen ($1*10^{15}$-$1*10^{16}$ Neutronen/cm^2) am FRM II Reaktor in München bestrahlt wurden. Durch diese Methode wird die Spaltung von ^{235}U angeregt, wodurch Spaltfragmente entstehen und beim Auftreffen auf die Mineralproben induzierte Spaltspuren erzeugen können. Es kann angenommen werden, dass diese induzierten Spaltspuren den spontanen Spaltspuren sehr ähneln, welche in natürlichen Proben aufgrund deren ^{235}U-Gehalt vorkommen können.

Der **Forschungsschwerpunkt** bestand in der Visualisierung von Schwerionenspuren auf Dolomit und Siderit mithilfe chemischer Ätzmethoden, inklusive deren Quantifizierung mittels optischer Mikroskopie. Die Qualität der benutzten Mineralproben war hierfür von großer Bedeutung; sofern möglich, wurden Proben mit sehr glatten Oberflächen benutzt, aber insbesondere im Fall von Siderit waren die verfügbaren Proben zu rau, sodass eine Bearbeitungsmethode entwickelt werden musste, um polierte Oberflächen von hoher Qualität zu schaffen. Zunächst wurden die in der Literatur veröffentlichten Ätztechniken für Minerale auf ihre Benutzbarkeit getestet sowie deren Tauglichkeit für die Visualisierung induzierter oder natürlicher Spuren auf Mineralproben. Um ein optimales Ätzrezept zu entwickeln, mussten diese

Ätzmethoden leicht verändert werden, indem die Konzentration des Ätzmittels, die Ätzzeit sowie die Ätztemperatur angepasst wurden. Dazu gehörte auch die Notwendigkeit, eine Methode zu finden, um bei erhöhten Temperaturen (50-70 °C) die Ätzung sicher durchführen zu können. Idealerweise sollten möglichst sichere Ätzmethoden verwendet werden, d.h. ungiftige, leicht handzuhabende Ätzlösungen, die keine speziellen Sicherheitsvorkehrungen erfordern. Für die Visualisierung von ioneninduzierten Spuren auf Dolomit wurde eine geeignete Ätzlösung gefunden: 0.001 mol/l HCl bei einer Temperatur von 20 °C, welche annähernd dreieckige Ätzgruben nach 60-120 Minuten Ätzzeit produziert. Zwei Ätzlösungen erwiesen sich als nutzbar für die Visualisierung von Schwerionenspuren auf Siderit: 10% HCl bei einer Temperatur von 50 °C resultiert in dreieckigen Ätzgruben nach 10 Minuten Ätzzeit, während 10% H_2SO_4 bei einer Temperatur von 50 °C nach einer Ätzzeit von 30-60 Minuten hexagonale Ätzgruben produziert. Diese Ätzmethoden sind jeweils so optimiert, dass sie eine vollständige Visualisierung aller Spuren auf einer Probe bewirken, welche mit einer Ionenfluenz von etwa $1*10^6$ Ionen/cm^2 generiert wurden. Die Beobachtung verschiedener Formen der Ätzgruben auf Siderit je nach verwendetem Ätzmittel deckt sich mit den in der Literatur veröffentlichten Beschreibungen, inklusive einiger sehr alter Publikationen, welche ebenfalls unterschiedliche Ätzgrubenformen je nach benutzter Ätzlösung zeigen.

Nachdem die Ätzmethoden für die Visualisierung von Schwerionenspuren etabliert waren, wurden diese an neutronenbestrahlten Proben mit induzierten Spaltspuren getestet. Sowohl für Dolomit als auch Siderit erwiesen sich die hier entwickelten Ätzrezepte als brauchbar, um induzierte Spaltspuren zu visualisieren, welche durch Bestrahlung mit Spaltfragmenten einer Energie von etwa 170 MeV geschaffen wurden. Die Resultate zeigten, dass die für die Visualisierung von Schwerionenspuren verwendeten Ätzbedingungen gleichermaßen auf induzierte Spaltspuren anwendbar sind. Dies bedeutet, dass die Minerale Dolomit und Siderit als Archive für Fission-Track Dating nutzbar sind, solange deren Urangehalt hoch genug ist.

Um diese Bestrahlungs- und Ätzexperimente durchführen zu können, war es wichtig, geeignete Methoden für die Präparation von Mineralproben zu entwickeln, sodass diese für die Bestrahlung mit Schwerionen oder thermischen Neutronen geeignet sind. Dazu wurde eine Schleif- und Poliermethode entwickelt, welche in der Lage ist, sehr glatte Mineraloberflächen zu schaffen und somit den negativen Effekt zu minimieren, den die natürliche Kristalltopografie auf die Sichtbarkeit geätzter Spuren hat.

Die **zweite Fragestellung** befasst sich mit dem Test der thermischen Stabilität von induzierten Spaltspuren auf Dolomit und Siderit, sowie der Erforschung ihres Verheilungsverhaltens. Für Dolomit wurde festgestellt, dass Spuren, welche mittels Schwerionenbestrahlung erzeugt wurden, nach dem Erhitzen der Probe auf 500 °C für 100 h verschwinden, während natürliche Dislokationen bei diesen Temperaturen bestehen bleiben. Somit kann diese Methode als Werkzeug benutzt werden, um natürliche und künstliche Spuren zu unterscheiden. Siderit wird dagegen zersetzt, wenn er für 5 h einer Temperatur von 400 °C ausgesetzt ist; es bleibt lediglich ein schwarzer pulvriger Rückstand aus Zerfallsprodukten zurück, von dem angenommen wird, dass es sich entweder um Wüstit (FeO) oder Graphit (C) handelt. Wird Siderit für 4.5 h auf 300 °C erhitzt, bildet sich eine dünne Schicht von schwarzem Pulver auf der Oberfläche, wobei die auf der Probe vorhandenen Schwerionenspuren weiterhin angeätzt werden konnten, d.h. die Verheilungstemperatur der Ionenspuren auf Siderit liegt oberhalb der Zersetzungstemperatur.

Desweiteren wurden Online-Raman-Messungen durchgeführt, um das Verhalten von Sideritproben während der Bestrahlung zu erforschen und Änderungen der chemischen Zusammensetzung der Probe zu dokumentieren. Die Ergebnisse zeigten, dass alle drei Sideritbanden (180, 282 und 1084 cm^{-1}) bei steigender Ionenfluenz in ihrer Intensität abnehmen, mit einem völligen Verschwinden der Banden bei einer Fluenz von etwa $1*10^{12}$ Ionen/cm^2. Nach Abschluss des Experiments stellte sich heraus, dass die Sideritprobe zu demselben schwarzen Rückstand geworden war, der auch in den Verheilungsexperimenten beobachtet wurde. Dies weist darauf hin, dass Siderit sich zersetzt, wenn er einer hohen Strahlungsdosis ausgesetzt wird.

Acknowledgement

I would like to express my special thanks to my supervisor Prof. Dr. Ulrich A. Glasmacher, who introduced me to the world of mineral dating techniques and made this study possible. Many thanks also go to Prof. Dr. Christina Trautmann for all the help provided with heavy ion irradiation experiments and online Raman measurements.

I hereby want to thank all my colleagues in Heidelberg for all the scientific discussions and the great time we spent together. In particular, I want to thank Margit Brückner for her invaluable support in the chemistry laboratory and Hans Ebert for always helping patiently with the design and construction of various accessories for the laboratory. Without you, this study would not have been possible.

With eternal gratitude I acknowledge the financial support offered by the BMBF for funding this study within the “BMBF Verbundprojekte” framework.

My very special thanks go to my parents for their long-time support and infinite patience during my doctoral study.

Thank you very much!

Table of Contents

1. Introduction

In geology, visualization and quantification of spontaneous fission tracks is an important method for determining the age and the temperature history of rocks and, therefore, of exhumation of crustal segments. Natural minerals containing uranium will have spontaneous fission tracks generated over time due to spontaneous fissioning of uranium (^{238}U, ^{235}U) and thorium (^{232}Th) isotopes. Natural fissioning generated high-energy ions which are capable of damaging the host mineral. For calcite ($CaCO_3$), a method to visualize and count spontaneous fission tracks and artificial ion tracks by etching and optical microscopy has been successfully developed by Dedera (2015). In addition, Dedera (2015) used the technique of UV-c pulsed laser stimulated fluorescence spectroscopy. The content of the thesis focuses on the research of methods to visualize spontaneous and induced fission tracks and artificial ion tracks in dolomite and siderite. Dolomite ($CaMg(CO_3)_2$ is an ubiquitous mineral of various colour in carbonate rocks that can be dissolved by water over time, resulting in the formation of natural caves that are capable of acting as a natural oil and gas reservoir.
Siderite ($FeCO_3$) often occurs in shales, sandstones, and hydrothermal veins and also appears in shallow sedimentary rocks.

In this work, the processes of developing methods that allow visualization and counting induced fission tracks and artificial ion tracks on a polished internal surface of dolomite and siderite are described in detail. The description includes sample preparation, irradiation of grains with swift heavy ions or thermalized neutrons to generate artificial ion tracks and induced fission tracks, and chemical etching experiments. After irradiation and etching the results were imaged by using an optical microscope and imaging software. Furthermore, irradiated grains of both minerals were used for annealing experiments to determine the temperature at which the ion tracks and induced fission tracks disappear and can no longer be etched successfully.

Since the natural uranium content of mineral samples is highly variable, a defined amount of artificial ion tracks was generated by irradiating samples with ^{197}Au ions at the UNILAC linear accelerator of the GSI (Gesellschaft für Schwerionenforschung) in Darmstadt. This thesis presents the development of the first successful chemical etching method that is capable of visualizing ion tracks on polished internal surfaces of dolomite and siderite. The etching recipe was also successfully applied to samples with induced fission tracks, which were generated by coupling mineral samples with uranium glass standards (CN1 and CN5) and zircon grains that were irradiated by thermalized neutrons. In conclusion, this thesis shows that chemical etching methods are potentially capable of visualizing artificially induced ion tracks and induced fission

tracks on an internal polished surface of dolomite and siderite.

2. Literature research

2.1 Etching of carbonate minerals: Past to Present

In its perpetual thirst for knowledge, humankind has been interested in understanding the structure of minerals for centuries. One method of learning more about a mineral is to test its reaction to etchants. This chapter presents an overview of various researchers' works of mineral etching conducted in the past.

The first mineral etching experiments documented in literature date back to the early 19th century. Scientists from Germany and Austria were pioneers in this field, and many of their results are summarized in a book by German mineralogist Heinrich Baumhauer who describes etching experiments for a variety of minerals including dolomite and siderite (1894, Fig. **2.1**).

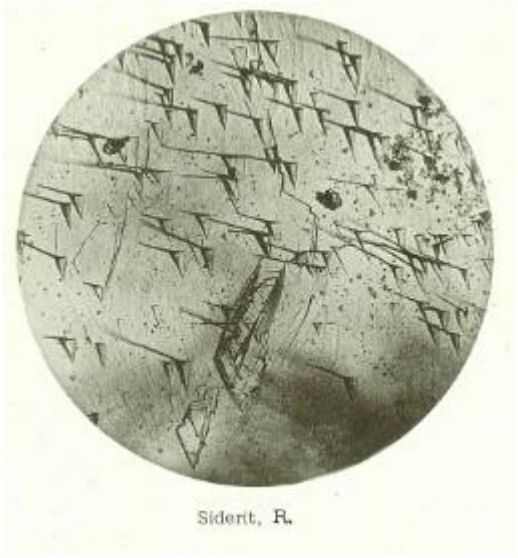

Fig. **2.1**: Etch pits on siderite etched with HCl (Baumhauer 1894).

According to Baumhauer (1894), the first documented mineral etching experiment was conducted by Daniell (1817), who investigated the effect of acids on calcite ($CaCO_3$), strontianite ($SrCO_3$), and witherite ($BaCO_3$) to test their solubility.

In 1854, Franz Leydolt (Leydolt 1854) published his research on using etching techniques for determining the crystal structure of minerals. He observed the principle that on a given crystal face all the etch pits will look alike, while they may look different on a different face of the same crystal.

Leydolt also discovered that the etchant concentration and temperature have an influence on the shape and size of etch pits. In his paper, Leydolt states that over-etching a sample is a possibility, marked as the point at which the etch pits on the crystal surface overlap and eventually reach a point where the individual pits can no longer be characterized; he suggests

working with diluted acid at reduced temperatures to prevent over-etching, or watching the etching process under a microscope so it can be stopped at a favourable point in time.

Etch figures on calcite and aragonite have been researched by Viktor von Ebner in 1884-1885, testing various etching solutions for their effect on calcite and observing their different growth rates (Ebner 1884-1885). In 1894, Gustav Tschermak (Tschermak 1894) did extensive etching experiments on dolomite, magnesite and siderite in an attempt to determine their crystal structure and symmetry (Fig. **2.2**); the results from his siderite etching experiment with hydrochloric acid are of special importance for this thesis.

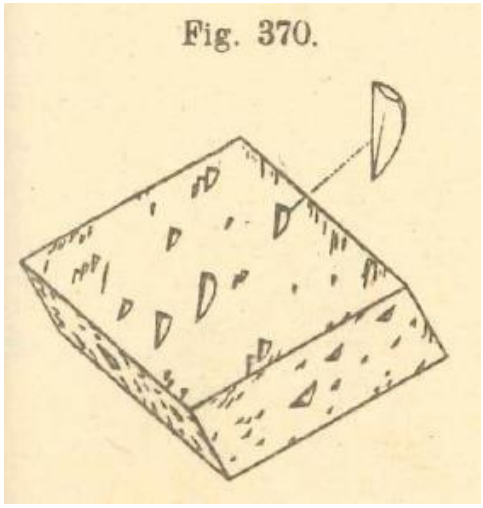

Fig. **2.2**: Etch pits on dolomite etched by hydrochloric acid (Tschermak 1894).

The early 20th century saw more mineral etching experiments, with their aim mainly being to better understand crystal structure. A paper from Waldemar Schaller (1906) mentions the formation of well-formed triangular etch figures when putting a siderite sample into diluted hydrochloric acid for several days. Paul Gaubert (1901) studied the effects of hydrochloric and acetic acid on calcite, dolomite and ankerite in 1901, describing the variety of etch pits observed (Fig. **2.3**); the works of Baumhauer (1894) and Tschermak (1894) are referenced in his work. Another important publication is the etch figure investigation performed by Honess & Jones (1937), who tested a variety of optically active organic acids on calcite, dolomite and other minerals in an attempt to gain knowledge about the symmetry of these minerals; they discovered that if the optically active etchant is used in high enough concentrations, a given crystal face may develop etch pits with reduced symmetry (Fig. **2.4**). This confirms the observations made by Royer (1930) who examined the etch figures produced by optically active acids on calcite.

Fig. **2.3**: Etch pits on dolomite (Binntal, Switzerland) etched with hydrochloric acid (Gaubert 1901).

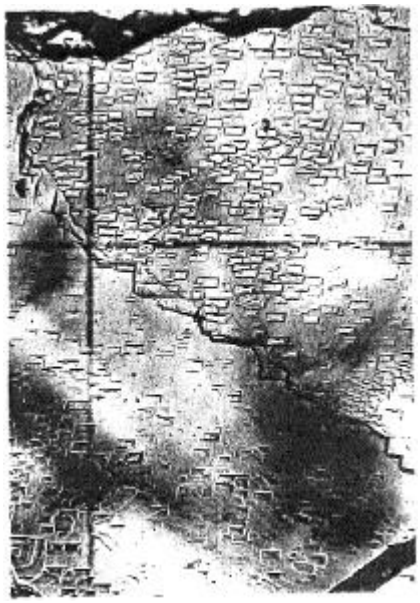

Fig. **2.4**: Etch pits on dolomite etched with l-malic acid, 70x magnification (Honess & Jones 1937).

In 1938-1940, Willi Kleber published several interpretations ("Einkristallätzung mit optisch aktiven Säuren" 1938, "Zur Deutung der mit optisch aktiven Säuren erzeugten Ätzerscheinungen" 1940) of the works of Honess & Jones (1937) and Royer (1930), where he discusses the effect of etchants on calcite crystals. Kleber (1938) says that optically active etchants can give etch figures matching the etchant's symmetry even if a non-optically active compound is added to the etchant, as long as the optically active one (e.g. tartaric acid) is strong enough to work as the main etchant. He also explains that depending on the crystal's face that is being attacked by the acid, there is usually one specific preferred direction in which the acid will attack due to the crystal's orientation, which is assumed to be the reason why one isomer of tartaric acid can produce etch pits that are a mirror image of the etch pits produced by the other isomer.

Another important work was presented by Arnold Boos (1941), who conducted a set of etching experiments on calcite, siderite, and rhodochrosite ($MnCO_3$). His aim was to collect more data on the effect of mineral acids and optically active acids on carbonate minerals, using various concentrations of hydrochloric, sulfuric, nitric and tartaric acid. Most of Boos's experiments were done on calcite, focusing on the effect of d-tartaric acid in particular. Being an optically active acid, tartaric acid can exist in two forms, called enantiomers (l- and d-tartaric acid), which are mirror images of each other. A defining trait of an optically active compound is that when hit by polarized light, the plane of light will rotate in a different direction depending on the enantiomer, with d-tartaric acid causing clockwise rotation and l-tartaric acid resulting in counter clockwise rotation. Boos' observations include a variety of etch pit shapes and sizes depending on which etchant is used, and Boos discusses the difference in etching speed depending on the analyzed mineral. A result that is important for this thesis is that calcite etching is fast, rhodochrosite is etched more slowly and siderite etching happens even more slowly. This bit of data influenced the experiments that were done to find a suitable etchant for siderite, as described in chapter 5.1.

In the second half of the 20th century, few etching attempts with carbonate minerals have been made. Experiments made in that timeframe that are relevant for this thesis include a study that visualizes induced fission tracks on siderite with sodium hydroxide solution by Nagpal (1972), as well as some attempts at calcite etching by Keith & Gilman (1960) that include a variety of etching recipes. A work about successful etching of induced fission tracks on calcite was published by Sippel & Glover (1964, Fig. **2.5**), and an attempt to etch spontaneous fission tracks on calcite was made by Macdougall & Price (1974); the latter paper mentions that tracks on calcite may anneal at room temperature and that calcite was therefore unsuitable for fission track dating, which is probably the reason why no publications about track etching of calcite were made from that point on. Later works are mainly about dissolution kinetics of carbonate minerals, including works by Orton and Unwin (1993) experimenting with flow system cells to dissolve dolomite in aqueous hydrochloric acid at room temperature, Gautelier (1999, 2007) who studied the dissolution of dolomite in aqueous solutions of hydrochloric acid at elevated temperatures, and Pokrovsky (2005, 2009) with a study of calcite, dolomite and magnesite dissolution in aqueous solutions of various pH values and a wide range of temperatures.

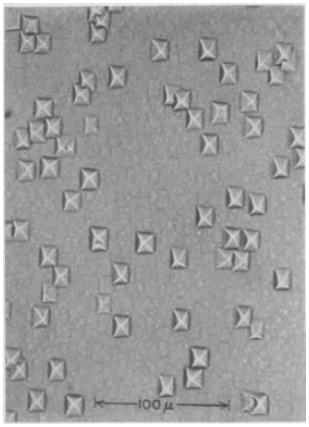

Fig. **2.5**: Etch pits of induced fission tracks on calcite etched with concentrated formic acid (Sippel & Glover 1964).

There is a recent doctoral thesis by Dedera (2015) which deals with the topic of track etching, which will be discussed in detail in Chapter 2.3. Dedera's main focus was the etching of heavy ion tracks and induced fission tracks on artificial internal surfaces of calcite samples, but his thesis also briefly discusses the etching of other carbonate minerals.

2.2 Fission track dating

Fission-track dating is a widely used method in thermochronology based on the natural decay of uranium (mainly ^{238}U) in minerals causing linear radiation damage. Such damage remains in a mineral as long as it is kept below the mineral-specific closure temperature, at which the radiation damage would start to heal and vanish. Since the half-life of ^{238}U is constant, the thermochronometer is able to give the time that has passed since the mineral was last cooled below the closure temperature (the "cooling age"); if the mineral cooled very quickly, the time when the mineral crystallized (the "crystallization age") can also be determined by this method.

For a mineral to be usable as a thermochronometer, several conditions must be fulfilled. The mineral's natural uranium content must be high enough so that a given sample will generate a sizable amount of spontaneous fission tracks over time. A method to visualize and quantify the spontaneous fission tracks is required, and the actual uranium content of the sample to be analyzed must be determined. Additionally, the closure temperature of spontaneous fission tracks must be known, i.e. the temperature at which fission tracks start to fade. Different minerals have different closure temperatures meaning that this temperature has to be specifically determined for each mineral.

An important overview of fission-track dating was published by Fleischer, Price & Walker ("Advances in Fission-Track Dating", 1975). The minerals most commonly used for fission track dating are zircon and apatite; tracks on those minerals can be visualized by etching, which

can be done with a mixture of H_2SO_4 and HF for zircon (Krishnaswami, 1974, Fig. **2.6**) and with HNO_3 for apatite (Wagner & Van den Haute, "Fission-track Dating", 1992). When the mineral's natural uranium content has been determined, it is then possible to polish and etch a previously internal surface to get the track density and thereby calculate the mineral's cooling age. It is also possible to determine the track length distribution and the size of etch pits. The aforementioned book, "Fission-track Dating", is an important compendium about the fission track dating method and its potential applications.

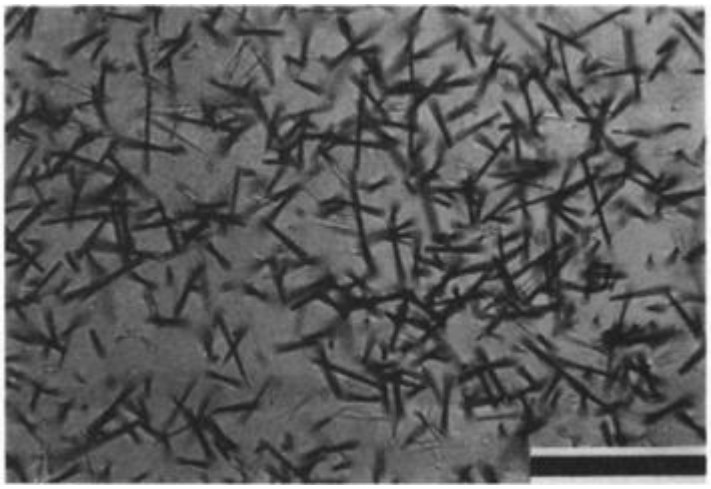

Fig. **2.6**: Etch pits of spontaneous fission tracks on zircon etched with a 1:1 mixture of HF/H_2SO_4 at 150-180 °C (Krishnaswami 1974).

2.3 Quantification of irradiation damage on an internal surface of calcite

Recently, a successful attempt to visualize ion tracks in calcite has been done by Sebastian Dedera (Dedera 2015, Visualization of Ion-Induced Tracks in Carbonate Minerals, PhD thesis). He used cleaved calcite crystals from Eskifjörður, Iceland and generated artificial ion tracks by preparing crystals and irradiating them with heavy ions, using etching techniques to enlarge the formed tracks into etch pits. Dedera's work was inspired by the paper "Fission Damage in Calcite and the Dating of Carbonates" by Sippel & Glover (1964), which investigated whether fission-track dating could be performed on calcite minerals. In an attempt to find a suitable acid, Dedera performed heavy ion experiments with calcite samples to create ion tracks, then tested concentrated formic acid (used by Sippel & Glover), hydrochloric acid, sodium hydroxide (based on works by Macdougall & Price 1974 and Afarideh et. al. 1993) and a mixture of EDTA and acetic acid (also used by Macdougall & Price) in an attempt to visualize the generated ion tracks via etching.

Out of these etchants, Dedera found EDTA + 5% acetic acid to produce the best results, but discovered that this etchant may cause problems when trying to etch a sample embedded in

epoxy. Dedera then proceeded to test an etching solution for calcite described by Keith & Gilman (1960), who used diluted nitric acid. By fine-tuning the conditions for etching, Dedera was able to successfully visualize the heavy ion tracks on cleaved surfaces of calcite samples and quantify them, thereby verifying that the irradiation worked and showing that HNO_3 can be used to etch ion tracks on calcite. He established a standard etching recipe using 0.091% HNO_3 at a temperature of 15 °C for 2-8 seconds, which produced good shapes and sizes of etch pits (Fig. **2.7**). Dedera then did experiments with thermal neutron irradiation of calcite crystals where the cleaved surfaces were covered with a uranium source (zircon grains or CN5 uranium glass) and etching the irradiated samples with nitric acid, using the method he established for heavy ion irradiated samples. He successfully managed to get etch pits that could be attributed to the irradiation process, thereby showing that it is indeed possible to visualize fission damage on calcite with this method.

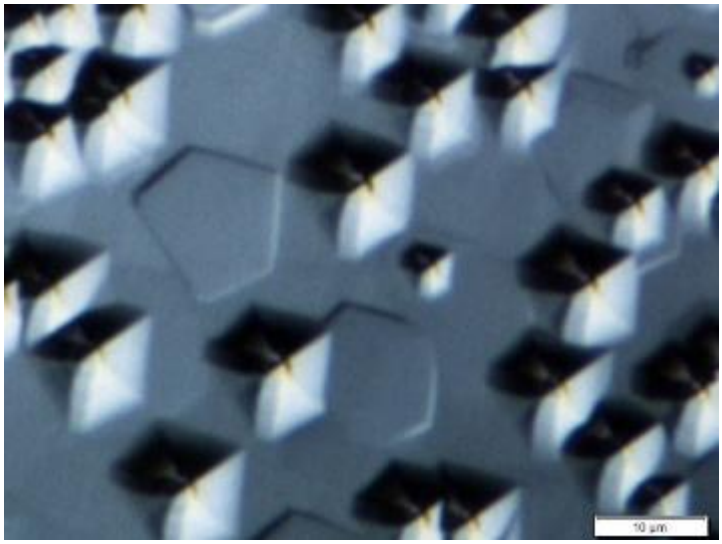

Fig. **2.7**: Etch pits of ion tracks on calcite etched with 0.091% HNO_3 for 2 s at 15 °C, Dedera (2015). The etch pits have a hexagonal shape with a distinct circular-shaped trail in the centre.

2.4 Use of dolomite and siderite for fission-track dating

Not many research papers deal with the subject of using dolomite or siderite for fission-track dating. An important study by Nagpal (1972) describes attempts at visualizing induced fission tracks on various minerals, including siderite; the etchant used by them is a 6N NaOH solution in water. The group of Nagpal saturated this etching solution with etch products of the lexan pieces they used during irradiation; they state that the quality of etch pits on the sample increases that way. Nagpal successfully etched tracks generated by irradiation with thermalized neutrons of siderite samples covered with uranium-doped glass (Fig. **2.8**).

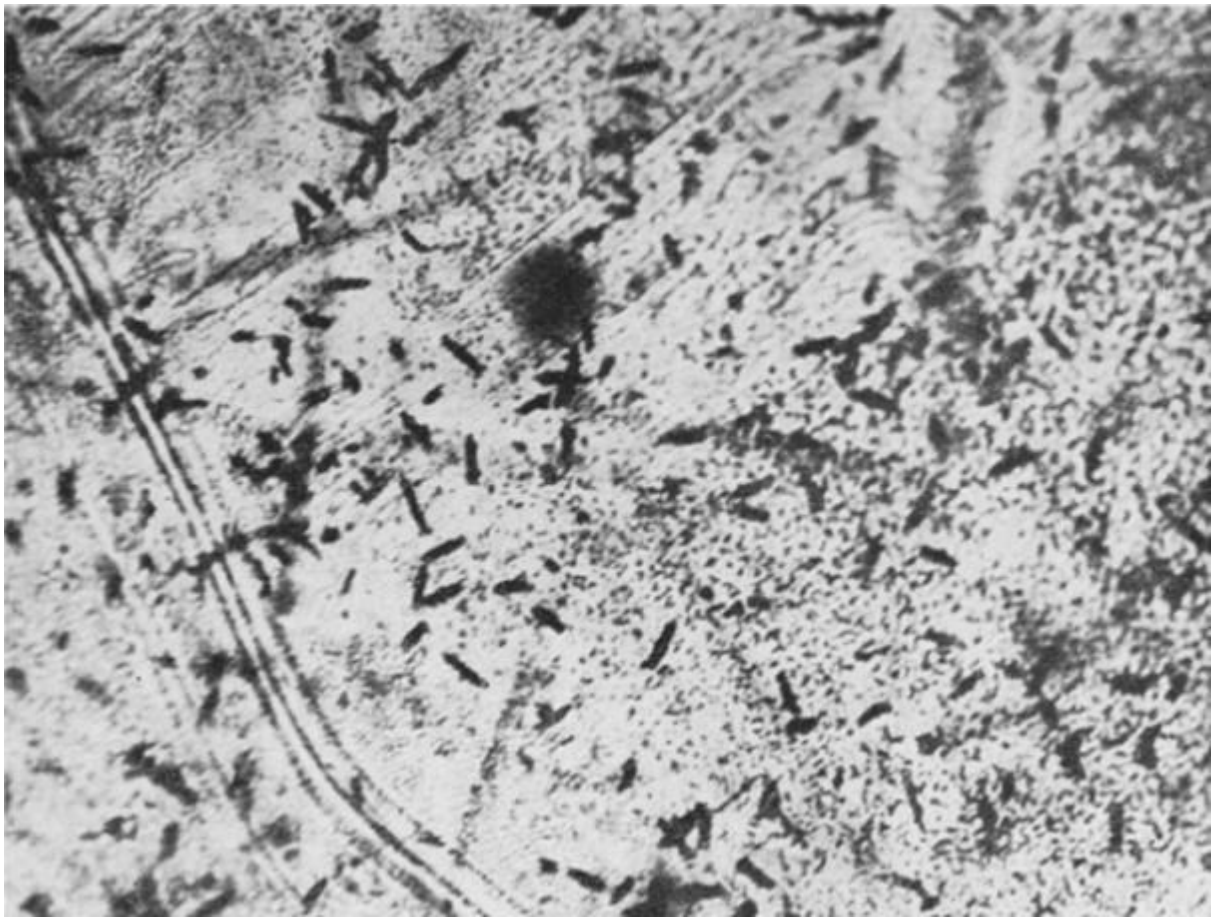

Fig. **2.8**: Etch pits on siderite produced with 6N NaOH, Nagpal (1972). The etch pits appear line-shaped and with various orientations on the sample surface.

2.5 Uranium content of dolomite/siderite

In order to be suitable for fission-track dating, minerals need to have a sufficiently high uranium content. The minerals most used for fission-track dating are apatite and zircon, with apatite usually having a uranium content between 10-50 µg/g and zircon averaging 100-300 µg/g. For determining whether fission-track dating using dolomite or siderite as the uranium-bearing mineral, literature research was performed to determine the average uranium content of these minerals.

Works that give average uranium contents of dolomite and siderite are plentiful, with Tab. **2.1** presenting an overview of the ones relevant for this study. As shown in Caruso & Simmons' study (Caruso & Simmons 1985), siderite can have uranium contents of 10-20 µg/g, but the siderite samples used in Nagpal's work (1972) were said to only contain about 0.5 µg/g of uranium. Nagpal also researched the uranium content of dolomite samples; they found that their samples had contents of about 0.27 µg/g of uranium, although a study by Copeland (2007) found uranium contents in dolomite samples of up to 4.1 µg/g. It can thus be assumed that not all siderite

and dolomite samples may be suitable for fission-track dating and that their uranium content has to be measured in advance.

Tab. **2.1**: Uranium content of various carbonate minerals.

Author	Year	Mineral	Source	U content (µg/g)
Nagpal	1972	Dolomite	unknown	0.26-0.28
Nagpal	1972	Siderite	unknown	0.53-0.62
Caruso	1985	Siderite	New Hampshire	Up to 24.6
Copeland	2007	Calcite/dolomite	Oklahoma et. al.	Up to 4.1

The siderite samples were also chemically analyzed for the presence of uranium, with the detailed procedure described in chapter 7.2. It turned out that the samples used in this study have very low uranium contents, meaning that the likeliness of being able to visualize spontaneous fission tracks on these samples is close to zero. Therefore, the only way to test the applicability of heavy ion track etching methods for fission tracks with the samples at hand is to create samples with induced fission tracks, which is described in chapter 5.7.

3. Methodology

The experiments performed on dolomite and siderite in this study are displayed schematically in the flow charts (Fig. **3.1, 3.2**) which show the individual steps that have been performed for this work. For both dolomite and siderite, the first step was to conduct literature research to see which experiments have been made on these minerals in the past, followed by the selection of samples to be used in experiments and their preparation. In order to be able to see the effects of etching on samples when viewing them with an optical microscope, their surfaces have to be sufficiently smooth; this factor had to be considered when selecting mineral samples. The available dolomite samples were found to be of sufficient quality, but in the case of siderite the available samples were found to be too coarse which led to the development of a preparation method for obtaining samples with smooth, polished surfaces.

Since the primary goal of this study is to establish an etching method capable of displaying fission tracks in carbonate minerals, swift heavy ion irradiation was performed at the GSI Darmstadt to create artificial tracks on the samples to ensure that tracks exist on the samples, leading to the next step: etching experiments with various etchants to determine the conditions (etchant, etching time and temperature, as well as the etchant concentration) necessary to visualize these artificial ion tracks.

Once an etchant was found that resulted in visible etched tracks when viewing the sample with a microscope, various conditions were tested to develop a standard etching recipe for the mineral in question, one which produces good quality tracks that can be counted to verify that the etching was complete and all the heavy ion tracks have in fact been etched successfully.

For both dolomite and siderite, experiments with induced fission tracks were performed once the standard etching method had been established. First, samples had to be prepared by embedding them in epoxy resin so that a uranium glass with a known concentration of ^{235}U can be mounted on top of them. This uranium glass serves as a source of fission fragments which are created by irradiation with thermal neutrons ($1*10^{15}$-$1*10^{16}$ neutrons/cm^2) at the FRM II reactor in Munich. The fission fragments can hit the surface of the mineral sample and generate induced fission tracks, which are similar in nature to those that occur on minerals as a result of spontaneous fission of ^{235}U. After the irradiation had been performed, the etching method was used in an attempt to visualize the induced fission tracks; in the case of siderite, a problem resulted when the unpacked samples showed high radioactivity after unpacking due to the formation of an iron isotope with long half-life (^{59}Fe) so a new attempt had to be made using very small and thin siderite samples to reduce the amount of ^{59}Fe that forms during irradiation. Both dolomite and siderite samples with

induced fission tracks were successfully etched, displaying the fission tracks as clusters of etch pits when viewing the samples with a microscope.

In order to determine the closing temperature at which ion tracks disappear for the samples, annealing experiments were conducted. These were successful for dolomite, but siderite was decomposed during the annealing attempt so the annealing temperature of tracks on siderite could not be determined.

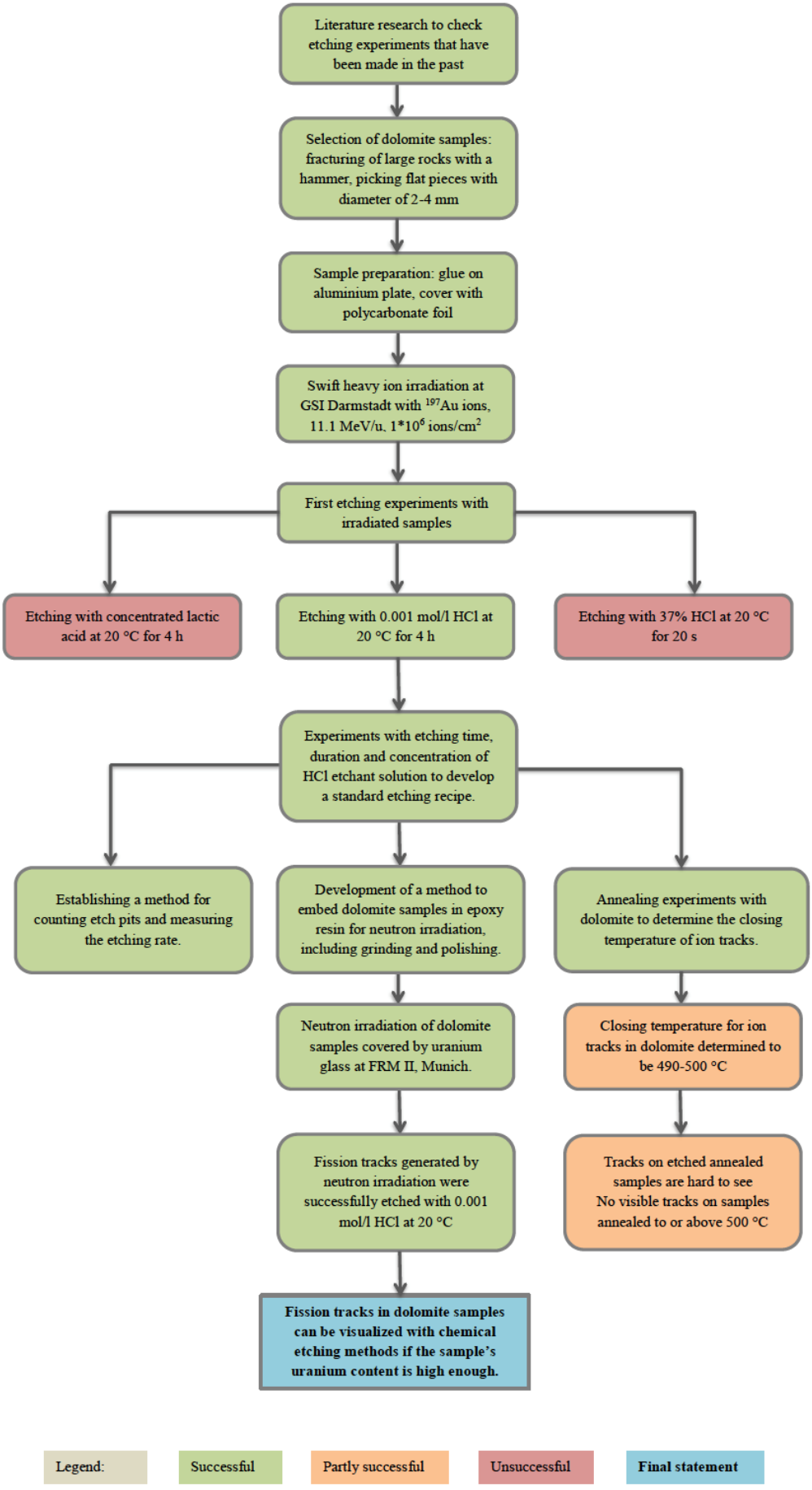

Fig. **3.1**: Flow Chart of experiments conducted with dolomite minerals.

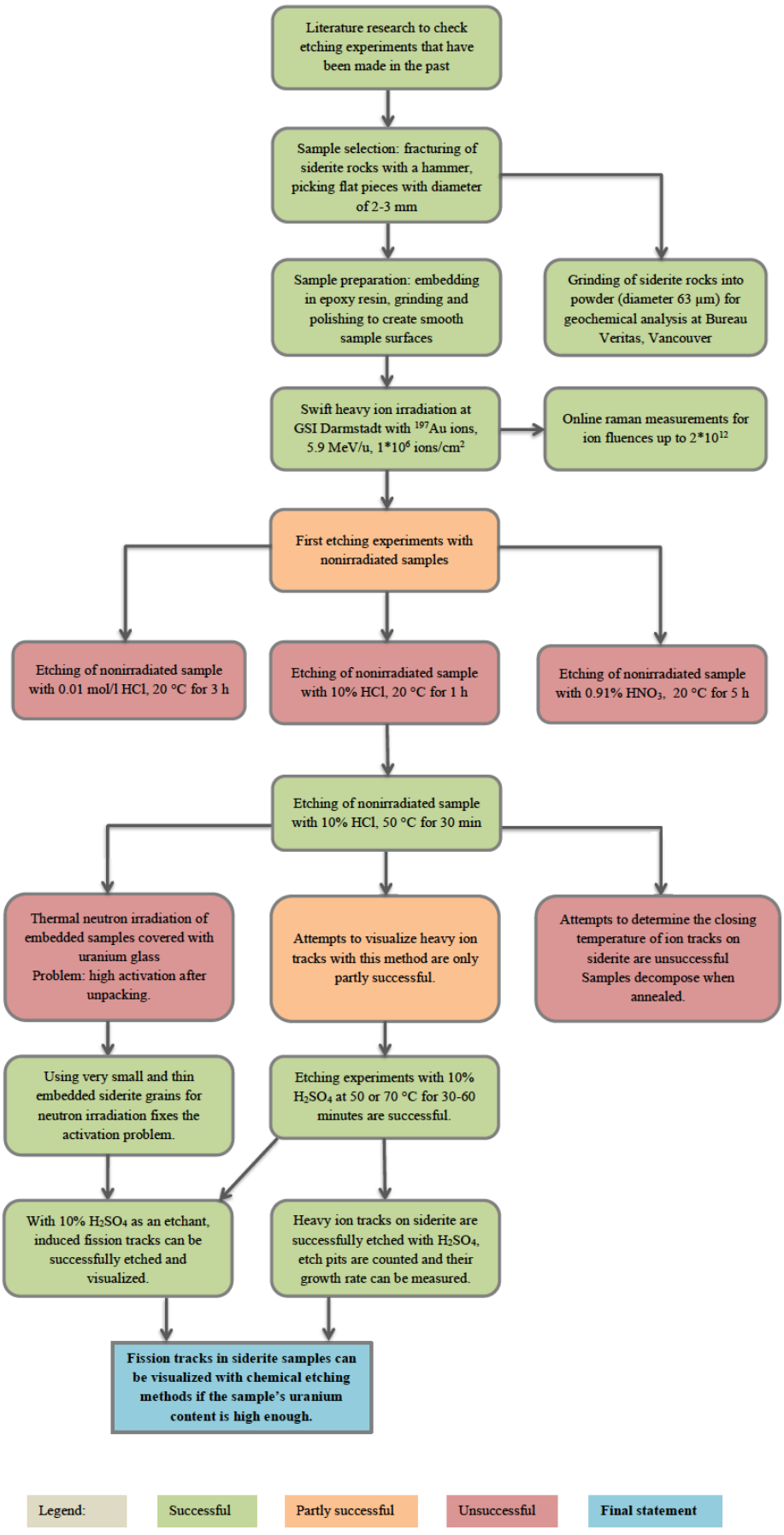

Fig. **3.2**: Flow Chart of experiments conducted with siderite minerals.

3.1 Characterization of dolomite and siderite

Dolomite and siderite are classified as carbonate minerals (Chang, L., Deer, W.A., Zussman, R.A., 1998). Carbonate minerals are commonly found in sediments and metamorphosed rocks. Rock-forming carbonate minerals are divided into four types: calcite-type, aragonite-type, dolomite-type minerals, and malachite/azurite type. Chemically, all carbonate minerals share the carbonate anion CO_3^{2-} with an ion radius of 1.76 Å. The crystal structure depends on the ion radius of the associated cation. When the cation is small, carbonate minerals will crystallize ditrigonal-scalenoedrically, e.g. siderite with the Fe^{2+} ion's radius of 0.82 Å; this is called the "calcite type". Carbonate minerals with big cations, e.g. witherite with a Ba^{2+} cation (1.35 Å), crystallize rhombically; minerals of this type are "aragonite type" minerals. Carbonate minerals with several cations also exist, with the "dolomite type" defined by the mineral dolomite whose structure alternates between Ca^{2+} (1.08 Å) and Mg^{2+} (0.65 Å) cations and crystallizes in the trigonal-rhombohedral system. The minerals malachite and azurite form the "malachite/azurite type", crystallizing monoclinic-prismatically; in addition to the carbonate anion, their chemical composition also includes a hydroxide (OH^-) anion.

Dolomite is the main mineral of the "dolomite type" group of carbonate minerals (Cai et al 2021). It was characterized by D. G. de Dolomieu, a French geologist who researched occurrences of dolomite in Rome and the Dolomite Alps, the latter getting their name in honour of Dolomieu's works. (described in: Paul Caminada (2006), Das abenteuerliche Leben des Forschungsreisenden Déodat de Dolomieu)

The chemical composition of Dolomite is $CaMg(CO_3)_2$. It belongs to the trigonal crystal system and usually forms crystals of tabular habit, although other crystal habits (columnar, stalactitic) are also possible. Dolomite has a Moh´s hardness of 3.5-4, and its crystals are usually colourless but grey and occasionally pink varieties exist. The mineral usually appears transparent or translucent. A distinctive property of dolomite is a high birefringence index, which causes incoming rays of light to be split into two rays that are refracted at different angles, a phenomenon that can be observed by putting a dolomite crystal on graph paper under a light source; this property is shared by some other carbonate minerals, including calcite and siderite.

Dolostone is the name for sedimentary rocks that consist mainly of dolomite; due to the chemical composition of dolomite, their stoichiometric ratio of magnesium to calcium is approximately 1:1. Dolostone is very common in the earth's crust and can be found all around the world; it often occurs together with calcite-rich limestone. The dolostone rocks are usually appearing opaque due to the birefringence of dolomite, and it usually forms sharp edges and

rough surfaces. When subjected to hydrochloric acid, dolostone will dissolve very slowly, producing weak bubbles of carbonic acid. Dolostone is capable of acting as an oil and gas reservoir. A major dolostone deposit is found in the Italian Alps and northeastern Italy, called "The Dolomites", a mountain range formed mostly of dolostone and limestone. Dolomite is believed to be formed when calcite, e.g. in limestone, gets into contact with magnesium-rich water, which starts a process called dolomitization. Limestone can partially or completely be changed to dolostone that way. However, dolomite can also be formed by precipitation from supersaturated solutions (Banerjee, Journal of the Geological Society of India Vol.87, May 2016). Calcite dissolution happens according to the formula

$$CaCO_3 + H^+ \leftrightarrow Ca^{2+} + HCO_3^-$$

If the solution contains sufficient amounts of magnesium, dolomite can then be formed according to the following equation:

$$Ca^{2+} + Mg^{2+} + 2\ CO_3^{2-} \leftrightarrow CaMg(CO_3)_2$$

Dolomite precipitation is believed to follow the second part of the reaction, occurring if calcium, magnesium and carbonate ions are present in a solution with a sufficiently high saturation index. Magnesium-rich sea water can, as a consequence, reach a point where dolomite is precipitated.

Siderite is a "calcite type" carbonate mineral, which was known since ancient times and started being used as an iron ore in the early Iron Age. It got its name in the 19th century; at first, in 1832 F. S. Beudant called it "siderose" (Beudant, 1832) based on its iron content (the Greek word for iron is σίδηρος, sideros), and W. K. Haidinger, who did the first scientific paper about the mineral, renamed it to "siderite" in 1845 (Haidinger, 1845). Like dolomite, siderite crystallizes in the trigonal crystal system and usually forms tabular crystals. Its Moh´s hardness is around 4, and it often forms yellowish or brown crystals but colourless, red, green, and black varieties exist. Siderite is a brittle mineral that is very likely to break when mechanical force is applied. When exposed to hydrochloric acid, siderite shows no visible reaction with cold acid and only a very weak reaction with hot acid (Chang, L., Deer, W.A., Zussman, R.A., 1998).

The world's biggest siderite deposit is found in the Erzberg mine of Austria, located in the city of Eisenerz (German for "iron ore"). Dolomite and ankerite are also found there. Several other siderite mines exist in Austria too, and as a result, iron ore processing is an important branch of the country's industry. The Erzberg mine alone is currently producing about 3 million tons of

refined iron ore per year.

Like dolomite, siderite can be formed by precipitation from supersaturated solutions. (Krylov, Geophysical Research Letters, vol. 35, 2008) The reaction for siderite formation is assumed to be:

$$Fe^{2+} + 2\ HCO_3^- \leftrightarrow FeCO_3 + CO_2 + H_2O$$

which requires the solution's pH to be where dissolved carbon is mostly present in the form of bicarbonate.

3.2 Samples used

The dolomite samples used in this study are from Binntal, Switzerland, specifically the "Grube Lengenbach", a quarry where a large variety of minerals can be found (Tab. **3.1a, b**). It is the type locality for over 30 minerals, some of which have not been found anywhere else yet.
Lengenbach has a big dolomite deposit. For this study, mostly translucent white dolomite crystals were used but also some more opaque blue crystals that get their colour from the presence of impurities. Originally the material consisted of large chunks with diameters of several cm, which were fractured into small fragments of 0.5-1 cm diameter by using a hammer. The resulting dolomite crystals often had flat surfaces even without further preparation and could therefore generally be used as they are. (Fig. **3.3**)

Fig. **3.3**: Raw dolomite crystals from Binntal, Switzerland.

Siderite samples used in this study are spathic iron ores from Siegen, Germany, collected in the "Grube Pfannenberger Einigkeit", a former mine that was closed in 1962 (Tab. **3.1a, b**). A total of over 8.5 million tons of iron ore was hauled from this mine while it was running; the siderite found in this mine usually appears in paragenesis with chalcopyrite. Other minerals found in Pfannenberger Einigkeit include galena, pyrite, sphalerite and ankerite. (Fig. **3.4**) The raw siderite samples were originally massive rocks with diameters of 5 cm and bigger, which were fractured into small fragments of 0.5-1 cm diameter by using a hammer (Fig. **3.5**).

The resulting siderite crystals are opaque and of a dark brown colour, exhibiting a layered structure and considerable brittleness; particularly thin crystals tend to crumble even when exposed to slight mechanical force and therefore have to be handled with care. Due to the majority of resulting siderite crystals having no flat surfaces that could easily be viewed under a microscope, embedding them in epoxy resin was generally required. The embedding process is described in detail in chapter 5.3-5.4.

Tab. **3.1a**: Samples used in this study.

Sample No.	Mineral	Results	Irradiation	Etching
DolSD01	Dolomite		^{197}Au 1*10^{6}, 11.1 MeV/u	HCl 37% RT 20s
DolSD02	Dolomite		^{197}Au 1*10^{6}, 11.1 MeV/u	conc. lactic acid 210 min RT + 30 min 50 °C + 30 min 80 °C
DolSD03	Dolomite		^{197}Au 1*10^{6}, 11.1 MeV/u	HCl 0.001 mol/l 260 min RT + 150 min 50 °C
BK0309Dol001-02	Dolomite		^{197}Au 1*10^{6}, 11.1 MeV/u	HCl 0.001 mol/l 225 min 50 °C
BK0309Dol001-01	Dolomite	overetched	^{197}Au 1*10^{6}, 11.1 MeV/u	HCl 0.001 mol/l 240 min 50 °C
BK0309Dol001-10 to BK0309Dol001-15	Dolomite	Glued on specimen plate with nail polish	^{197}Au 1*10^{6}, 11.1 MeV/u	HCl 0.001 mol/l 120 min 20 °C
BK0309Dol001-16	Dolomite		^{197}Au 1*10^{6}, 11.1 MeV/u	HCl 0.001 mol/l 120 min 20 °C
BK0309Dol001-05 to BK0309Dol001-09	Dolomite	Glued on specimen plate with nail polish	^{197}Au 1*10^{6}, 11.1 MeV/u	HCl 0.001 mol/l 150 min 20 °C
BK0309Dol001-04	Dolomite		^{197}Au 1*10^{6}, 11.1 MeV/u	HCl 0.001 mol/l 240 min 20 °C
BK0309Dol001-03	Dolomite	Etch pits clearly visible	^{197}Au 1*10^{6}, 11.1 MeV/u	HCl 0.001 mol/l 260 min 20 °C
BK0309Dol001-17	Dolomite		^{197}Au 1*10^{6}, 11.1 MeV/u	HNO_3 0.91% 120 min 20 °C
DolB010-G	Dolomite, blue		1*10^{15} Neutrons on zircon	HCl 0.001 mol/l 60 min 25 °C
DolW04-G	Dolomite	Embedded, etched with sample holder	1*10^{15} Neutrons on zircon	HCl 0.001 mol/l 165 min 40 °C
DolW11-G	Dolomite	Clusters of etch pits	1*10^{15} Neutrons on zircon	HCl 0.001 mol/l 180 min 20 °C
DolW13-G	Dolomite	Etch pits distributed randomly on surface	1*10^{15} Neutrons on CN1	HCl 0.001 mol/l 240 min 20 °C + 150 min 40 °C + 30 min 50 °C
BK2705-01-Sid	Siderite		Not irradiated	HCl 0.001 mol/l 180 min 20 °C + HCl 0.01 mol/l 210 min 20 °C + HNO_3 0.91% 120 min 20 °C
Sid-1209-Ätztest 1	Siderite	Triangular etch pits	Not irradiated	HCl 10% 30 min 50 °C
Sid-1209-Ätztest 2	Siderite	Triangular etch pits	Not irradiated	HCl 10% 10 min 50 °C
Sid-1209-Ätztest 3	Siderite	Very small etch pits	Not irradiated	HCl 10% 30 min 20 °C
Sid-H_2SO_4-Ätztest	Siderite		Not irradiated	H_2SO_4 10% 30 min 20 °C + 60 min 50 °C
Sid-H_2SO_4-Ätztest b	Siderite	Irregular distribution of etch pits	Not irradiated	H_2SO_4 10% 30 min 50 °C
Sid-001-01-04	Siderite		^{197}Au 1*10^{6}, 5.9 MeV/u	H_2SO_4 10% 30 min 50 °C
Sid-001-01-02	Siderite	Etch pits in hexagonal area	^{197}Au 1*10^{6}, 5.9 MeV/u	H_2SO_4 10% 30 min 70 °C
Sid-001-01-05	Siderite		^{197}Au 1*10^{6}, 5.9 MeV/u	H_2SO_4 10% 60 min 50 °C
Sid-001-02-01	Siderite	Etch pits well visible	^{197}Au 1*10^{6}, 5.9 MeV/u	H_2SO_4 10% 60 min 50 °C
Sid-001-01-06	Siderite		^{197}Au 1*10^{6}, 5.9 MeV/u	H_2SO_4 10% 60 min 50 °C
Sid-001-05	Siderite	Sample was polished for 15 min with OP-S suspension first, etch pits well visible	^{197}Au 1*10^{6}, 5.9 MeV/u	H_2SO_4 10% 60 min 50 °C
Sid-001-06b	Siderite		^{197}Au 1*10^{6}, 5.9 MeV/u	H_2SO_4 10% 60 min 50 °C

Tab. **3.1b**: Samples used in this study

Sample No.	Mineral	Results	Irradiation	Etching
Sid-001-12	Siderite	OP-S suspension used after etching to improve visibility of etch pits	^{197}Au 1*10^{6}, 5.9 MeV/u	H_2SO_4 10% 60 min 50 °C
Sid-001-01-07	Siderite	Etch pits well visible	^{197}Au 1*10^{6}, 5.9 MeV/u	H_2SO_4 10% 60 min 70 °C
Sid-001-06a	Siderite		^{197}Au 1*10^{6}, 5.9 MeV/u	H_2SO_4 10% 75 min 50 °C
Sid-001-01-01	Siderite	Etch pits in hexagonal area (hard to see)	^{197}Au 1*10^{6}, 5.9 MeV/u	H_2SO_4 10% 90 min 50 °C
Sid-001-01-03	Siderite	Etch pits well visible	^{197}Au 1*10^{6}, 5.9 MeV/u	H_2SO_4 10% 120 min 50 °C
Sid-001-08	Siderite	Etch pits visible with transmitted light only (?)	^{197}Au 1*10^{6}, 5.9 MeV/u	H_2SO_4 10% 240 min 50 °C
Sid-001-03-01	Siderite	Etch pits visible only after 10% HCl etching	^{197}Au 1*10^{6}, 5.9 MeV/u	HCl 0.001 mol/l 300 min 20 °C + HNO_3 0.91 % 120 min 20 °C, 60 min 50 °C + HCl 10% 150 min 20 °C
Sid-001-03-02	Siderite	Many etch pits after etching at 50°C	^{197}Au 1*10^{6}, 5.9 MeV/u	HCl 10% 90+90 min 20 °C + 60 min 50 °C
Sid-001-04-01	Siderite		^{197}Au 1*10^{6}, 5.9 MeV/u	HCl 2% 480 min 20 °C + HCl 10% 60 min 20 °C
Sid-001-04-03	Siderite		^{197}Au 1*10^{6}, 5.9 MeV/u	HCl 10% 30 min 50 °C
Sid-001-04-02	Siderite		^{197}Au 1*10^{6}, 5.9 MeV/u	HCl 10% 60 min 50 °C
Sid-Disl01	Siderite		Not irradiated	H_2SO_4 10% 60 min 50 °C
Sid-Disl02	Siderite	Surface damaged (overetched)	Not irradiated	HCl 10% 30 min 50 °C
Sid-EB-Ätztest	Siderite	Embedded in epoxy	Not irradiated	H_2SO_4 10% 30 min 50 °C
SPT3	Siderite	For photos that document grinding and polishing	Not irradiated	H_2SO_4 10% 30 min 50 °C
Sid-AH-1	Siderite	Annealed at 250 °C for 14 d, then embedded, grinded and polished	Not irradiated	H_2SO_4 10% 60 min 50 °C
Sid-AH-2	Siderite	Annealed at 250 °C for 14 d, then embedded, grinded and polished	Not irradiated	H_2SO_4 10% 60 min 50 °C
Sid-Verheilungstest	Siderite	Annealed at 300 °C for 270 min, black residue on surface (maybe wuestite)	Not irradiated	H_2SO_4 10% 60 min 50 °C
1703-Sid-a	Siderite	Fission tracks visible with transmitted light	1*10^{16} Neutrons on CN5	H_2SO_4 10% 90 min 50 °C
1703-Sid-d	Siderite		1*10^{16} Neutrons on zircon	H_2SO_4 10% 210 min 50 °C
1703-Sid-e	Siderite		1*10^{16} Neutrons on zircon	H_2SO_4 10% 60 min 50 °C

Fig. **3.4**: A raw pristine siderite sample from Pfannenberger Einigkeit.

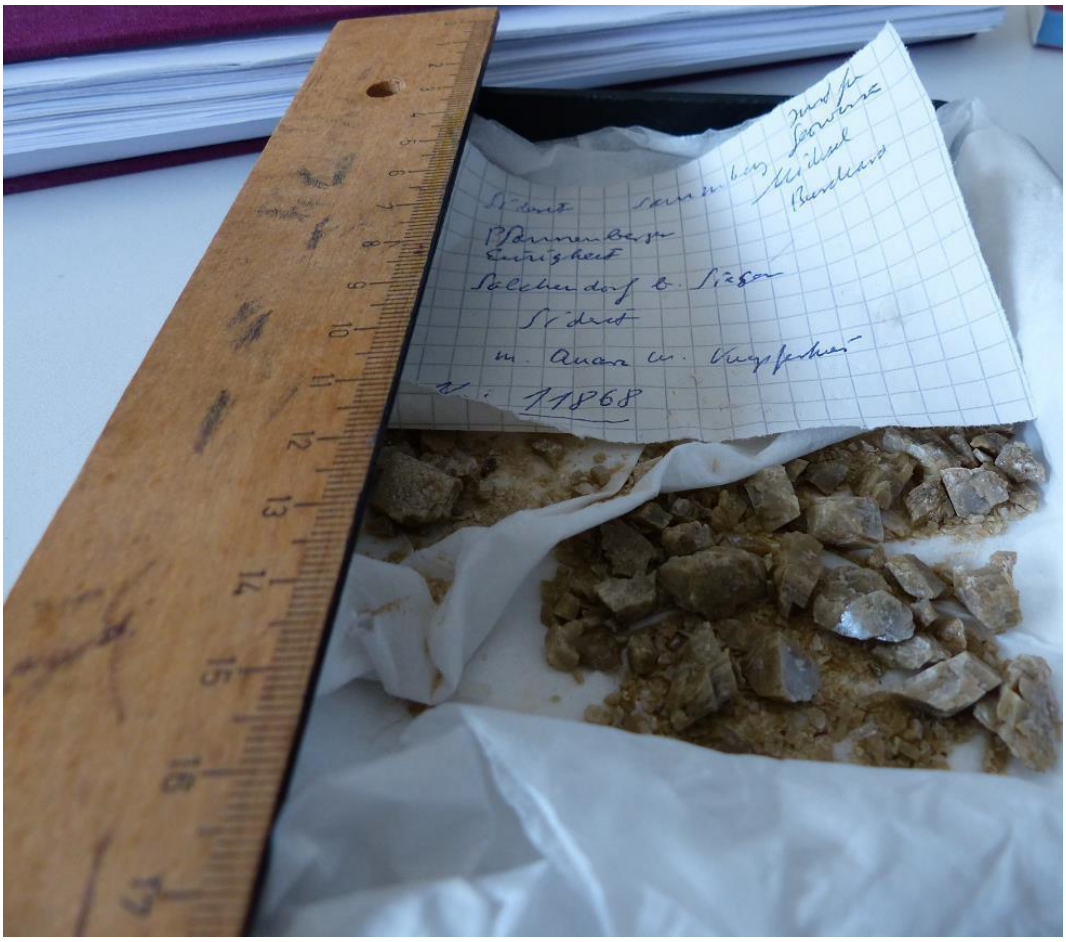

Fig. **3.5**: Raw siderite samples from Pfannenberger Einigkeit, fractured with a hammer.

In order to simulate fission fragments a uranium source was attached to the dolomite and siderite crystals prior to the irradiation with thermalized neutrons (Tab. **3.1a, b**). As a uranium source, zircon crystals from a titanium mine in Paraíba, Brazil were used. Furthermore, CN-5 uranium glasses standards from Corning, New York were also used as a uranium source. The CN-5 glasses used for this work have an actual uranium content of 12.17 (± 0.62) µg/g (Bellemans et. al. 1995). In order to check the amount of induced fission tracks generated during irradiation with thermalized neutrons, one CN-5 glass covered with a mica of very low uranium content was irradiated with the natural dolomite and siderite samples.

Muscovite used for thermal neutron irradiation of siderite was purchased from "Richard Jahre GmbH", a company that specializes in manufacturing of electronic components. The mica plates offered come in different shapes and thicknesses; the ones used in this study are round or square in shape and have a thickness of 65-75 µm.

3.3 Swift heavy ion irradiation

One of the world's largest facilities for experiments with accelerated heavy ions is located in Darmstadt, Germany: the GSI (Gesellschaft für Schwerionenforschung). It is part of the Helmholtz Association, an organization that funds scientific research projects in Germany. The following accelerator facilities are used at the GSI:

- the linear accelerator UNILAC, which is used to accelerate elements from hydrogen to uranium. Ions can reach energies ranging from 2 to 11.4 MeV/nucleon, being accelerated to 15-20% of the speed of light. The fluence that can be achieved is 10^7-10^8 per bunch.

- the synchrotron SIS18, capable of accelerating ions to 90% of the speed of light, with a corresponding energy of about 1300 MeV/nucleon.

- the storage ring ESR, which is used to store the accelerated ions generated by the SIS18.

Altogether, the GSI's accelerator facilities have over 25 experimental areas. The GSI specializes in physics research, including plasma physics, atomic physics, as well as nuclear, biophysics, medical, and material research. From 1981 to 1996, the following elements have been created at the GSI: bohrium, meitnerium, hassium, darmstadtium, roentgenium and copernicium, corresponding to the atomic numbers 107-112. The existence of heavier elements up to an atomic number of 117 (tennessine) has been confirmed in experiments conducted at the GSI from 2009 to 2012. At the GSI, a method of cancer treatment via heavy ion beams of carbon has been developed, which is nowadays used in the "Heidelberger Ionenstrahl-Therapiezentrum" (HIT center of ion beam therapy).

Ions to be accelerated are generated at the ion source and sent to the UNILAC for the initial acceleration. In the linear accelerator, ions can reach a maximum energy of 11.4 MeV/u and are then sent either to one of the experimental sites (X0-X8), the M-branch (a multipurpose research chamber, M1-M3 experimental place, that has equipment for atomic force microscopy, x-ray diffraction, spectroscopy, and scanning electron microscopy) or the SIS18 synchrotron. In the latter case, the ions are accelerated again, reaching energies of up to 1300 MeV/u, and sent to the ESR storage ring where they can be stored for a few hours, the FRS fragment separator to generate radioactive isotopes and/or fission and fusion products, or one of the experimental caves located in the target hall.

Irradiation experiments for this study were conducted in the X0 experimental hall. For irradiation in the experimental area, sample magazines are used that can hold 20 sample holders each. The X0 beamline has an automatic sample exchange system for quickly irradiating the samples in a magazine without requiring further user input.

Irradiating any sample turns it into "activated material": due to the irradiation, the sample itself will emit radioactivity because of the interaction of the irradiation beam with the sample creating radioactive isotopes. With a digital dose rate meter, this radioactivity can be measured. As long as the radioactivity is significantly higher than the background radiation that is present everywhere, the samples are not ready for use in the laboratory of the Institute of Earth Sciences (Heidelberg University) yet; the GSI will usually release irradiated samples about one week after irradiation, after the generated radioactive isotopes have had time to decay. Before the samples can then be used in routine laboratory experiments, their radioactivity needs to be measured again by a radiation safety officer, and if the value is lower than a certain threshold (below 100nS), they can be unpacked and used. The same practice is also applied when doing thermal neutron irradiation, as described in chapter 3.6.

The dolomite samples in this study were irradiated with 11.1 MeV ^{197}Au ions at the X0 beamline, with a fluence of $1*10^6$ ions/cm^2. Siderite samples were irradiated with 5.6 MeV ^{197}Au ions and a fluence of $1*10^6$ ions/cm^2. In both cases, all irradiations were perpendicular to the natural or polished internal crystal surface. Due to difficulties with the calibration for ion beams for this comparatively low ion fluence, the actual number of ions applied to the sample varies quite a bit, including one case where etching experiments showed etch pits of over $1*10^7$ ions/cm^2 on the irradiated sample surface, as well as some samples for which the amount was less than $0.5*10^6$ ions/cm^2.

In order to be able to determine the exact fluence applied to an irradiated sample, the dolomite

and siderite grains were covered with a polycarbonate foil during irradiation. This foil is highly sensitive for irradiation and can be etched with a well-established method (Ditlov et. al. 1997; Picht, 2010) to display all ions when etched with 6 mol/l NaOH at 50 °C for 90 minutes. A hexagonal mask with 90% transmission was mounted on top of the foil, thereby allowing irradiated and non-irradiated areas to be formed next to each other on the sample surface. Etch pits in non-irradiated regions can thereby be classified as dislocations or natural defects, as opposed to etched ion tracks which will only occur in areas that were not covered by the mask.

For the determination of energy loss and projected ranges of heavy ions in the sample, the SRIM (Stopping and Range of Ions in Matter, developed by Ziegler et. al. 2010) software was used. Calculated results are a range of 86.71 µm for 11.1 MeV ^{197}Au ions on dolomite and 90.05 µm for 5.6 MeV ^{197}Au ions on siderite, with fission fragments of natural ^{238}U for comparison (Tab. **3.2**). The output includes electron and nuclear energy loss, projected range in the sample, and longitudinal/lateral straggling. Since the polycarbonate foil covering the siderite samples has a thickness of 30 µm, it is assumed that the remaining energy of ions hitting the siderite surface is reduced, resulting in an actual range of 28.77 µm on the sample as can be seen in the tables, the range that accelerated heavy ions will travel in the sample is much greater than that of fission fragments. The method used to generate fission fragments is shown in chapter 3.6.

Tab. **3.2**: Energy loss and projected ranges of ions in dolomite and siderite, calculated by SRIM software.

Ion Energy	Target	dE/dx Elec [keV/µm]	dE/dx Nuclear [keV/µm]	Projected Range
2.19 GeV ^{197}Au	Dolomite	2.653E+04	2.425E+01	86.71 µm
90.0 MeV ^{90}Kr	Dolomite	1.238E+04	4.388E+01	11.79 µm
90.0 MeV ^{143}Ba	Dolomite	1.328E+04	1.431E+02	11.67 µm
1.10 GeV ^{197}Au	Siderite	1.425E+04	2.113E+01	90.05 µm
672.5 MeV ^{197}Au	Siderite	3.368E+04	8.139E+01	28.77 µm

3.4 Etching equipment and procedure

Etching solutions were produced by diluting laboratory chemicals from Sigma-Aldrich, AppliChem and Roth with purified water. They were kept in a chemical storage cabinet with a constant temperature of 21 °C (± 0.5 °C). In order to find etchants suitable for the visualization of heavy ion tracks and induced fission tracks, etching solutions described in literature were tested on mineral samples with and without artificial irradiation damage. Etch pits (when available) were then characterized and compared with literature images.

Etching experiments were conducted in a laboratory equipped with an extractor hood. The temperature in this laboratory is kept constant by an air conditioning unit set to 21 °C. Etching

solutions were used in a beaker glass, and the samples were either put into the etchant with tweezers or, in the case of epoxy-embedded ones, a sample holder constructed at the precision mechanic workshop that only exposes the top of the sample to the etchant solution (Fig. **3.6**). For keeping the temperature constant during etching, the glass containing the etchant was put in a Lauda E 100 water bath after the latter had reached the desired temperature. The etching solution was stirred with a magnetic stir bar during the experiment. (Fig. **3.7**)

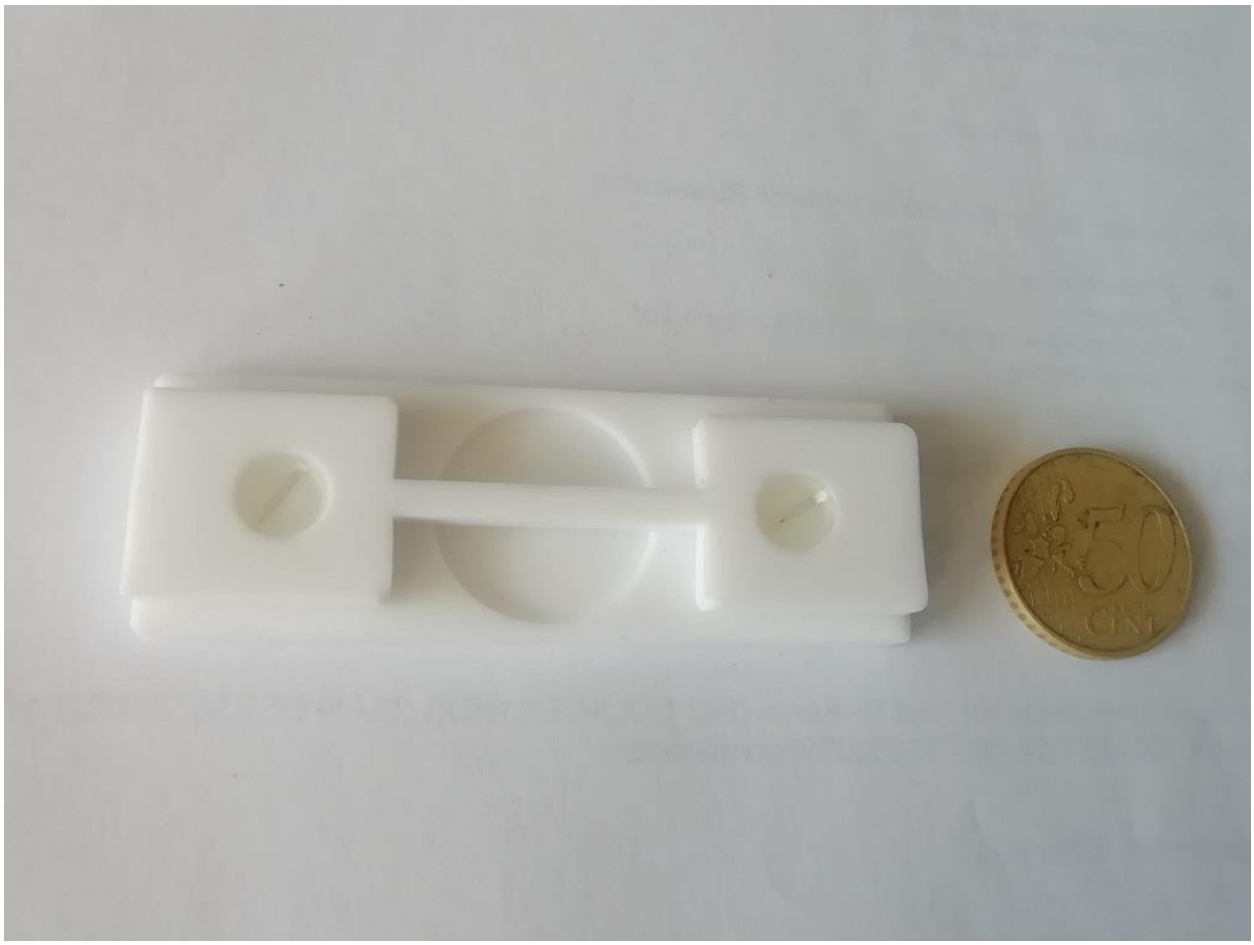

Fig. **3.6**: Special sample holder with a cavity for embedded samples, for ensuring that only the top of a sample is exposed to the etchant solution. The sample is put in the circular-shaped orifice.

Fig. **3.7**: Lauda E 100 water bath with temperature regulation unit.

After the etching was completed, the sample was washed with purified water, followed by ethanol or isopropanol; it was found that ethanol often leaves a liquid film behind on the sample surface, which is difficult to remove and proves to be troublesome when the sample is later viewed under a microscope. This problem was solved by switching to isopropanol, which leaves no impurities after wiping it off the sample with a tissue cloth. Care must be exercised when wiping the sample surface because too much force may result in accidentally removing part of it, or in the case of brittle samples (especially siderite), it can even result in the sample breaking apart.

3.5 Analytical methods used

The microscope used for optical analysis and characterization/counting of observed etch pits is an Olympus BX-50 reflected and transmitted light microscope with attached Nomarski Differential Interference Contrast (DIC) and attached camera. Stream Enterprise™ software was used for image analysis. Available objectives for the microscope are 5x, 20x, 50x and 100x,

and the lens allows magnifications of 1x, 1.25x, 1.6x and 2x. Images were mostly taken with reflected light and attached DIC, as the desired features can be hard to see without DIC. In some cases, transmitted light was used when the etch pits were indistinguishable against rough backgrounds with reflected light. (Fig. **3.8**).

Fig. **3.8**: Olympus BX-50 microscope with Nomarski DIC, attached camera and PC with Stream Enterprise™ software.

For quality control while performing the grinding and polishing process of embedded samples, a Leitz 307-148 microscope was used with 5x, 10x, 25x, 100x and 160x objectives. (Fig. **3.9**). Embedding of samples is done with casting molds (Struers), disposable scratch paper, double-sided duct tape (Tesa) and Struers EpoFix resin and hardener. The resin/hardener ratio used is always 50:6.

Fig. **3.9**: Leitz microscope for quality control of polished samples.

Fig. **3.10**: Struers RotoPol grinding machine with RotoForce sample holder.

Grinding and polishing are done with a Struers RotoPol 22 grinding machine and RotoForce sample holder, using silicium carbide grinding paper and Struers MD-DAC/OP-Chem polishing cloths. Diamond paste (3 and 1 µm), DP Lubricant Blue and OP-S suspension, all provided by Struers, are also used in the polishing process. Chapter 5.3 describes the procedure in detail. (Fig. **3.10**)

A Horiba Jobin Yvon iHR 320 Raman spectrometer equipped with a Laser Quantum Ventus 532 nm laser was used to determine the mineralogical composition of siderite samples. All Siderite crystals used in the experiments are single siderite grains. Components of the Raman spectrometer include a Pelletier cooled camera, a Laser Quantum MPC 6000 laser control unit, and a Horiba Superhead optional confocal optic with an Euromex EK1 cold light source. The microscope has 5x, 10x, 20x and 50x objectives. For controlling the system and microscope image analysis, Horiba LabSpec 5 software is used.

The principle of Raman spectroscopy is based on inelastic scattering of light (typically monochromatic laser beams) that results when light interacts with matter. Specifically, the light photons can interact with a molecule's vibrational modes; usually, visible or near- infrared lasers are used as the light source. When a molecule is hit by the beam, it is excited to a virtual energy state, a state where its energy level is higher than that of the ground state.
Most of the time, the molecule will then fall back to the same ground state it started in, emitting a scattered photon in the process that has the same energy as the photon which caused the excitation. This is called "Rayleigh scattering". However, if the molecule's vibrational modes interact with the polarization when the excitation happens, it's possible that the molecule absorbs energy, leading to the emission of a photon whose energy is lower than that of the absorbed photon; this is known as "Stokes scattering". The reverse case is also possible when the molecule loses energy and the emitted photon's energy is higher than that of the absorbed photon, an effect known as "anti-Stokes scattering". (Fig. **3.11**)

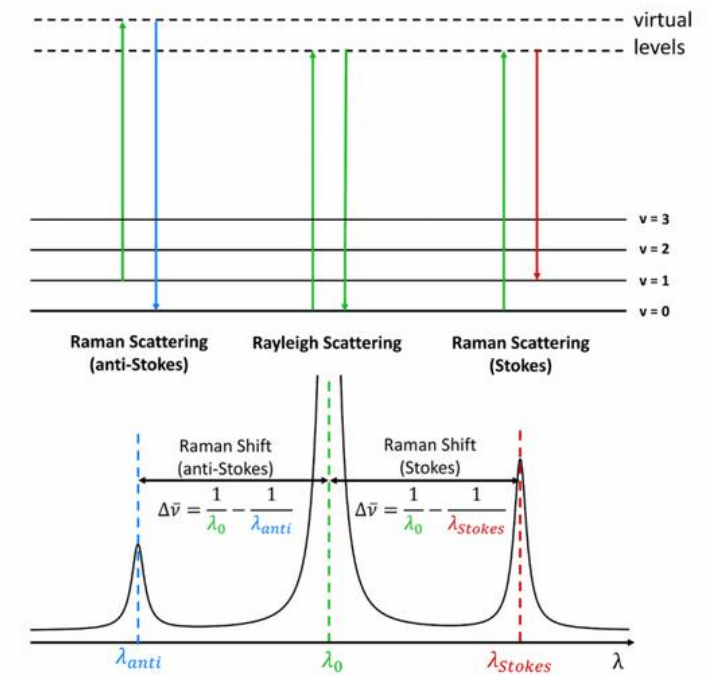

Fig. **3.11**: Rayleigh, Stokes and anti-Stokes scattering (G. Stokes, 1852).

A Raman spectrum shows the spectrum of scattered photons. The presence or absence of characteristic bands can be used to determine which chemical compounds exist in the sample, with the caveat that only those compounds whose polarization is changed in the process of excitation can have Raman bands.

For annealing experiments, a Heraeus Instruments M110 muffle furnace was used with a temperature uncertainty of ± 2 °C and a maximum operating temperature of 1100 °C. The furnace's temperature control allows the user to set the temperature in intervals of 10 °C. (Fig. **3.12**)

Fig. **3.12**: Heraeus Instruments M110 muffle furnace.

The chemical composition of the minerals was determined at the Bureau Veritas Commodities laboratory in Vancouver, Canada. The method used in the laboratory is called ICP-MS, which stands for Inductively Coupled Plasma Mass Spectrometry. This method tests samples for the presence of the following compounds: SiO_2, Al_2O_3, Fe_2O_3, CaO, MgO, Na_2O, K_2O, MnO, TiO_2, P_2O_5, Cr_2O_3. Additionally, the following elements can be detected: Au, Ag, As, Ba, Be, Bi, Cd, Co, Cs, Cu, Ga, Hf, Hg, Mo, Nb, Ni, Pb, Rb, Sb, Sc, Se, Sn, Sr, Ta, Th, Tl, U, V, W, Y, Zn, Zr, La, Ce, Pr, Nd, Sm, Eu, Gd, Tb, Dy, Ho, Er, Tm, Yb, Lu. In this analysis, the metal oxides are dissolved by lithium metaborate or tetraborate and nitric acid. Samples are then introduced to a plasma with temperatures of about 10’000 K, where the atoms are ionized and then transported to an attached mass spectrometer that detects the quality and quantity of incoming ions. The result is a chart that shows the concentration of all the atoms and compounds mentioned above in the analyzed sample. Chapter 7.2 shows the results of the geochemistry analysis. The detection limit for the different elements and analytical techniques used is provided in Tab. **3.3**.

Tab. **3.3** : Lower and upper detection limit for mass spectrometry analysis of various elements and oxides.

Element oxides/ Elements	Lower detection limit [%]	Upper detection limit [%]
SiO_2	0,01	100
TiO_2	0,01	10
Al_2O_3	0,01	100
$Fe_2O_3^T$	0,04	100
MnO	0,01	30
MgO	0,01	100
CaO	0,01	100
Na_2O	0,01	100
K_2O	0,01	100
P_2O_5	0,01	100
LOI	0,1	100
Sum	0,01	100
TOT/C	0,02	100
TOT/S	0,02	100
Elements	Lower detection limit [µg/g]	Upper detection limit [µg/g]
Sc	1,0	10.000
V	8,0	10.000
Cr	20	10.000
Co	0,2	10.000
Ni	0,1	10.000
Cu	0,1	10.000
Zn	1,0	10.000
Ga	0,5	10.000
Rb	0,1	1.000
Sr	0,5	50.000
Y	0,1	50.000
Zr	0,1	50.000
Nb	0,1	1.000
Cs	0,1	1.000
Ba	1,0	50.000
La	0,1	50.000
Ce	0,1	50.000
Pr	0,02	10.000
Nd	0,3	10.000
Sm	0,05	10.000
Eu	0,02	10.000
Gd	0,05	10.000
Tb	0,01	10.000
Dy	0,05	10.000
Ho	0,02	10.000
Er	0,03	10.000
Tm	0,01	10.000
Yb	0,05	10.000
Lu	0,01	10.000
Hf	0,1	10.000
Ta	0,1	1.000
Pb	0,1	10.000
Th	0,2	10.000
U	0,1	10.000
W	0,5	10.000
Mo	0,1	2.000
As	0,5	10.000
Au	0,5 [ng/g]	100.000 [ng/g]

3.6 Thermal neutron irradiation

A stack of samples within a special capsule was prepared for irradiation with thermalized neutrons. The capsules were provided by the FRM II. The stack consisted of dolomite and siderite embedded samples covered with zircon and uranium standard glass (CN 5), as well as CN5 glasses covered with nearly uranium-free Muscovites. Chapter 5.3 describes the procedure of creating suitable embedded samples in detail.

For best irradiation results, it is important that the samples have a completely flat polished surface, which is achieved via the grinding and polishing method described in Chapter 5.3. The uranium source is mounted directly on top of the sample with uranium-free adhesive tape.

Since neutron irradiation can transform stable isotopes of elements into heavier isotopes that may be radioactive, an irradiated sample may emit radioactivity for a while after irradiation, i.e. it turns into activated material. Ideally, the radioactive isotopes generated in a sample decay after a few weeks due to their short half-life, allowing the sample to be released and used for experiments.

Using larger siderite grains for irradiation experiments with thermalized neutrons, a high dose of radioactivity occurred after irradiation. This high dose did not decay significantly over the course of 6 months and disallowed the use of irradiated samples in etching experiments. A possible cause of the high dose might be neutron induced change of the stable ^{58}Fe-isotope to the radioactive ^{59}Fe-isotope. As described earlier siderite has 48% Fe. Stable iron isotopes present in natural siderite are ^{54}Fe (5.8 %), ^{56}Fe (91.72 %), ^{57}Fe (2.2 %), and ^{58}Fe (0.28 %). Neutron irradiation can form the radioactive isotope ^{59}Fe out of the stable isotope ^{58}Fe. The radioactive isotope ^{59}Fe decays with a half-life time of 45.1 days (gamma decay). If enough ^{59}Fe is formed during the neutron irradiation, the siderite sample cannot be used within a decent time.

In order to circumvent this irradiation problem, the volume of siderite was reduced by cutting, grinding and polishing siderite grains to 1 mm thickness and a shape of 3 mm diameter. The formed radioactivity of such samples will decay to acceptable levels within a few weeks after the irradiation is complete, allowing them to be used.

Thermal neutron irradiation experiments of dolomite did not run into this problem, because of the lack of long-lived heavy isotopes of calcium and magnesium. ^{45}Ca, which is likely to form from the stable isotope ^{44}Ca, has a half-life of about 162.61 d, while all heavier Ca isotopes and all Mg isotopes decay faster than that, so even if a significant number of radioactive isotopes

are generated from irradiating a dolomite sample, their activity will decay reasonably fast so it normally doesn’t take more than a few weeks until the samples can be released.

4. Dolomite

4.1 Preparation of cleaved dolomite samples for irradiation

Dolomite grains were gained from idiomorph crystals available at the Institute of Earth Sciences, Heidelberg University, by fracturing them with a hammer or similar tools. The pieces revealed are geometrically equivalent to the large initial piece due to the cleavage properties of dolomite, and are about 0.5-1 mm in diameter with a thickness of 0.2-0.4 mm. For irradiation at the UNILAC accelerator in Darmstadt, the samples were mounted on an aluminium plate (square-shaped, diameter of 5 cm) and inserted in a sample holder provided by the GSI. These fixed-size sample holders are part of the standard equipment used during irradiation at the X0 branch of the GSI. For maximum yield and comparability, the available space on the aluminium plate was filled with as many dolomite samples as possible; since the actual fluence applied can be different for each plate, it helps to have a bunch of samples that all got the same fluence of heavy ions.

For gluing the dolomite crystals to the aluminium plate, a strong double-side adhesive tape was used to ensure the crystals stay in place during irradiation. The available dolomite samples were of sufficient quality to be usable for experiments without the need of grinding and polishing, with smooth surfaces that were almost completely free of scratches. In nature, dolomite can also occur in the form of very fine grains with coarse surfaces, which would require a method of creating smooth surfaces for the purpose of etching experiments; this problem didn't occur for the dolomite samples used in this study, but a grinding and polishing method similar to the one used for siderite samples (as described in chapter 5.3) would render such samples usable for experiments.

4.2 Etching solutions tested

In order to find a suitable etching solution that can visualize heavy ion tracks on an internal surface of dolomite, acids described in literature have been tested. Specifically, the works of Honess & Jones (1937) which dealt with the effect of optically active acids on carbonate minerals included experiments that used lactic acid on dolomite, producing long oval or triangular etch pits. However, attempts to reproduce these results by etching an irradiated dolomite sample with concentrated lactic acid did not produce etched ion tracks. The lactic acid only generated a couple of long scratches after 210 minutes of etching at room temperature, which are probably natural defects in the crystal structure being enlarged by the acid. Etching at 50 °C or 80 °C resulted in more of the same kind of scratches, which appear mostly as lines

with lengths up to 500 µm but also curved and irregular-shaped ones. They are distributed seemingly randomly on the surface. (Fig. **4.1**)

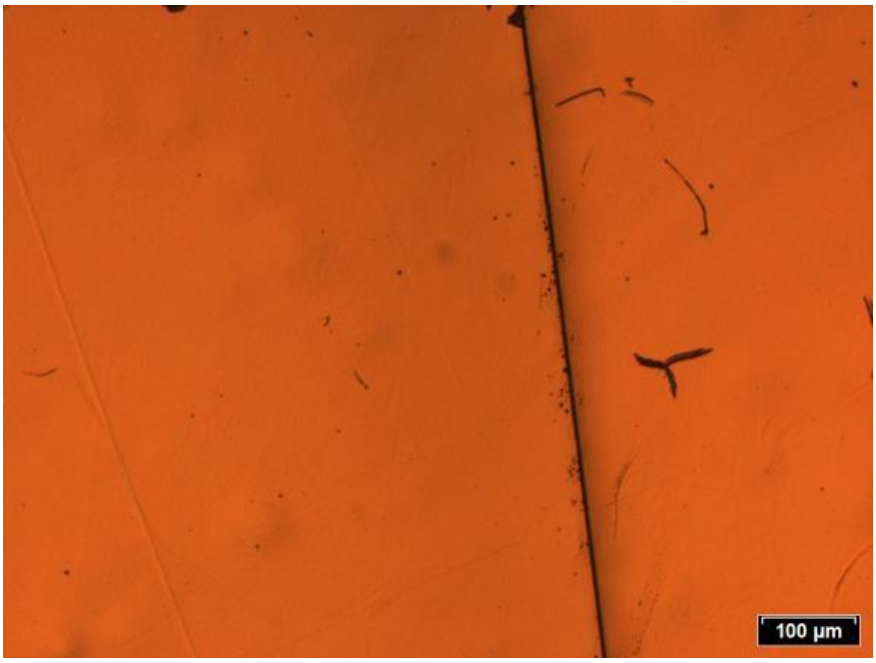

Fig. **4.1**: Heavy ion irradiated dolomite sample (DolSD02) etched with lactic acid, 210 min at 20 °C. A few scratches on the surface became enlarged by the etching, but no heavy ion etch pits are visible.

Another method described in literature involves etching dolomite with hydrochloric acid (Tschermak 1894), which created etch pits of a trigonal, asymmetric shape. An attempt to reproduce their results by etching an irradiated dolomite sample with concentrated HCl for 20 seconds at room temperature resulted in a completely destroyed surface, which means that the acid concentration needs to be reduced in order to receive meaningful results. A paper from Lüttge (2003) talks about dolomite dissolution with a 0.001 mol/l HCl and an etching time of 30-60 minutes, showing the development of roughly circular, scraggy etch pits. This method was also tested on irradiated dolomite samples, but first attempts at room temperature failed to visualize ion tracks even after 260 minutes of etching (Fig. **4.2**). When using the same 0.001 mol/l HCl at 50 °C and etching for 150 minutes, triangular-shaped etch pits of ion tracks were generated (Fig. **4.3**).

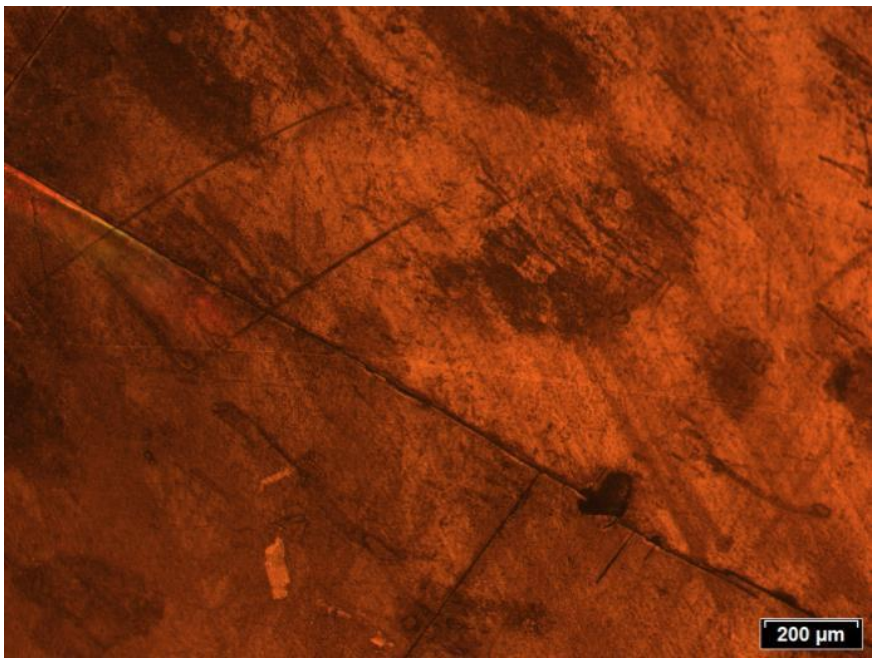

Fig. **4.2**: Heavy ion irradiated dolomite (DolSD03) etched with 0.001 mol/l HCl, 260 min, 20 °C. No etched ion tracks.

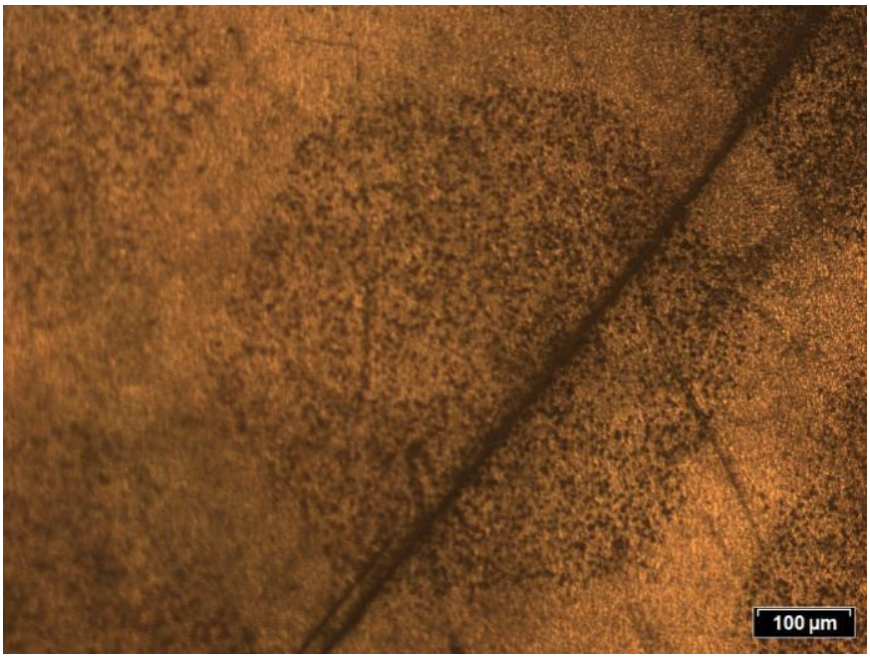

Fig. **4.3**: The same irradiated dolomite sample (DolSD03) after an additional 150 min of etching with the same etchant at 50 °C. Etch pits of heavy ion tracks are visible in hexagonal areas defined by the mask that covered the sample during irradiation.

There is also an etching method for dolomite described in literature that uses sulfuric acid (Baumhauer 1894, Fig. **4.4**) which, due to the good results obtained with HCl, was not investigated any further in this study. The method used by Baumhauer (1894) created trigonal, symmetric etch pits that slightly vary in size.

Fig. **4.4**: Dolomite etched with 1% H_2SO_4 (Baumhauer 1894). Very small trigonal etch pits are visible on the surface.

4.3 Visualization of ion tracks on dolomite with hydrochloric acid

After determining that 0.001 mol/l HCl is capable of etching ion tracks on dolomite into pits, experiments were performed to optimize the etching conditions and obtain statistical data. In order to check whether the etching method is capable of converting all ion tracks into etch pits, the polycarbonate foil that covered the sample during irradiation was etched with a 6 mol/l aqueous solution of NaOH at 50 °C for 90 minutes. This converts all ion tracks on the foil into pores, which are then counted with Olympus Stream imaging software (Fig. **4.5**).

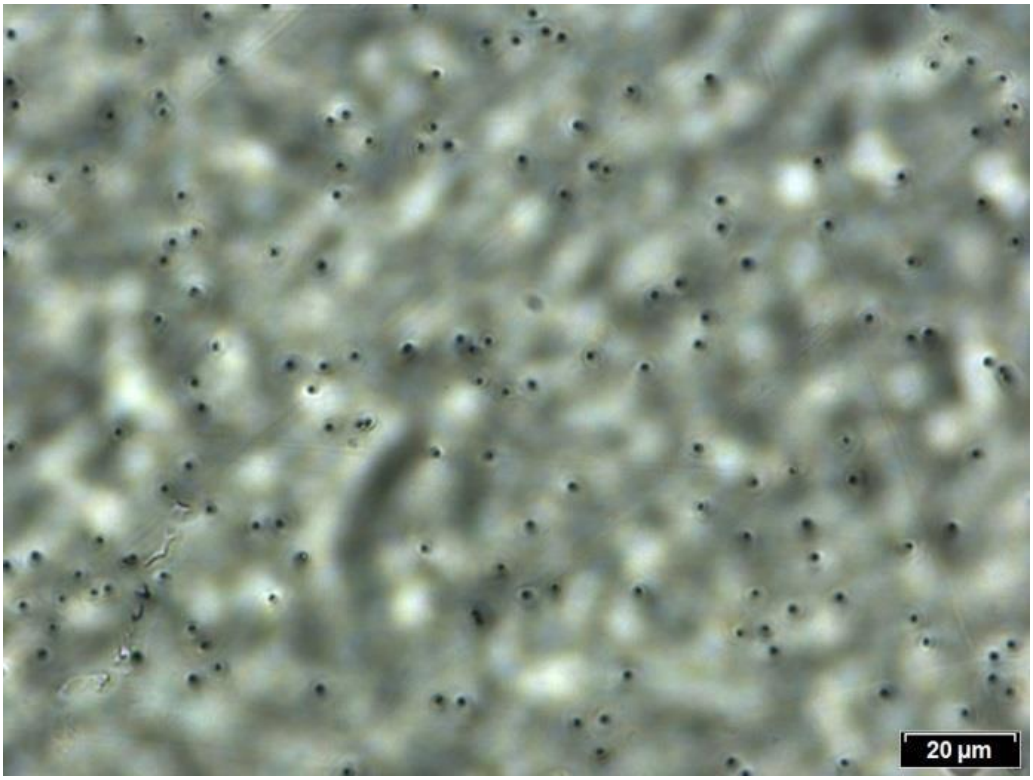

Fig. **4.5**: Irradiated polycarbonate foil etched with 6 mol/l NaOH, 50 °C, 90 min. This etching method visualizes ion tracks as circular-shaped pores which can be counted.

A microscope image with 50x magnification covers a surface of 22950 µm^2. In order to compare the amount of etch pits with the nominal fluence of heavy gold ions that has been applied to the sample, the count of etch pits has to be multiplied by a factor of 4357 to obtain the areal density for 1 cm^2. For both the etched dolomite sample and the foil that was used to cover it during irradiation, several (usually 8 to 25) different areas were evaluated.

The first successful etching experiment did create etch pits of ion tracks in the hexagonal area not covered by the mask during irradiation, but when counting their areal density and comparing it with the etched foil, the values didn't match. The applied fluence should be 1 * 10^6 ions/cm^2; the counted areal density on the foil was 0.706 (± 0.467) * 10^6 ions/cm^2. This can happen due to the very short irradiation time making it difficult to reach the exact fluence requested, meaning that the actual fluence can randomly be greater or smaller than 1 * 10^6 ions/cm^2. However, the areal density on the etched dolomite sample was only 0.450 (± 0.064) * 10^6 ions/cm^2, showing that the conditions used for etching were not satisfactory and the acid did not visualize all the ion tracks that should be there. Tab. **4.1** shows the areal density and calculated fluence for an etched dolomite sample and the corresponding etched foil.

Tab. **4.1**: Areal density of etch pits on dolomite sample (DolSD03, irradiated with heavy gold ions and etched with 0.001 mol/l HCl for 260 min at 20°C and 150 min at 50 °C) compared with the areal density of etched pores on the foil (etched with 6 mol/l NaOH for 90 min at 60 °C). The amount of etch pits on the dolomite sample is too low compared to the calculated fluence of the foil.

Index no.	Areal density (dolomite, 22950 µm²)			Index no.	Areal density (foil, 22950 µm²)		
1	85			1	174		
2	123			2	157		
3	103			3	162		
4	125			4	155		
5	102			5	180		
6	84			6	163		
7	105			7	160		
8	85			8	146		
9	117						
10	99						
11	107						
	Area	Calc. Fluence (10^6 ions/cm²)			Area	Calc. Fluence (10^6 ions/cm²)	
Mean	103	449563		Mean	162	706379	
Std. deviation	15	63523		Std. deviation	11	46662	

By performing etching experiments with different temperatures and etching times, it was determined that etching with 0.001 mol/l HCl at 20 °C for 60-120 minutes produces well-defined etch pits that don't overlap and are easy to distinguish from the background. When using too long etching times or high etching temperatures, the entire dolomite surface will be etched, making it impossible to see all the etched ion tracks against the etched background.

With an etching time of 120 minutes for a batch of irradiated samples, an average areal density of 1.761 (± 0.121) * 10^6 ions/cm^2 was determined by counting the etch pits, which is within error in agreement with the areal density of the corresponding etched foil of 1.754 (± 0.132) * 10^6 ions/cm^2 (Tab. **4.2**). As illustrated in Fig. **4.6**, the areal density of etch pits that appear outside the irradiated zones is small enough to be negligible.

Tab. **4.2**: Areal density of etch pits on dolomite sample (irradiated with heavy gold ions and etched with 0.001 mol/l HCl for 120 min at 20 °C) compared with the areal density of etched pores on the foil (etched with 6 mol/l NaOH for 90 min at 60 °C). The amount of etch pits on the dolomite sample is in agreement with the calculated fluence of the foil (within error).

Index no.	Areal density (dolomite, 22614 µm²)			Index no.	Areal density (foil, 22614 µm²)		
1	407			1	408		
2	377			2	409		
3	430			3	407		
4	401			4	425		
5	348			5	356		
6	367			6	379		
7	389			7	391		
8	399			8	398		
9	439			9	392		
10	382			10	384		
11	414			11	441		
12	437			12	431		
13	360			13	447		
14	392			14	423		
15	334			15	380		
16	378			16	361		
17	407			17	359		
18	429			18	401		
19	416			19	393		
20	424			20	421		
				21	356		
	Area	Calc. Fluence (10^6 ions/cm²)			Area	Calc. Fluence (10^6 ions/cm²)	
Mean	397	1754424		Mean	398	1761905	
Std. deviation	30	131513		Std. deviation	27	120940	

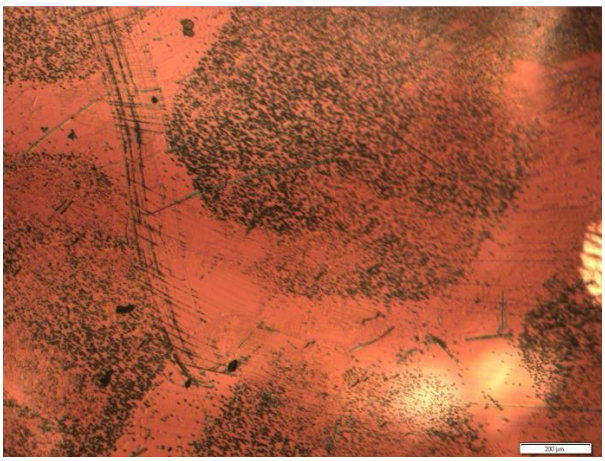

Fig. **4.6**: Heavy ion irradiated dolomite sample (BK0309Dol001-10) etched with 0.001 mol/l HCl at 20 °C, 120 min. Etch pits of heavy ion tracks appear in hexagonal areas as a result of the mask that covered the sample during irradiation.

On sufficiently thin parts of the dolomite crystals, the backside can also develop etched ion tracks. This is due to the penetration depth of heavy gold ions, which according to SRIM calculations (as seen in Chapter 3.3) is 86.71 µm in dolomite for an ion energy of 11.1 MeV. The ions will hit the dolomite crystal in an angle perpendicular to the exposed surface, and the variety of shapes that cleaved crystals can exhibit will sometimes allow the ion beam to penetrate the crystal completely, resulting in ion tracks on surfaces that were not directly exposed to the beam. Fig. **4.7** illustrates this observation. When irradiated samples embedded in epoxy are used instead, this phenomenon can occur only if the samples are very thin, but usually their thickness exceeds the ions' penetration range.

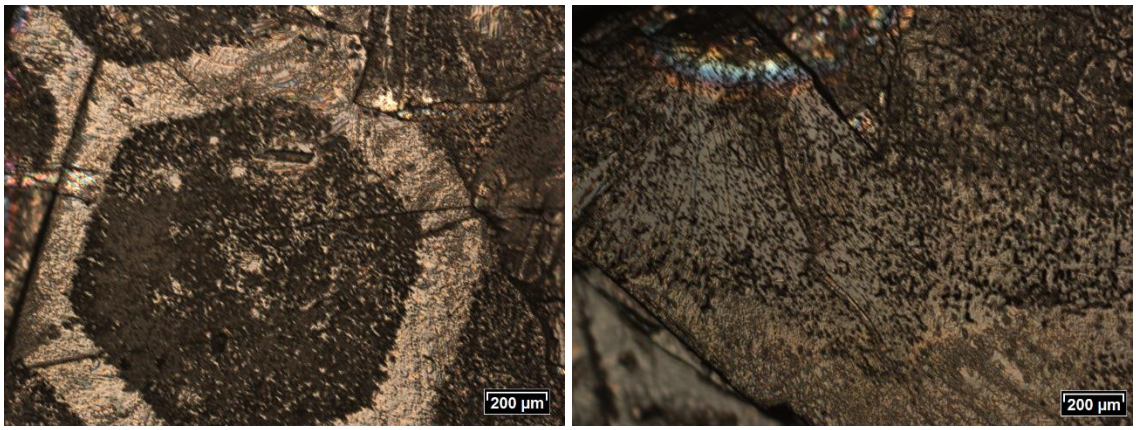

Fig. **4.7**: Heavy ion irradiated dolomite sample (BK0309Dol001-01) etched with 0.001 mol/l HCl for 240 min at 50 °C. Left image: irradiated surface with etch pits in an area defined by the hexagonal mask used as a cover. Right image: etch pits on a side of the crystal (not the irradiated surface), which are assumed to be the result of heavy ions penetrating the crystal and exiting on the side.

4.4 Statistics

With the established etching method for ion-irradiated dolomite, experiments have been performed to gain information on the statistics of the etching process. The growth rate of etch pits has been measured by determining their length and width once every 15 minutes, using Stream Imaging Software to obtain 100 values for each point in time to get a statistically significant result. Fig. **4.8** shows the etch pit growth rate as a function of etching time. At etching times from 15-45 minutes, the etch pits weren't of sufficient quality for statistical analysis.

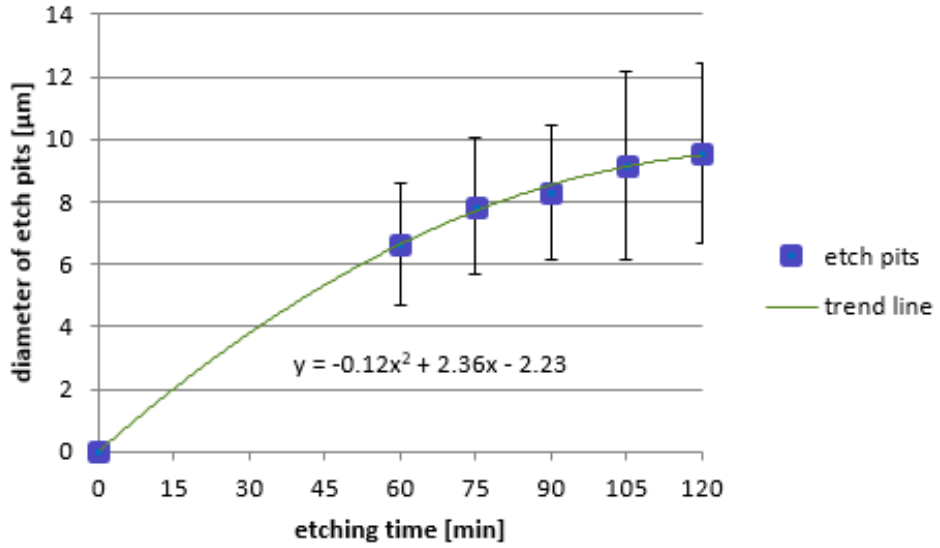

Fig. **4.8**: Diameter of etch pits on heavy ion irradiated dolomite (BK0309Dol001-12) at various points in time when etched with 0.001 mol/l HCl at 20 °C.

The diagram shows that the growth rate of etch pits starts out high and then becomes slower as etching time increases. A possible explanation of this phenomenon is that as etch pits become bigger, more material of the sample has to be etched away to further increase the etch pits' size. As a result, the diameter of etch pits will eventually reach a plateau value where they barely increase in size with additional etching time, and eventually a point is reached where etch pits become too large, causing them to overlap. When conducting etching experiments, it is therefore important to not overetch the sample to make sure the individual etch pits are still recognizable.

In order to determine the vertical etching speed, irradiated dolomite crystals were glued on a specimen plate using Pro Shine Base Coat nail polish. This was done in an attempt to fixate their position so that the sample's height could then be measured with TrackScan software. In a first experiment, the stability of this nail polish under acidic conditions was tested, using 0.001 mol/l HCl as an etchant. It was found that the glue does not dissolve, which ensures its usability for etching experiments.

When using this method on irradiated samples, the optical microscope is not capable of measuring the depth of individual etch pits themselves, making it impossible to determine their etching speed with this method. Only the bulk vertical etching rate can be measured. For this, a reference copper dot has been glued on the specimen plate (Fig. **4.9**) and the relative vertical position of etched dolomite samples to this reference dot was measured once every 15 minutes of etching. Results are given in Tab. **4.3** and Fig. **4.10**; the observed average rate of vertical etching was 0.4 (± 0.1) µm/min. The vertical etching rate is slow enough that samples can generally be etched for several hours.

Fig. **4.9**: Dolomite samples glued onto a specimen plate, with a reference copper dot (marked by the red circle).

Tab. **4.3**: Bulk vertical etch rates for dolomite sample (DolGarW04), with 0.001 mol/l HCl at 20 °C as an etchant, determined with Stream software.

Etching time [min]	Height [µm]			Average	Error
0	428.6	369.9	439	412.5	11.5
15	423.5	372.5	436.5	410.8	10.7
30	423	382	398.6	401.2	6.8
45	425.3	397.5	443.4	422.1	7.7
60	421.1	353.5	393	389.2	11.3
75	414.5	350.2	407.5	390.7	10.7
90	418.4	341	389	382.8	12.9
105	405.5	376.7	423.8	402.0	7.9
120	384	372.9	424.3	393.7	8.6
135	385.3	345.6	409.9	380.3	10.7
150	380.1	332.7	373.2	362.0	7.9
165	356.9	335.4	351	347.8	3.6

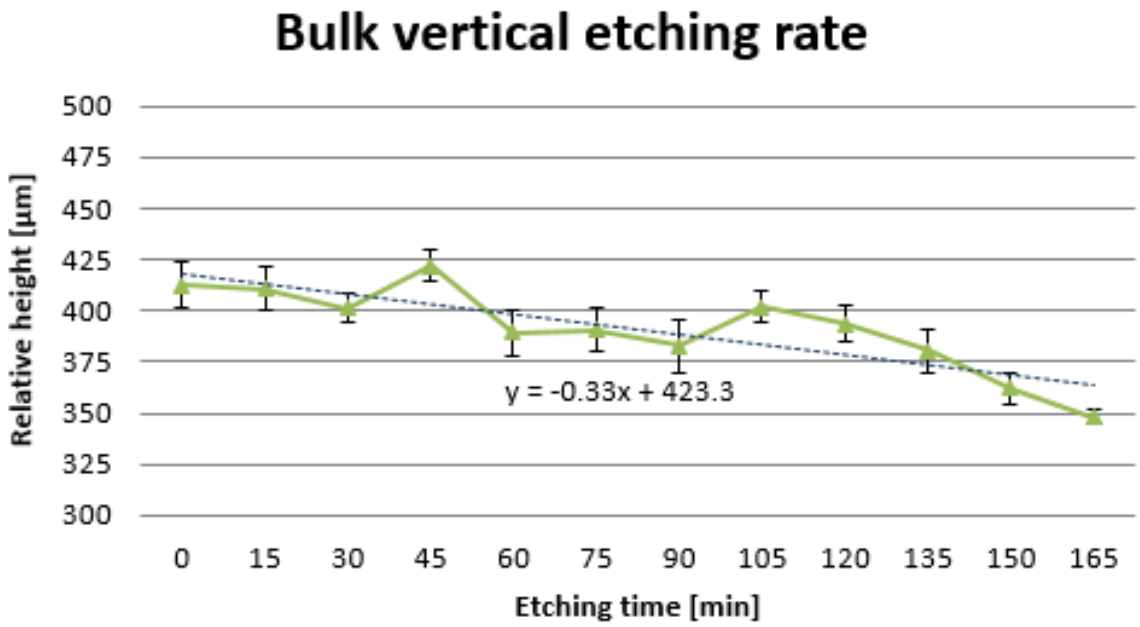

Fig. **4.10**: Vertical etching rate of dolomite (DolW04-G) with 0.001 mol/l HCl at 20 °C as an etchant, determined with Stream software.

Another method for measuring the bulk etching rate involved the construction of a sample holder with the help of the precision mechanic workshop (seen in chapter 3.4). This sample holder is capable of holding the sample in a fixed position and allows the sample to be etched exclusively on the exposed surface, and it is constructed in a way that allows it to be examined under the optical microscope by reflected light as well. A specific spot on the sample was selected to be the point of focus. Using TrackScan software, the difference in height between the focused spot and the sample holder's horizontal bar was measured once every 15 minutes of etching (Fig. **4.11**). Here, the vertical etching rate was determined to be 0.7 (± 0.4) µm/min. Within error, this result is in agreement with the vertical etching rate determined via Stream software.

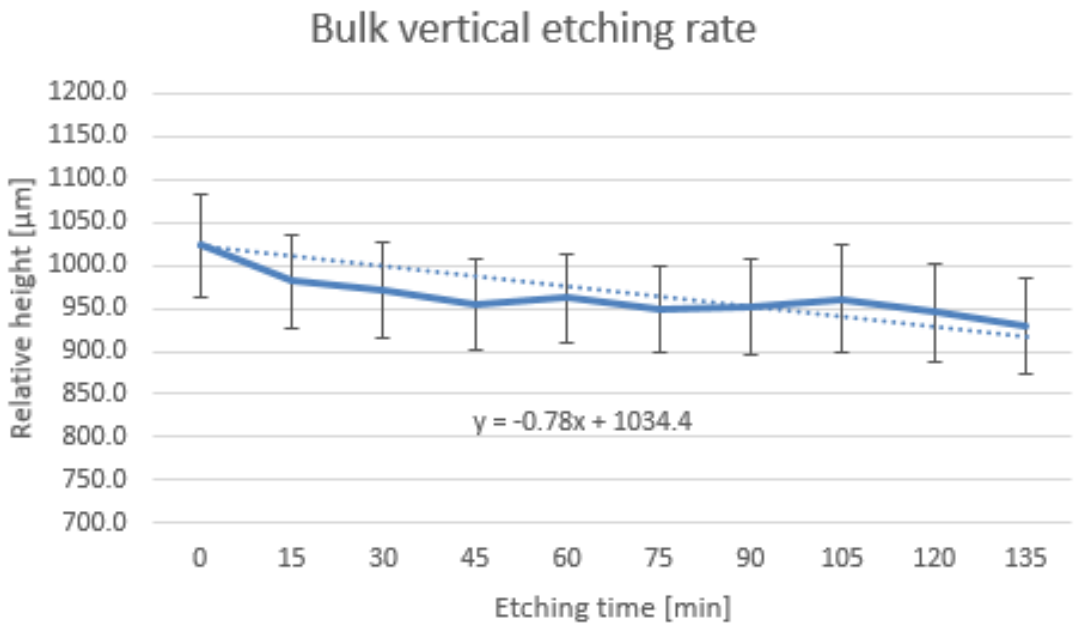

Fig. **4.11**: Vertical etching rate of heavy gold ion irradiated dolomite (BK0309Dol001-06) with 0.001 mol/l HCl at 20 °C as an etchant, determined with TrackScan software.

The optimized etching method for dolomite was used for annealing experiments on several batches of dolomite samples. Chapter 6 deals with the results of etching annealed dolomite samples in detail.

4.5 Visualization of induced fission tracks on dolomite

Dolomite samples for this set of experiments were embedded in epoxy resin. Induced fission tracks on dolomite samples were created by irradiation with thermal neutrons at the FRM II reactor in Munich. The samples were covered with uranium-doped CN-5 glass or zircon grains during irradiation. A fluence of $1*10^{15}$ neutrons/cm^2 was applied during irradiation.

Etching of irradiated samples was performed with 0.001 mol/l HCl at 20 °C with etching times of 60-240 min. Long etching times were required to obtain statistical data including the growth rate of etch pits as a function of etching time. Length and width measurements as well as counting the etch pits was done with Olympus Stream and/or TrakScan software, using microscope images taken at 50x magnification (Fig. **4.12**). Induced fission tracks could be successfully etched with this method, generating line-shaped etch pits with lengths of up to 6.7 µm after 180 minutes of etching. The etch pits are oriented randomly due to the random angle at which fission fragments leave the source, resulting in etch pits with variable trail lengths. Dot-shaped etch pits also appeared, which are likely the result of fission fragments hitting the dolomite sample almost perpendicularly.

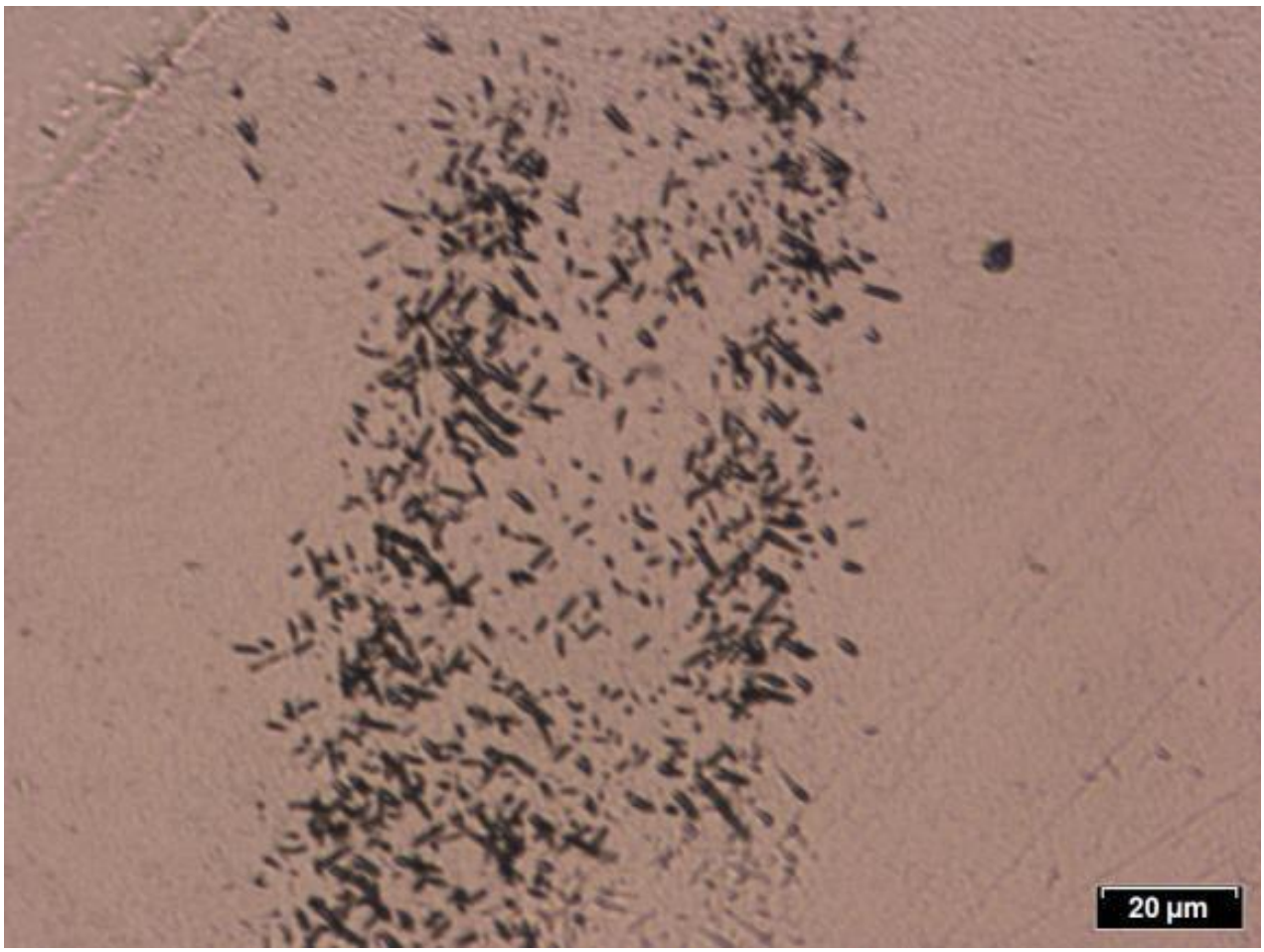

Fig. **4.12**: Neutron-irradiated dolomite sample (DolW11, covered with zircon during irradiation) etched with 0.001 mol/l HCl at 20 °C for 180 min. Clusters of line-shaped etch pits are visible in a defined area on the sample surface.

The etch pit growth rate is shown in Tab. **4.4** and Fig. **4.13**. Up until an etching time of 120 min, etch pits are growing bigger over time; after that time, it becomes increasingly difficult to measure the etch pit lengths due to overlapping. It appears that an etching time of 120-150 min is suitable for obtaining well-defined etch pits.

Tab. **4.4**: Etch pit length on neutron-irradiated dolomite sample (DolW11, covered with zircon during irradiation) as a function of etching time, using 0.001 mol/l HCl at 20 °C as etchant.

Time (min)	Min length [µm]	Max length [µm]	Mean [µm]
75	1.2	6.0	3.1 (± 1.2)
90	2.6	6.1	4.0 (± 0.9)
105	2.1	6.8	4.2 (± 1.0)
120	2.4	7.0	4.4 (± 1.0)
135	2.3	7.8	4.4 (± 1.2)
150	3.3	6.5	4.5 (± 0.9)
165	3.0	7.0	4.5 (± 1.0)
180	2.9	6.7	4.3 (± 0.8)

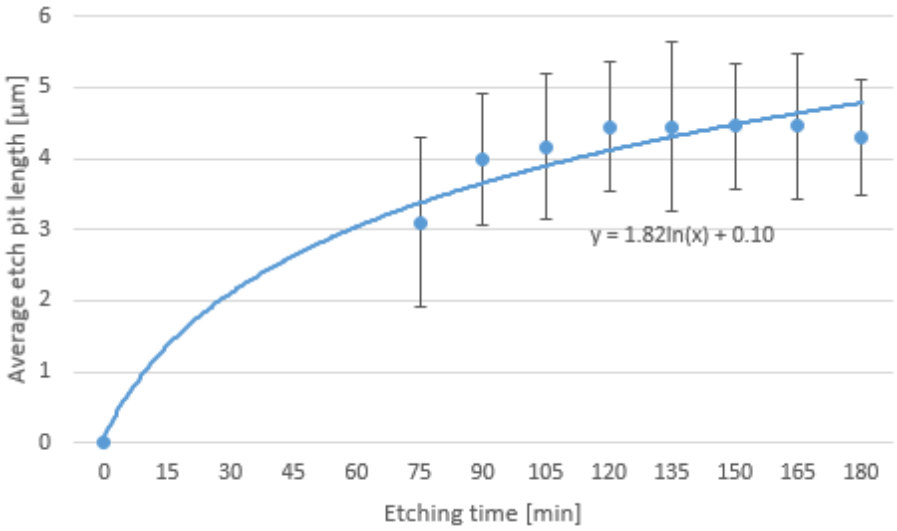

Fig. **4.13**: Etch pit length as a function of etching time for neutron-irradiated dolomite sample (DolW11, covered with zircon during irradiation) etched with 0.001 mol/l HCl at 20 °C for 180 min.

In summary, it can be said that fission tracks on dolomite can be successfully etched with 0.001 mol/l HCl using etching times of about 2 hours. Induced fission tracks generated by covering the sample with zircon during irradiation will form well-defined clusters of etch pits. It can therefore be assumed that spontaneous fission tracks on dolomite can be etched by this method as well.

5. Siderite

5.1 First experiments

Siderite etching attempts in literature used a variety of acids. A paper from Boos (1941) mentions the use of hydrochloric, nitric, and sulfuric acid of different concentrations, and Boos (1941) obtained results that show a reduction in etching speed with the ionic radius of the elements. According to Boos (1941), calcite with its large Ca^{2+} ionic radius is etched quickly, while siderite etching is rather slow due to the small ionic radius of the Fe^{2+} cation. Siderite etching with HCl is also mentioned by Baumhauer (1894) and seems to be the etchant of first choice for siderite in literature. Therefore, HCl was the first etchant used on siderite in this thesis to attempt to reproduce the results obtained by Baumhauer (1894) and Boos (1941).

Cleaved siderite samples often have non-rectangular shapes, which when put on a specimen plate and viewed under an optical microscope are impossible to put in focus due to the differences in height. In order to alleviate this problem, samples had to be prepared in a way that results in smooth, planar surfaces. A method of embedding, grinding and polishing siderite samples that results in sample surfaces of sufficient quality is described in Chapter 5.3.

First attempts to etch heavy ion irradiated siderite with HCl solutions at 20 °C didn't visualize ion tracks (Fig. **5.1**). Tested concentrations were 0.001 mol/l and 0.01 mol/l for 4 hours each. Nitric acid was likewise tested, using a concentration of 0.91% by mixing 1 part of a 65% HNO_3 solution with 99 parts of purified water; etching an irradiated siderite with this solution did not result in etch pits of ion tracks either. Increasing the etching temperature to 50 °C and etching the same sample for another hour did not change this result.

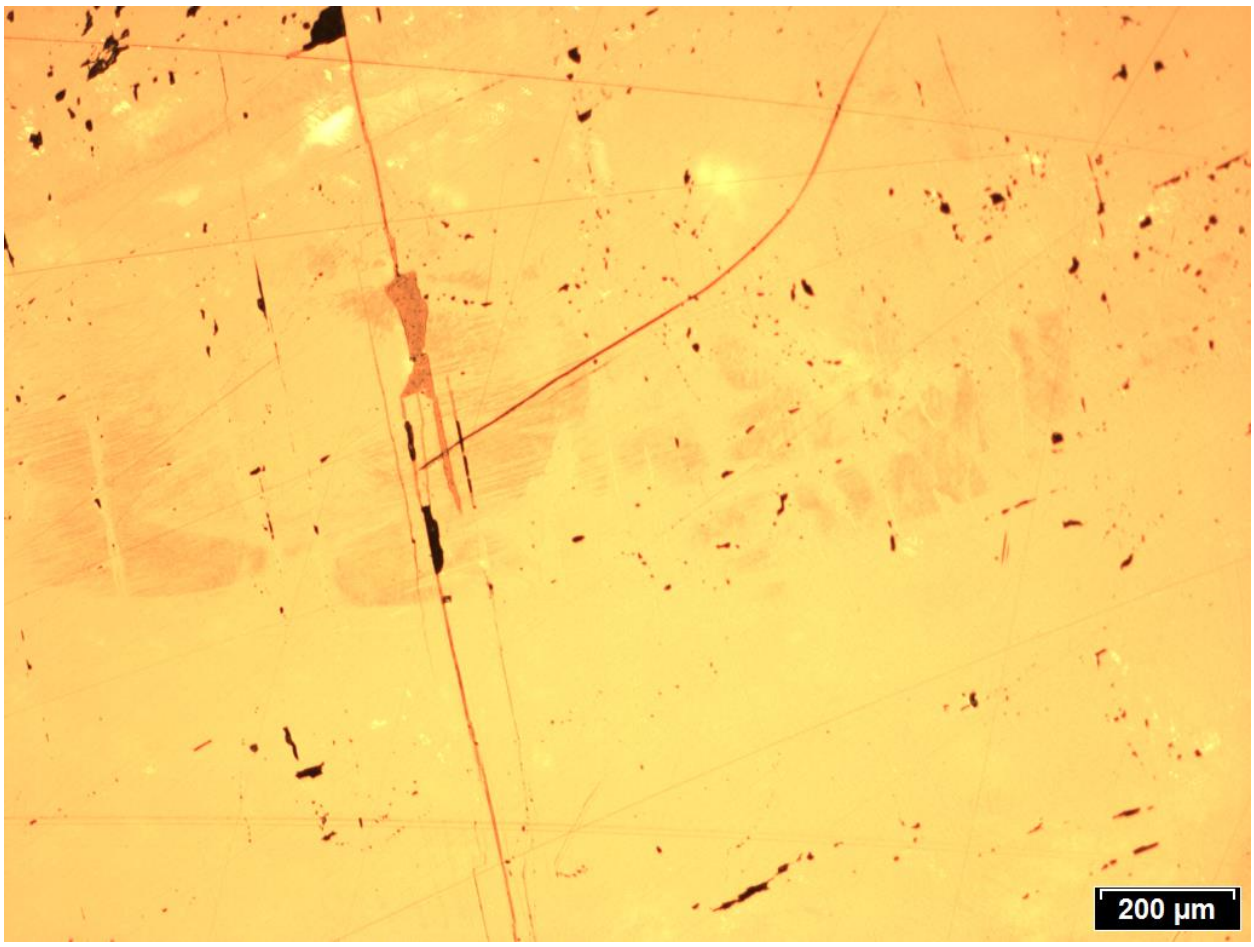

Fig. **5.1**: Siderite sample (Sid-001-03-01), irradiated with $1*10^6$ ^{197}Au, 5.9 MeV/u, etched with 0.001 mol/l HCl at 20 °C for 4 hours. No etch pits of heavy ion tracks are visible.

The lack of etch pits on siderite when using diluted acid as an etchant suggested that a higher concentration may be necessary to obtain the desired results. In the papers by Baumhauer (1894) and Boos (1941) on the etching of carbonate minerals, well-defined etch pits on siderite are presented after all. Boos (1941) used HCl concentrations ranging from 5% to 36% for his etching experiments, and mentions that out of the three minerals he etched (calcite, rhodochrosite and siderite) the siderite etching was the slowest. Therefore, for the next experiment, an irradiated siderite sample was etched with 10% HCl, using temperatures of 20 °C and 50 °C. This method resulted in lots of triangular etch pits on the sample surface. Of note is the fact that on a given surface, all of these etch pits have the same orientation. (Fig. **5.2**)

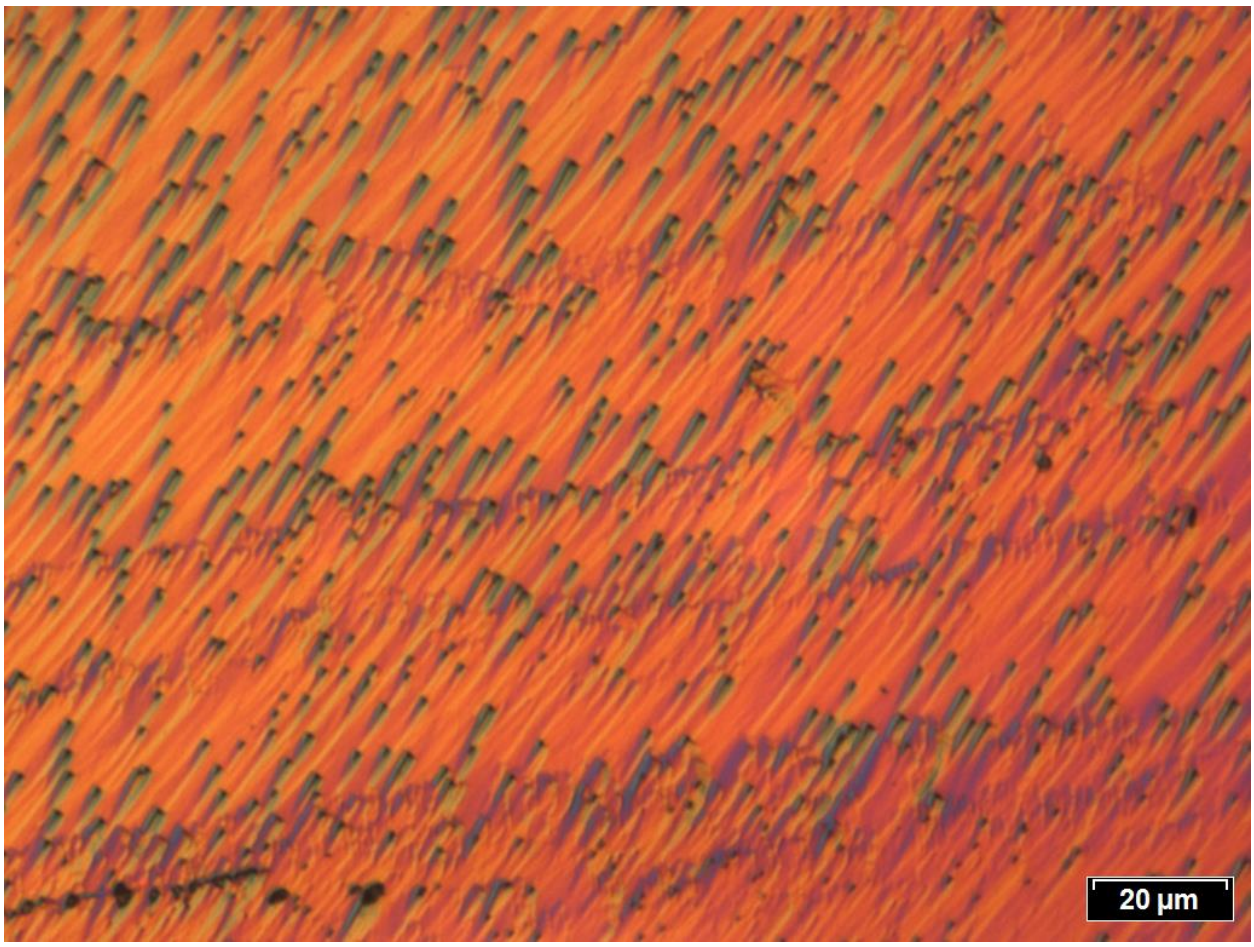

Fig. **5.2**: Siderite sample (Sid-001-03-02), irradiated with $1*10^6$ ^{197}Au, 5.9 MeV/u, etched with 10% HCl at 20 °C for 3 hours and at 50 °C for 30 minutes. Many triangular etch pits are visible which all have the same orientation, indicating etched heavy ion tracks.

In order to optimize the etching method, several attempts with various HCl concentrations and etching times were conducted (Tab. **5.1**). It was determined that a 2% HCl may already be too weak to create good quality etch pits; no visible ones were generated after 4 hours of etching at 20 °C. Visualization attempts with 10% HCl at 20 °C were moderately successful, generating etch pits of ion tracks on some areas of the siderite samples after about one hour of etching, but it also formed destroyed areas on the sample where no clearly defined etch pits are visible at all. When a 10% HCl is used at 50 °C, etched ion tracks can already be seen after 10 minutes of etching when using sufficient magnification (usually 20x; Fig. **5.3**), but prolonged etching often resulted in destroyed areas being formed as well.

Tab. **5.1**: Siderite etching experiments with HCl at various conditions.

Sample No.	Mineral	Results	Irradiation	Etching
Sid-001-03-01	Siderite	Etch pits visible only after 10% HCl etching	^{197}Au 1*10^{6}, 5.9 MeV/u	HCl 0.001 mol/l 300 min 20 °C + HNO_3 0.91 % 120 min 20 °C, 60 min 50 °C + HCl 10% 150 min 20 °C
Sid-001-03-02	Siderite	Many etch pits after etching at 50°C	^{197}Au 1*10^{6}, 5.9 MeV/u	HCl 10% 90+90 min 20 °C + 60 min 50 °C
Sid-001-04-01	Siderite	No etch pits with 2% HCl, bad quality pits with 10% HCl	^{197}Au 1*10^{6}, 5.9 MeV/u	HCl 2% 480 min 20 °C + HCl 10% 60 min 20 °C
Sid-001-04-03	Siderite	Etch pits and destroyed zones	^{197}Au 1*10^{6}, 5.9 MeV/u	HCl 10% 30 min 50 °C
Sid-001-04-02	Siderite	Good quality etch pits	^{197}Au 1*10^{6}, 5.9 MeV/u	HCl 10% 60 min 50 °C

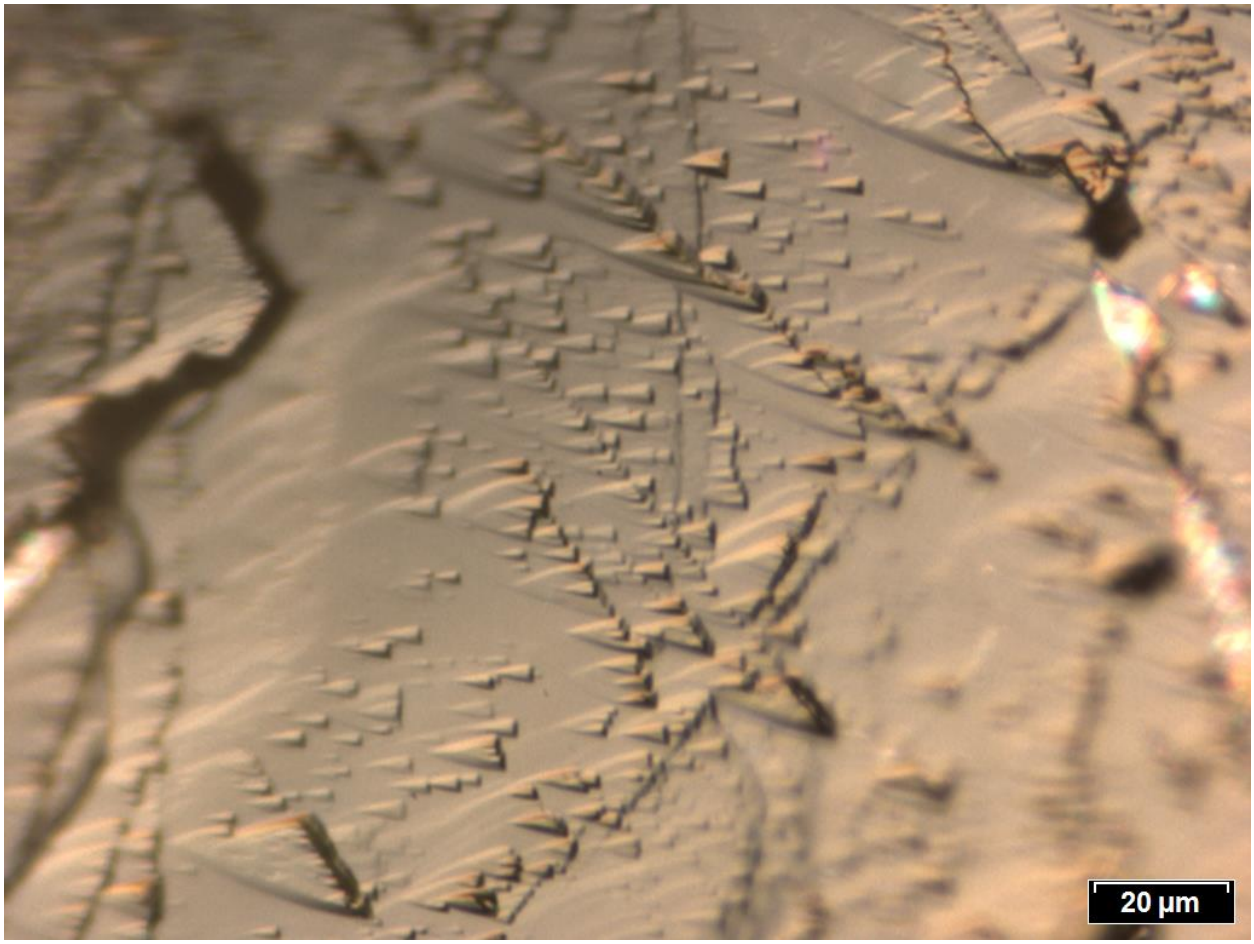

Fig. **5.3**: Siderite sample (Sid-1209-Ätztest 2), non-irradiated, etched with 10% HCl at 50 °C for 10 minutes. Flat triangular etch pits are visible, which are assumed to be etched dislocations.

5.2 Visualization of ion tracks on siderite with sulfuric acid

Sulfuric acid was used by Boos as an etchant for siderite, as explained in chapter 5.1. Another mention of siderite etching with H_2SO_4 goes back to Tschermak (Min. Petr. Mitt. 4, 1882. S. 99). Since the results obtained with hydrochloric acid were not satisfactory due to the proliferation of destroyed areas forming on the samples with prolonged etching, the applicability of H_2SO_4 as an alternate etchant for siderite was researched.

A series of test etchings was performed on non-irradiated siderite samples first, using 10% H_2SO_4 with temperatures of 20 or 50 °C and etching times of 30-60 min. After 30 minutes of etching, etch pits started to develop on the surface, showing hexagonal shapes with a diameter of about 0.5 µm. These are possibly etched dislocations, appearing in line patterns sometimes but there are also single etch pits distributed randomly. (Fig. **5.4**)

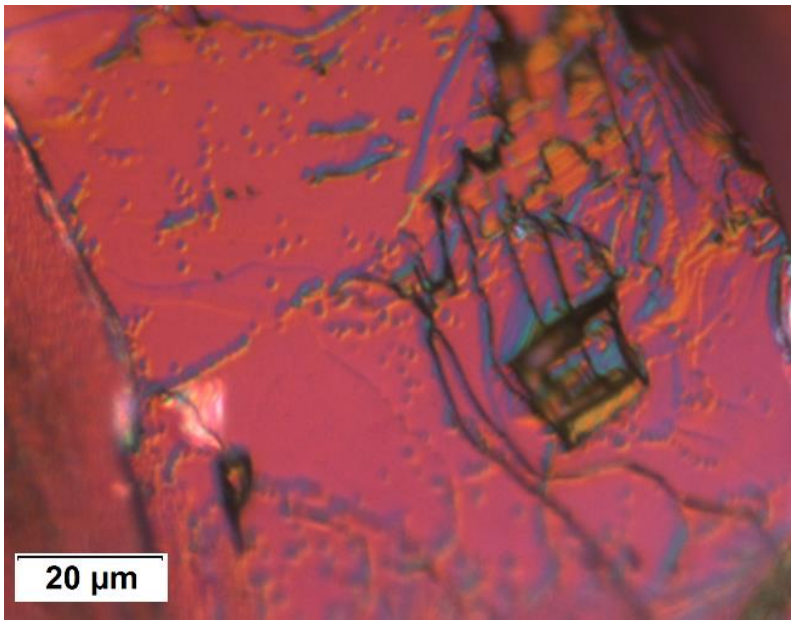

Fig. **5.4**: Siderite sample (Sid-H_2SO_4-Ätztest b, unirradiated), etched with 10% H_2SO_4, 30 min at 50 °C. A couple of roughly circular-shaped etch pits are visible which are attributed to etched dislocations.

.

Attempts to visualize ion tracks were conducted on irradiated siderite samples using 10% H_2SO_4 with temperatures of 50 or 70 °C. Etching for 30-60 min resulted in etch pits of ion tracks and dislocations, but like the earlier HCl experiments, destroyed areas were also formed on the crystal. It seems that siderite surfaces have inherent structures that will always be enlarged by the etching process, even when the grinding and polishing method has been applied perfectly. In order to verify that there are indeed etch pits of irradiation damage on the crystal, as opposed to etched dislocations, a sample that had been etched for 60 min at 70 °C was viewed with transmitted light, where the etch pits are much more differentiated against the background.

When using reflected light, natural features on the siderite surface superimpose the etch pits, making the latter hard to see. This phenomenon is illustrated in Fig. **5.5** and Fig. **5.6**, where the nonirradiated zone is clearly visible when viewed with transmitted light but hard to see with reflected light. While it's still possible to see the nonirradiated zone when using reflected light, there is a lot of background noise. This suggests that transmitted light is better for viewing siderite etch pits.

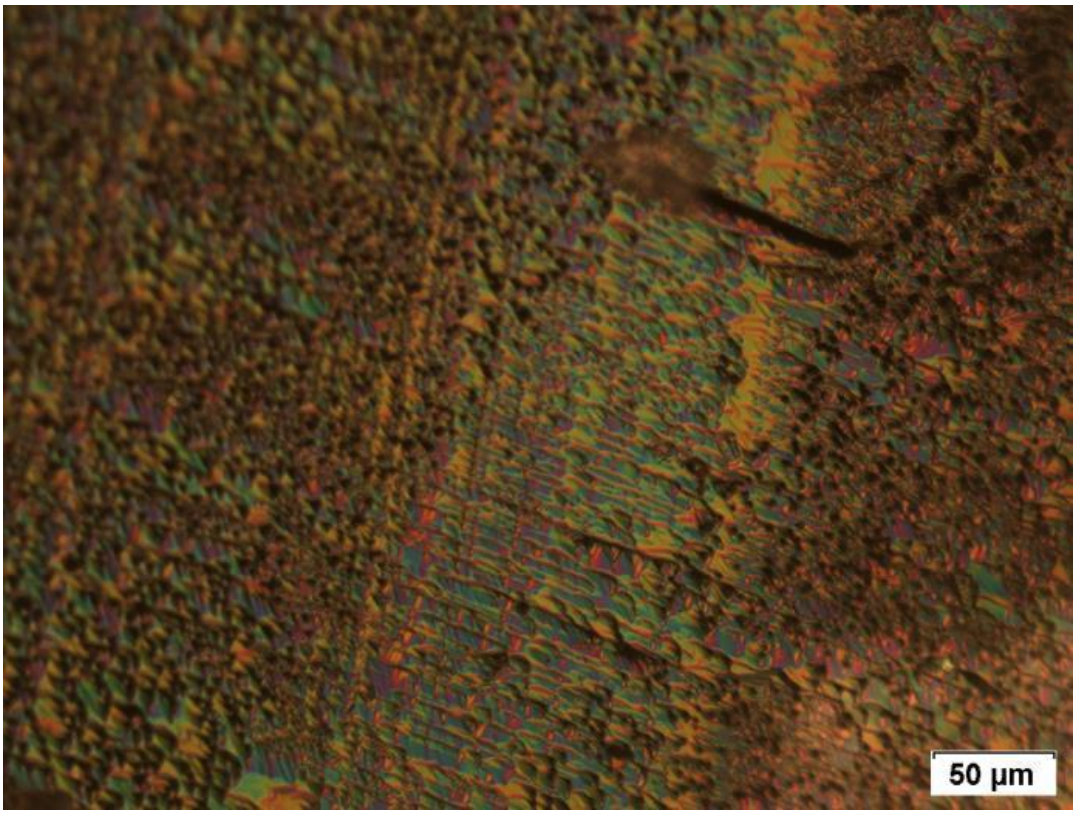

Fig. **5.5**: Heavy ion (5.9 MeV/u Au^{197}) irradiated siderite sample (Sid-001-01-07) etched with 10% H_2SO_4 at 70 °C, 60 min, viewed with Nomarski DIC and reflected light. Etch pits appear in areas to the left and right of the centre, but are hard to see against the background.

Fig. **5.6**: Heavy ion (5.9 MeV/u Au^{197}) irradiated siderite sample (Sid-001-01-07) etched with 10% H_2SO_4 at 70 °C, 60 min, viewed with transmitted light. Etch pits appear in areas to the left and right of the centre in well-defined areas.

5.3 Grinding and polishing of siderite samples

In order to improve the quality of siderite sample surfaces and their ability to display etch pits, a preparation method for dolomite and siderite crystals had to be developed that will produce samples with very smooth surfaces. The method involves three steps: embedding, grinding and polishing. A similar method was described for calcite by Dedera (2015); the sample preparation method for siderite is based on Dedera's sample preparation, but with some adjustments to accommodate for the different properties of siderite.

The GSI in Darmstadt and the FRM II reactor in Munich have facilities which require that the sample to be irradiated has a circular shape with a diameter of about 21 mm. In order to get mineral samples that fulfil this requirement, cleaved siderite crystals are put into a casting mold of appropriate size to begin the embedding process. The mold is glued onto leakproof paper and filled with Struers EpoFix resin.

Care must be taken to prevent the resin from spilling, due to its tendency to stick to desks or other contaminated surfaces which would make it difficult to clean them. The mounted sample should have a thickness of at least 7 mm for the next step to work; occasionally some of the

resin may spill out of the casting mold and onto the paper, in which case it's necessary to add more resin every once in a while, until it has hardened. After about 1 h the resin will usually be hardened enough that no spill can occur anymore, and the samples are left to dry for one day. Now the samples can be pressed out of the casting mold. Depending on the thickness of the sample, this can either be done by hand, or it might require the use of pressing tools at the precision mechanic workshop.

The next step of sample preparation is grinding. For the grinding and polishing steps, all data presented here has been obtained with the Struers equipment available in the Institute of Earth Sciences, Research Group Thermochronology and Archaeometry; they can serve as guidelines but the actual grinding and polishing times required for best results may vary depending on the equipment used.

For the first step of grinding, Struers coarse silicium carbide (SiC) paper with a grit size of 1200 is used. Samples are ground for 4-10 minutes with distilled water used as a lubricant. The mineral must not be covered with epoxy any longer after this step is done; if necessary, continue grinding until this is the case. It also helps to grind the sample's edges a bit, which will make them round and thereby cause them to wear out the grinding papers and polishing cloths less quickly. After this step, the samples are ground with grit 2400 SiC paper for 25-30 minutes, again using distilled water as lubricant. Grinding is now complete and the samples are ready for polishing.

Polishing is done in three steps, starting with 3 µm diamond paste (Struers DP paste). A Struers MD-DAC polishing cloth is used with DP Lubricant Blue as a lubricant. After 30-40 minutes, the sample surface usually appears sufficiently smooth under an optical microscope and is ready for the next polishing step. Now, 1 µm DP paste is used with a new MD-DAC cloth. The lubricant is DP Lubricant Blue again. This step also takes 30-40 minutes. The sample is cleaned and checked under an optical microscope, and if the polishing result is satisfactory, the final polishing step can be performed.

The last polishing step uses OP-S suspension and an OP-Chem polishing cloth. The OP-S suspension consists of colloidal silica gel and is used for final polishing of ductile materials. Also, the polishing cloth must be very wet for the polishing procedure to succeed, which can be achieved by operating the cloth with the water running for about 10 minutes.

To start the final polishing, some OP-S suspension is put on the cloth and the water flow set to about one drop per second; it is important that the water flow is fast enough to prevent the OP-S suspension from drying out, but slow enough that it doesn't wash the OP-S off the cloth too

quickly. Nonetheless, more OP-S needs to be added every 5-8 minutes. Once every 20 minutes the sample is checked under an optical microscope to see whether further polishing is necessary; it should be absolutely free of visible scratches or coarseness when viewed by an Olympus BX 50 optical microscope with an Nomarski DIC in reflected light mode. In the case of siderite, it is to be noted that the mineral samples often have natural defects that cannot be removed by grinding and polishing, though.

In order to be able to use the polished samples for irradiation experiments, their thickness has to be reduced to 0.5-0.7 mm. This allows them to be put in the standardized sample holders used at the GSI in Darmstadt, as well as making it possible to fit a sizable stack of samples in an irradiation batch for the FRM reactor in Munich. To achieve the desired thickness, we used special sample holders forged in the precision mechanic workshop at the Institute of Earth Sciences (Heidelberg University). The special sample holder is constructed in such a way that a sample with a diameter of about 21 mm will fit inside, protecting the polished surface while grinding is performed. Using grit 180 SiC paper and distilled water as a lubricant, the sample thickness can be reduced to the desired dimensions thanks to the special sample holder having an indentation for the sample that is about 0.7 mm thick, so that the grinding process automatically comes to a halt once the sample thickness has been reduced to that value. These finished samples can now be used for irradiation experiments. Fig. **5.7** illustrates the process of etching and polishing with microscope images of a siderite sample taken after each step of the process.

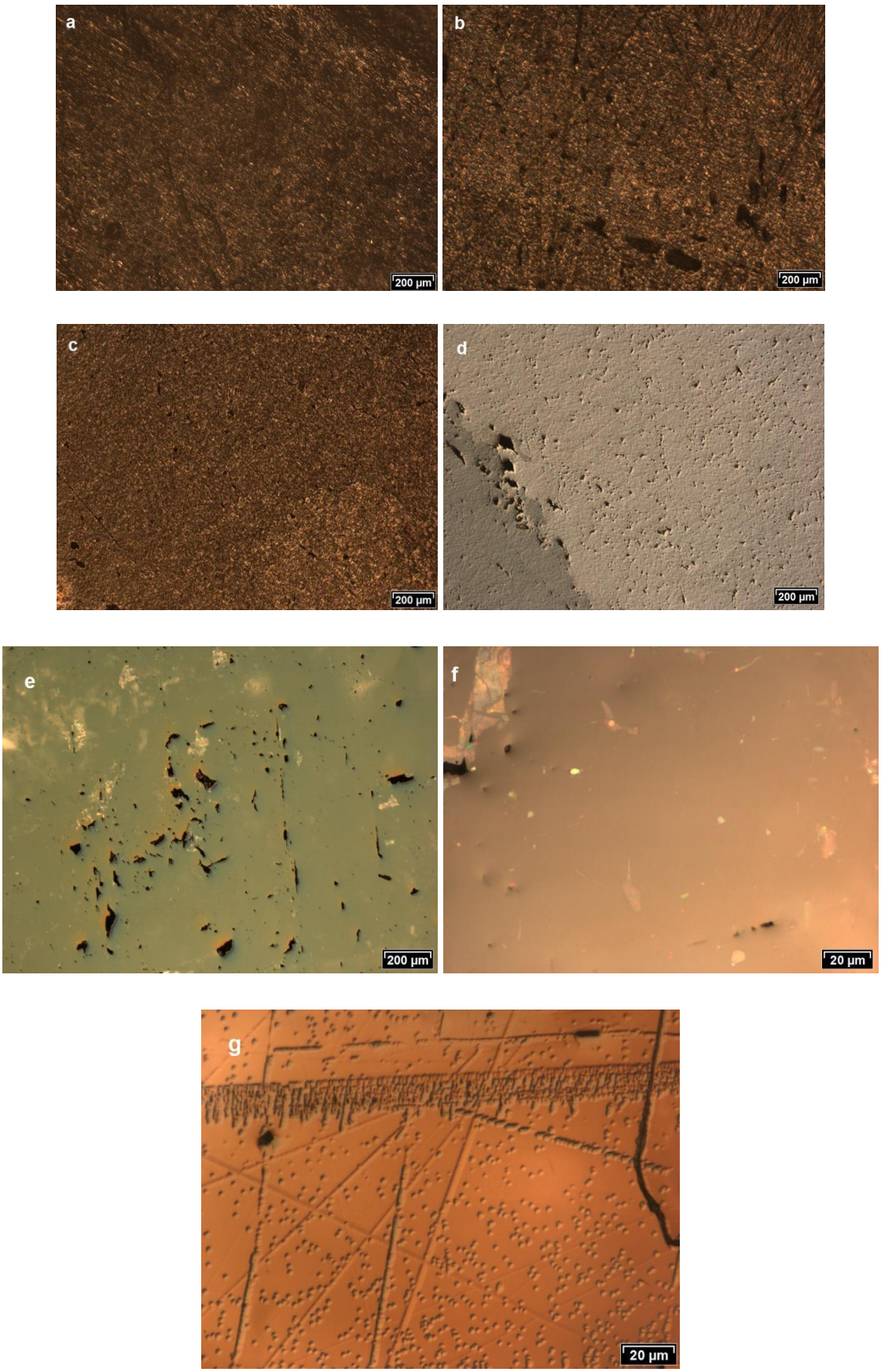

Fig. **5.7**: Grinding and polishing process for a siderite sample (SPT3). The images show the sample surface a) prior to grinding, b) after coarse grinding, c) after fine grinding, d) after polishing with 3 µm DP paste, e) after polishing with 1 µm DP paste, f) after polishing with OP-S suspension, g) after irradiation (5.9 MeV/u Au^{197}) and etching with H_2SO_4 for 30 minutes at 50 °C, with well-visible, roughly hexagonal etch pits indicating etched heavy ion tracks.

By applying the grinding and polishing method, the quality of siderite sample surfaces can be greatly increased. After the process of polishing is finished, large parts of the surface appear smooth under the microscope (Fig. **5.8**), but usually some cracks will remain that cannot be removed. The majority of the surface is capable of displaying etched ion tracks after polishing. It is therefore important that siderite samples which are to be used for ion track etching experiments are put through the grinding and polishing process, as it seems to be the key to getting useful results. Even with this method, though, etched siderite samples will almost always also display etched cracks and other features on their surface, which can impede the ability to clearly identify etch pits of ion tracks.

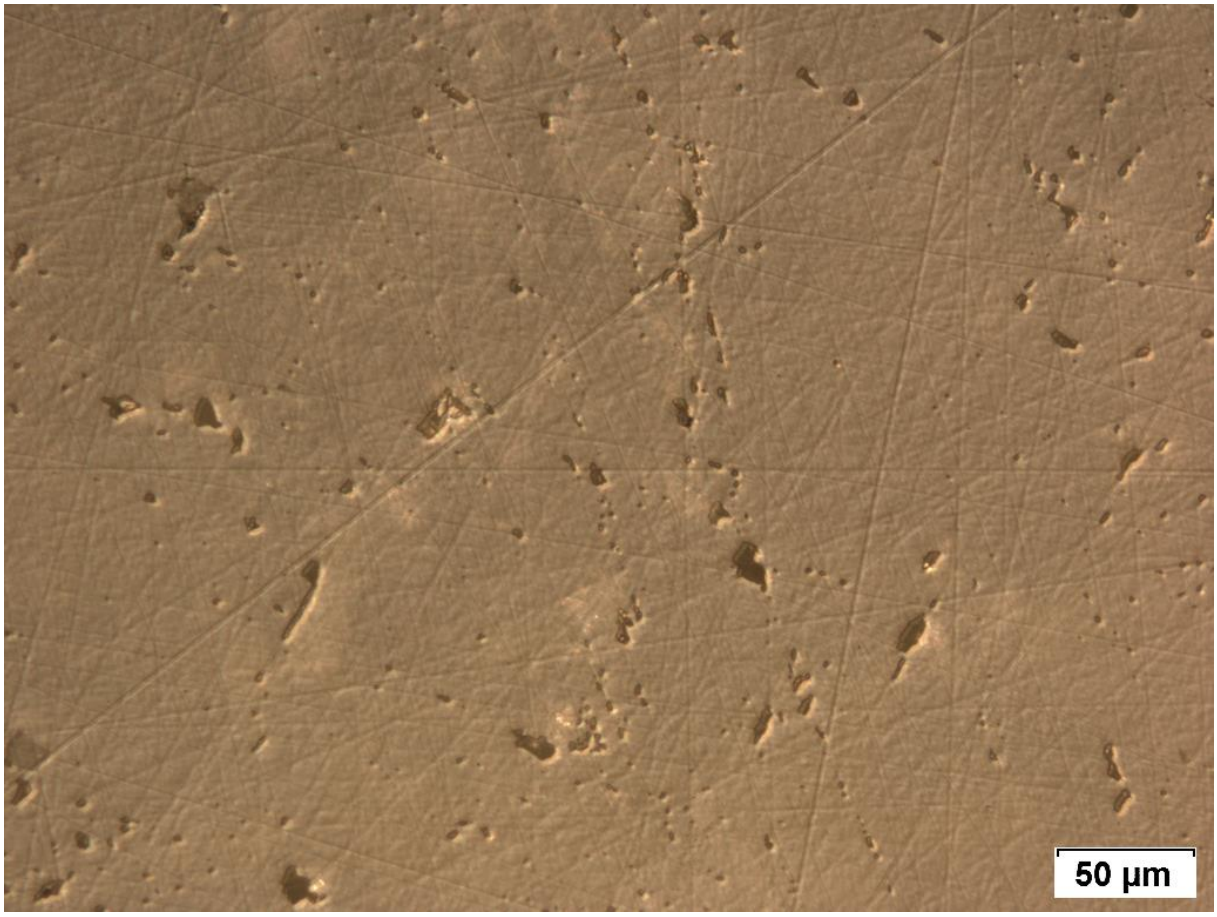

Fig. **5.8**: Siderite sample surface (SPT3) after grinding and polishing. The surface appears very smooth, but some cracks remain that couldn't be removed.

5.4 Etching experiments with polished samples

The main reason for performing the grinding and polishing was to create flat polished mineral internal surfaces capable of displaying irradiation damage after etching. Finished siderite samples were tested for their quality by etching with sulfuric acid (10%, 50 °C, 60-120 min, as described in chapter 5.2).

On polished siderite grains, the etching method produces shallow pits of roughly triangular or

circular shapes, which are about 2-4 µm in diameter. Some of them are arranged randomly while others are forming line patterns; the formation of these pits is attributed to dislocations present on the siderite samples, which are not removed by the preparation method. In order to test the quality of the polishing procedure, prepared siderite samples were irradiated at the GSI (5.9 MeV/u Au^{197} ions, $1*10^6$ ions/cm^2) and etched with sulfuric acid (10%, 60 min, 50 °C). Fig. **5.9** shows an etched surface with clearly visible irradiated and non-irradiated areas next to each other. The etched heavy ion tracks are easily distinguishable against the background, thereby proving that the polishing method works and produces sample surfaces of sufficient quality.

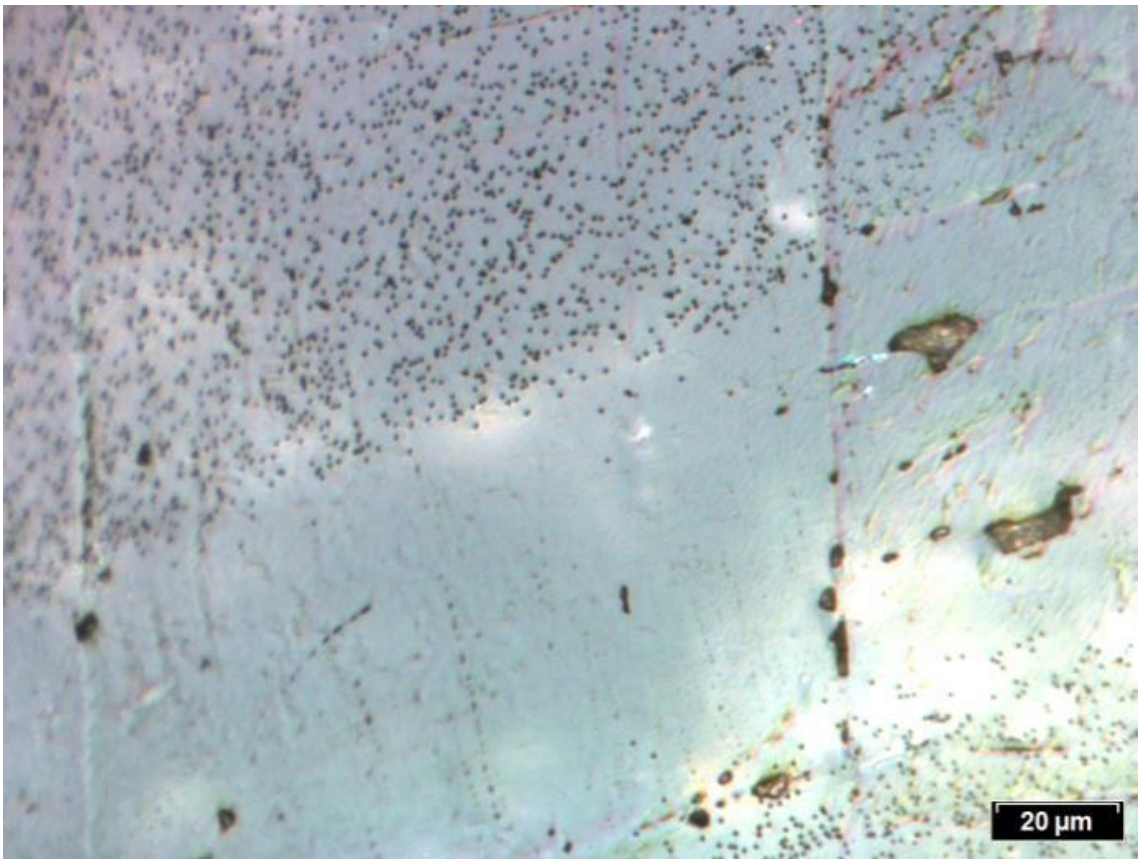

Fig. **5.9**: Siderite sample (Sid-001-06b) etched with 10% H_2SO_4, 60 min at 50 °C, after grinding/polishing and 5.9 MeV/u Au^{197} ion irradiation. Circular-shaped etch pits of heavy ion tracks appear in well-defined areas. The area without etch pits was covered by a mask during irradiation.

5.5 Comparison of the etching results revealed by HCl and H_2SO_4 solution

Heavy ion tracks on siderite can be visualized by etching with HCl or H_2SO_4. The results obtained show that the shape and size of etch pits differs between the two, with HCl etch pits usually showing a sharp triangular shape while H_2SO_4 generates approximately hexagonal pits. Both acids also result in etched dislocations, and over-etched areas can occur after prolonged etching. The results obtained make it seem like HCl produces this over-etching effect more

quickly, which suggests that H_2SO_4 may be more suitable for visualizing ion tracks on siderite.

Statistical data on an irradiated sample etched with 10% H_2SO_4 for 120 min at 50 °C was evaluated (Fig. **5.10**) and compared with the fluence calculated from counting the etch pits on the etched reference foil (Fig. **5.11**). The result (Tab. **5.2**) shows that within error, the fluence determined by the amount of etched ion tracks on a siderite sample surface is $2.18*10^6$ ($\pm$ $0.17*10^6$) ions/cm^2, which is in agreement with the applied fluence from the amount of pores on the etched foil, which was calculated as $2.13*10^6$ ($\pm$ $0.11*10^6$) ions/cm^2. Only few (about 1-2% of the total amount) etch pits appear in the nonirradiated zone, which may be the result of straggling in the ion beam. The results show that the H_2SO_4 etching method is capable of visualizing heavy ion tracks on siderite.

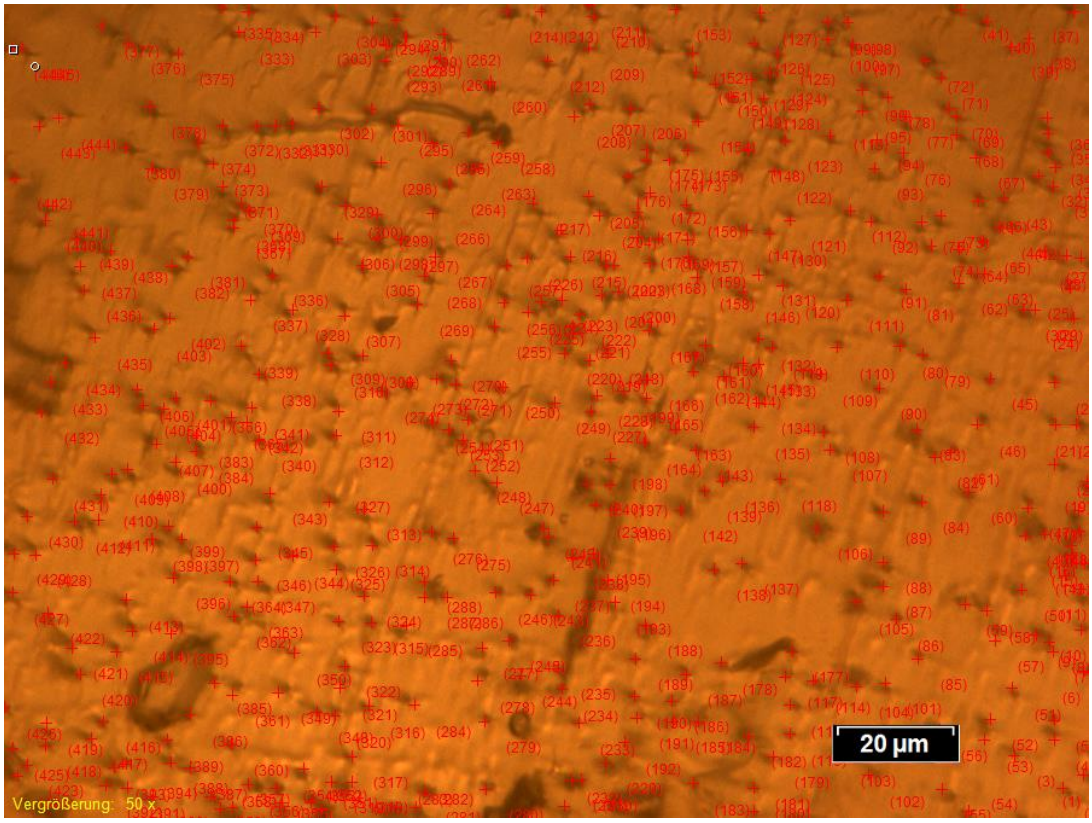

Fig. **5.10**: Etch pits on heavy ion (5.9 MeV/u Au^{197}) irradiated siderite sample (Sid-001-01-03) after etching with 10% H_2SO_4 at 50 °C for 120 minutes. Etch pits were counted with Stream Enterprise software. On this particular image, a total of 444 etch pits was counted.

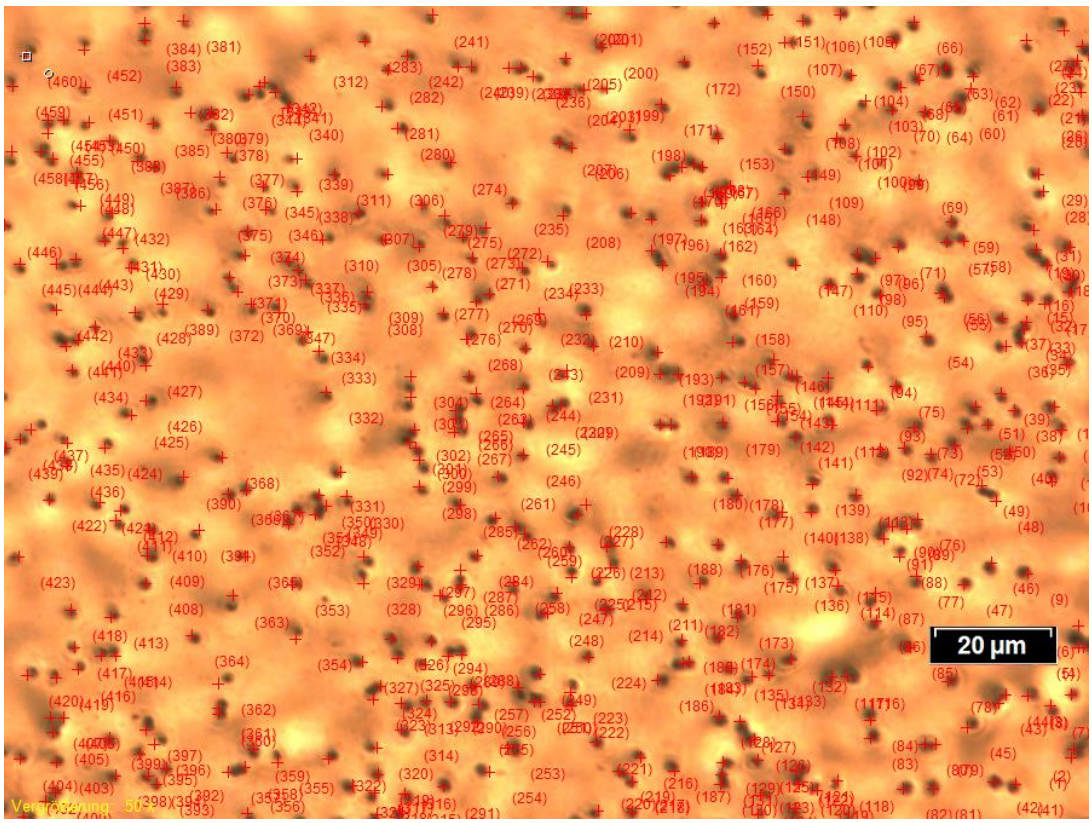

Fig. **5.11**: Etch pits on heavy ion (5.9 MeV/u Au^{197}) irradiated polycarbonate foil that was used to cover a siderite sample (Sid-001-01-03) during irradiation, after etching with 6 mol/l NaOH at 50 °C for 90 minutes. Etch pits were counted with Stream Enterprise software. On this particular image, a total of 460 etched pores was counted.

Tab. **5.2**: Areal density of etch pits for heavy ion irradiated siderite (Sid-001-01-03) etched with H_2SO_4 at 50 °C, compared with the areal density of the polycarbonate foil etched with 6 mol/l NaOH at 50 °C.

Index no.	Areal density (siderite, 22950 µm²)			Index no.	Areal density (foil, 22950 µm²)		
1	481			1	482		
2	444			2	500		
3	514			3	526		
4	434			4	505		
5	521			5	475		
6	521			6	485		
7	539			7	450		
8	479			8	448		
				9	479		
				10	506		
				11	510		
				12	462		
				13	471		
				14	460		
				15	505		
				16	450		
				17	506		
				18	453		
				19	496		
				20	456		
	Area	Calc. Fluence (10^6 ions/cm²)			Area	Calc. Fluence (10^6 ions/cm²)	
Mean	492	2175328		Mean	481	2129421	
Std. deviation	38	169993		Std. deviation	24	107582	

The etch pit growth rate was also investigated for H_2SO_4 etching at 50 °C, measuring the length and width of etch pits as a function of time. Results are shown in Tab. **5.3**, showing the length and width of etch pits at several points of etching. For each point in time, about 30 etch pits were measured for their length (x) and width (y). It can be seen that the etch pits grow bigger over time; the values obtained for 60 minutes of etching seem too high and may be the result of a measuring error.

Tab. **5.3**: Etch pit growth rate for heavy ion irradiated siderite etched with H_2SO_4 at 50 °C, with the mean value and standard deviation (dev) calculated for various etching times.

Etching time	x(mean) [µm]	dev(x) [µm]	y(mean) [µm]	dev(y) [µm]
20 min	0.357	0.043	0.289	0.049
30 min	0.380	0.050	0.331	0.040
40 min	0.406	0.046	0.357	0.041
50 min	0.444	0.049	0.364	0.042
60 min	0.566	0.058	0.508	0.056

Attempts to obtain similar statistical data for the HCl etching method proved difficult due to the samples being over-etched too quickly, making it hard to clearly identify etched ion tracks due to overlapping with etch figures produced by the etchant attacking other structures present on the sample surfaces. On one etched sample (Fig. **5.12**) the quality of etch pits was found to be reasonably good enough to count them and compare the calculated areal density with the fluence calculated from counting the etch pits on the etched reference foil (Fig. **5.13**).

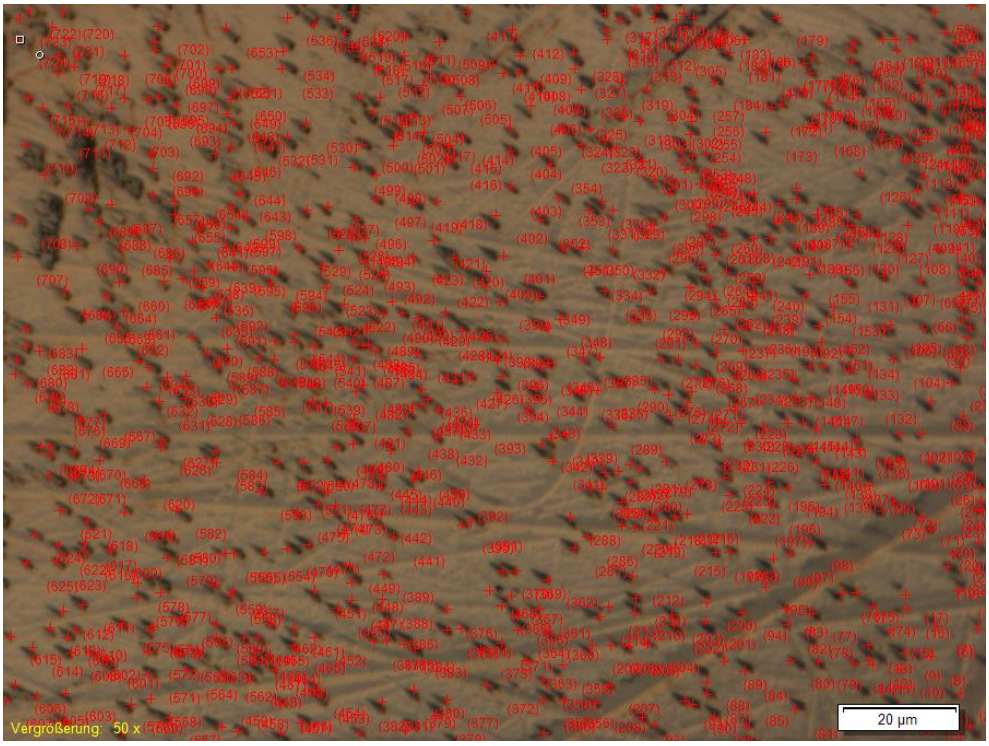

Fig. **5.12**: Areal density of etch pits on heavy ion (5.9 MeV/u Au^{197}) irradiated siderite sample (Sid-001-03-02) etched with 10% HCl at 20 °C. Etch pits were counted with Stream Enterprise software. A total of 724 etch pits was counted on this particular surface area.

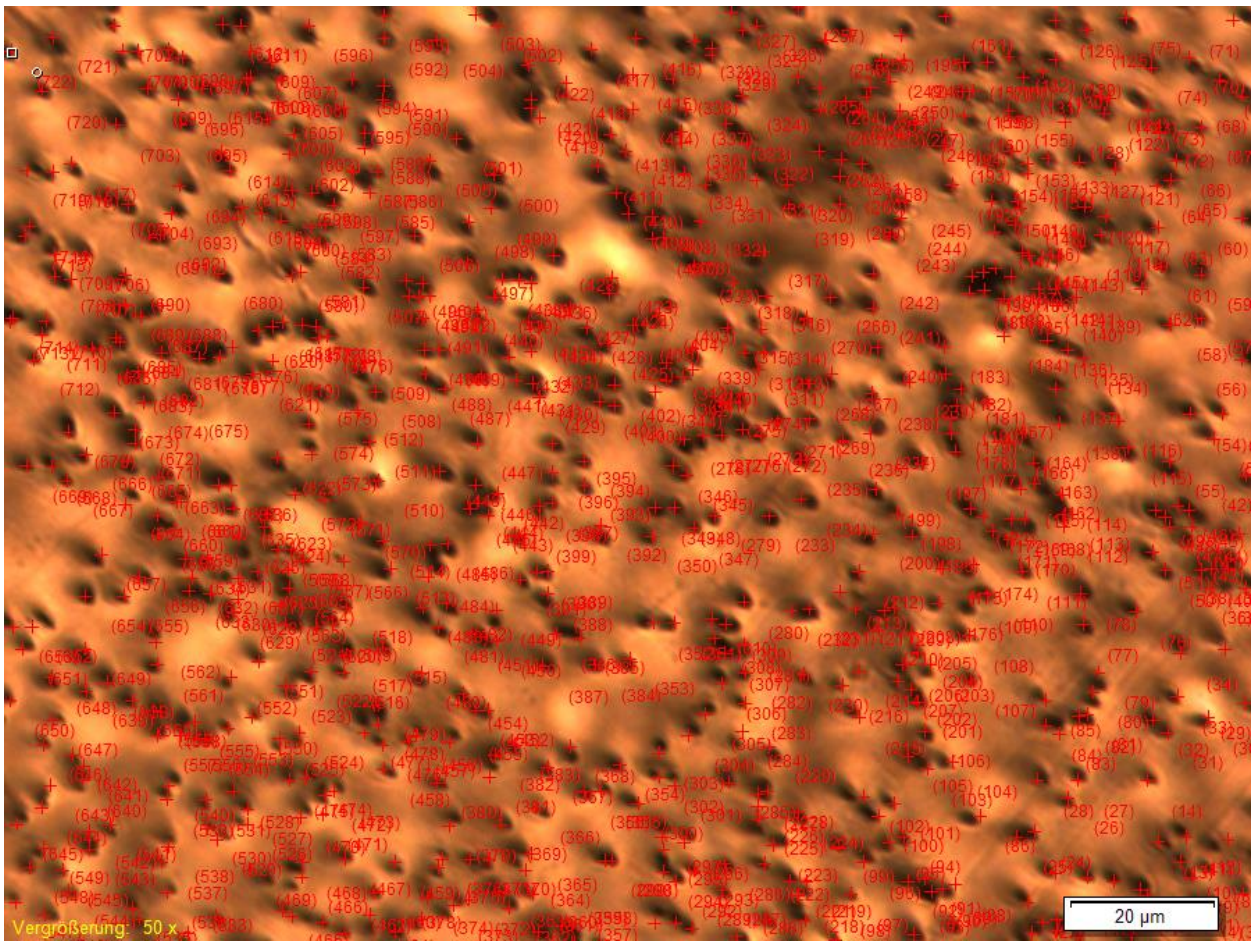

Fig. **5.13**: Etch pits on heavy ion (5.9 MeV/u Au^{197}) irradiated polycarbonate foil that was used to cover a siderite sample (Sid-001-03-02) during irradiation, after etching with 6 mol/l NaOH at 50 °C for 90 minutes. Etch pits were counted with Stream Enterprise software. On this particular image, a total of 722 etched pores was counted.

The areal density of etch pits on the siderite sample was in agreement with the amount of etched pores on the polycarbonate foil, indicating that the etching method worked and heavy ion tracks can be successfully visualized with the HCl etching method. The fluence determined by the amount of etched ion tracks on a siderite sample surface is $3.22*10^6$ ($\pm$ $0.37*10^6$) ions/cm^2, which is in agreement with the applied fluence from the amount of pores on the etched foil, which was calculated as $3.10*10^6$ ($\pm$ $0.13*10^6$) ions/cm^2; these results are visualized in Tab. **5.4**.

Tab. **5.4**: Areal density of etch pits for heavy ion irradiated siderite (Sid-001-03-02) etched with HCl at 50 °C, compared with the areal density of the polycarbonate foil etched with 6 mol/l NaOH at 50 °C.

Index no.	Areal density (siderite, 22950 µm²)		Index no.	Areal density (foil, 22950 µm²)	
1	632		1	661	
2	669		2	736	
3	748		3	665	
4	697		4	729	
5	895		5	690	
6	724		6	672	
7	726		7	676	
			8	692	
			9	750	
			10	685	
			11	675	
			12	732	
			13	659	
			14	691	
			15	697	
			16	696	
			17	742	
			18	722	
			19	753	
			20	710	
	Area	Calc. Fluence (10^6 ions/cm²)		Area	Calc. Fluence (10^6 ions/cm²)
Mean	727	3218072	Mean	702	3104640
Std. deviation	84	370042	Std. deviation	30	134939

In summary, it was decided that the H_2SO_4 etching method is more suitable for experiments with siderite than the HCl method because it visualizes ion tracks more reliably with less risk of over-etching, making it easier to obtain results that are usable for statistical evaluation. For experiments dealing with the visualization of induced fission tracks on siderite, which are described in chapter 5.7, only the H_2SO_4 etching method was used.

5.6 Annealing experiments of siderite

Annealing experiments on siderite were attempted, but the mineral's thermal instability proved problematic. When heated, siderite will eventually decompose to hematite (Fe_2O_3, Luo et. al. 2016), sometimes forming intermediate products like wüstite (FeO) or magnetite (Fe_3O_4). An earlier work by Gotor et. al. (2000) states that siderite decomposition starts at different temperatures depending on the exact composition of a sample. According to Gotor, siderite may require temperatures of 500-700 °C to decompose, while Luo mentions wüstite- and magnetite-forming reaction mechanisms that happen slightly below 400 °C.

In order to test the thermal stability of siderite samples and therefore the applicability of heating to determine the closure temperature of heavy ion tracks on siderite, non-irradiated samples were heated in the Heraeus muffle furnace under various conditions. A cleaved sample heated to 400 °C for 5 hours was almost completely decomposed; after taking the pot containing the sample out of the furnace, only a small amount of black powdery residue was left. This indicates

that at least one step of the decomposition reaction must have happened. According to Luo, this happens when the boiling temperature is reached, which means that the carbonate dissociation pressure exceeds the system's total pressure leading to a rapid decomposition of the mineral.

A second cleaved siderite sample was heated to 300 °C for 270 min. After removing it from the furnace, a thin black layer had formed on the upper surface, but the remaining sample appeared to be intact. This result might be due to the heat flow inside the furnace, which causes some areas of a sample inside the pot to be exposed to a higher amount of heat compared to the others. Apparently, the top of the sample had received temperatures high enough to start the decomposition process while all the other sample faces had not.

The black residue on the sample that was heated to 300 °C was removed mechanically, and the sample was then etched for 60 min with H_2SO_4 (10%) at 50 °C. Shallow and deep etch pits were visible under the microscope after etching, forming mostly line patterns. Since the sample has not been exposed to the grinding and polishing procedure, the surface appeared rough when viewed with an optical microscope, and the observed etch pits are probably the result of dislocations. Whether the annealing process has removed natural radiation damage on the mineral or not cannot be determined due to the large amount of dislocation etch pits. The dislocations themselves do not anneal at 300 °C according to this result, and it seems plausible that their annealing temperature is above the decomposition temperature of siderite. (Fig. **5.14**)

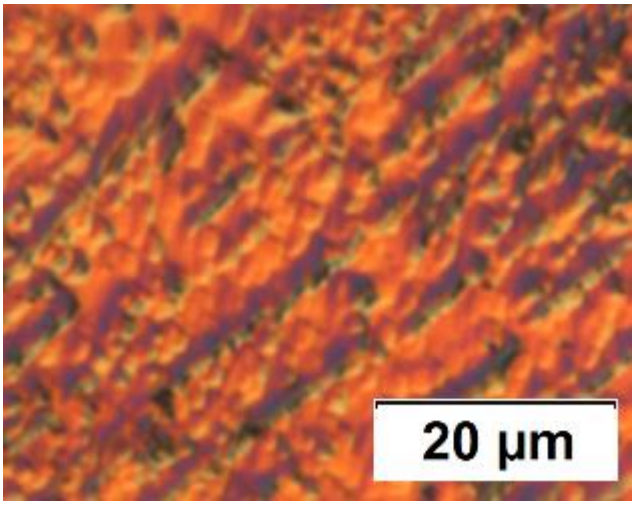

Fig. **5.14**: Unirradiated siderite sample (Sid-Verheilungstest), annealed for 270 min at 300 °C, etched with H_2SO_4 (10%) for 60 min at 50 °C. The rough surface is covered with plenty of roughly triangular etch pits, which are probably the result of dislocations. Due to the surface's considerable coarseness, the etch pits are hard to see against the background.

5.7 Visualization of induced fission tracks on siderite

Siderite samples for this set of experiments were embedded in epoxy resin and prepared with the grinding and polishing method described in chapter 5.3. Induced fission tracks on siderite samples were created by irradiation with thermal neutrons at the FRM II reactor in Munich. The samples were covered with uranium-doped CN-5 glass or zircon grains during irradiation, with one sample being covered with muscovite to serve as a reference, as muscovite contains almost no uranium and therefore results in a sample free of induced fission tracks. A fluence of $1*10^{16}$ neutrons/cm^2 was applied during irradiation.

Etching was performed with 10% H_2SO_4 at 50 °C for 90 min. Of the five samples used, one showed etched tracks that can clearly be attributed to induced fission damage (1703-Sid-a, covered with CN-5 glass during irradiation). The tracks appear as line shapes of various orientation when viewed under transmitted light, with lengths of up to 9 µm (Fig. **5.15**). When using reflected light, the trail is usually not visible, with the result that etched tracks look like little dots which are hard to distinguish against the background. Therefore, for analytical purposes, e.g. counting the areal density of etch pits, transmitted light has to be used to verify that the observed etch pits aren't the result of dirt or dislocations. Tab. **5.5** shows the length distribution of etch pits on the sample surface after 90 minutes of etching, with etch pit lengths ranging from 1.2 to 4.6 µm; for a more comprehensive statistics, future experiments with longer etching times are needed to produce larger etch pits for easier visualization and measurements.

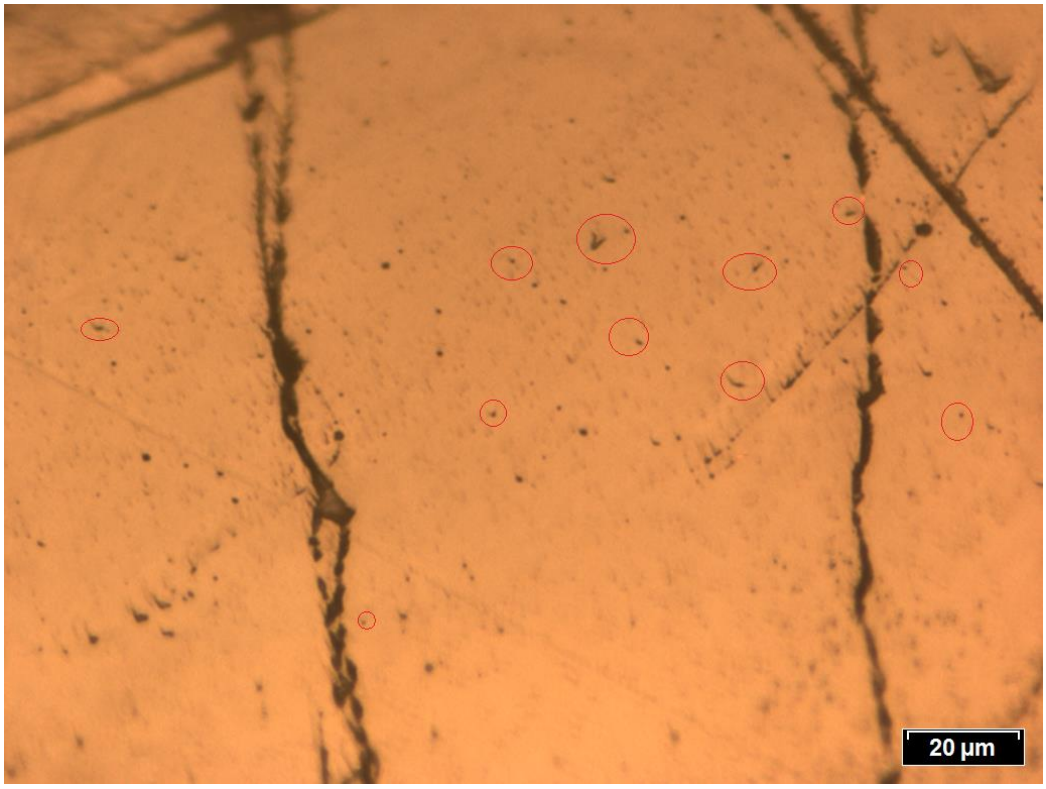

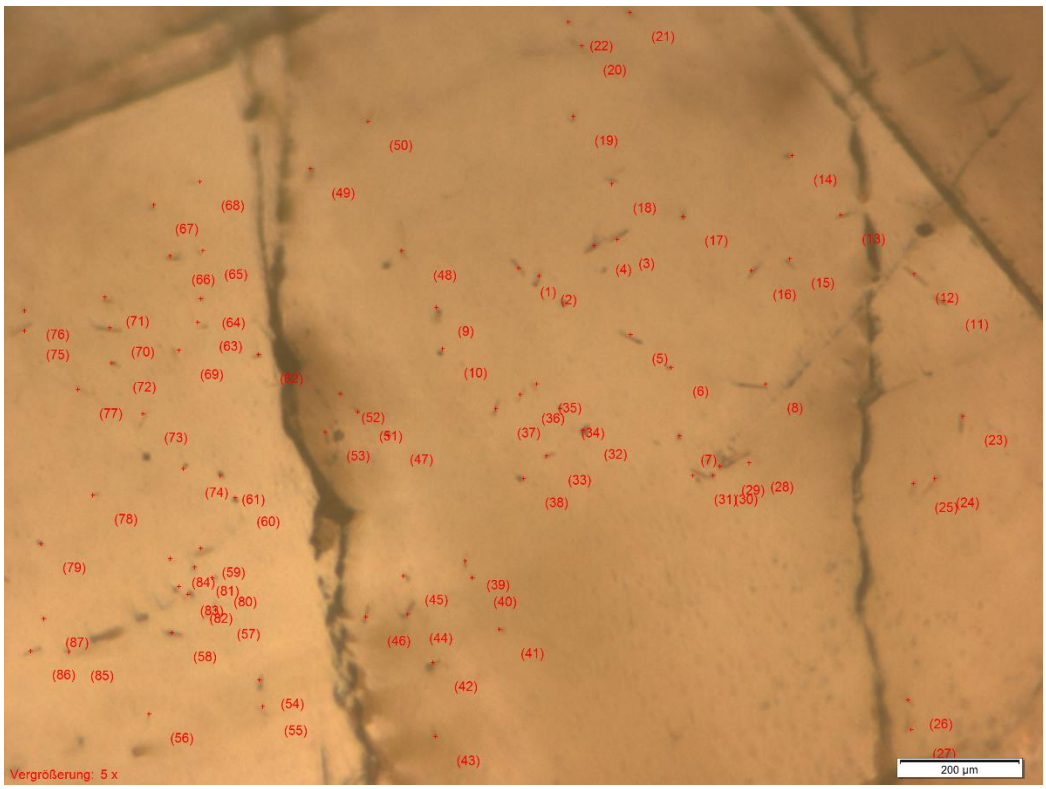

Fig. **5.15**: Neutron-irradiated siderite sample (1703-Sid-a, covered with CN-5 glass during irradiation) etched with 10% H_2SO_4, 50 °C, 90 min. Top: etched sample surface viewed with reflected light. Bottom: same etched sample surface viewed with transmitted light and etch pits counted with Stream Enterprise software. The line-shaped trails of etched induced fission tracks are visible only with transmitted light.

Tab. **5.5**: Etch pit length on neutron-irradiated siderite sample (1703-Sid-a, covered with CN-5 glass during irradiation) etched with 10% H_2SO_4, 50 °C, 90 min.

Time (min)	Min length [µm]	Max length [µm]	Mean [µm]
90	1.2	4.6	2.6 (± 0.8)

On the remaining samples, sometimes etch pits appeared as well but it's not clear whether they are etched fission tracks or etched dislocations; it was found that the quality of the sample surfaces was rather low, with areas that appeared smooth before the etching procedure becoming very coarse after etching, often forming destroyed zones where etch pits can barely be seen. Sample 1703-Sid-d produced good results, as seen in Fig. **5.16** which shows a surface etched with 10% H_2SO_4 at 50 °C for 150 min, displaying a lot of large etch pits. They all appear to have the same orientation though, a result that is not in accordance with the theory that fission fragments can hit the sample from a random angle.

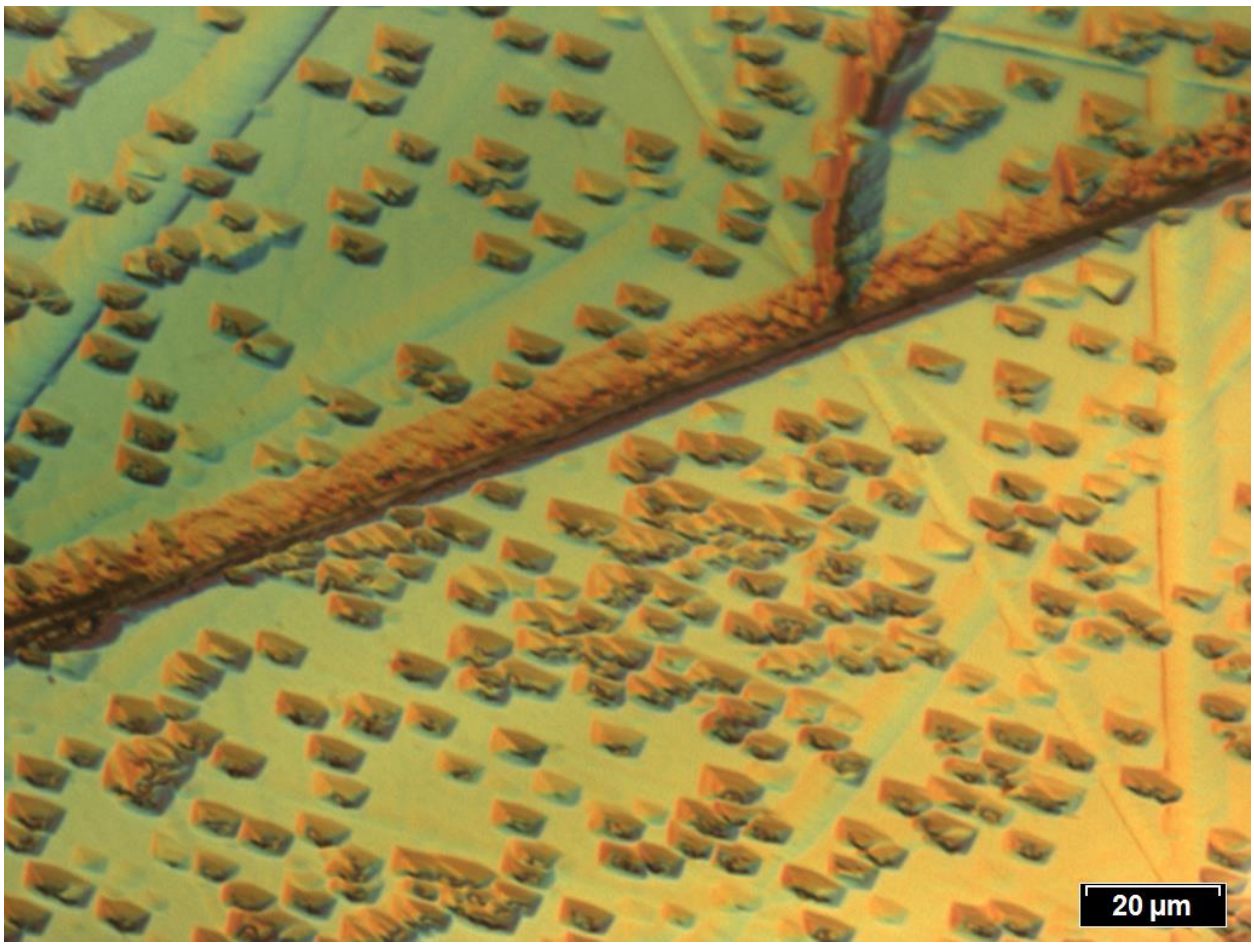

Fig. **5.16**: Neutron-irradiated siderite sample (1703-Sid-d, covered with zircon during irradiation) etched with 10% H_2SO_4, 50 °C, 150 min. Lots of rather large etch pits are visible, although it's not clear whether they are the result of etched fission tracks or dislocations.

In summary, it can be said that visualization of fission tracks on siderite is generally possible but requires samples with excellent quality surfaces so that the etched tracks are visible against the background. In particular, the etching and polishing method described in chapter 5.3 should be used to obtain smooth surfaces and minimize the amount of coarseness. Thin samples are preferable for their ability to be viewed under a microscope with transmitted light, where the line-shaped trails of etch pits are visible.

6. Annealing experiments for irradiated dolomite

6.1 Introduction

In chapter 4 the development of an etching method for ion tracks on irradiated dolomite has been discussed. This chapter deals with the annealing behaviour of tracks, testing the effect of heating irradiated samples up to temperatures of 300-500 °C. The goal is to establish annealing kinetics to determine the speed at which tracks are annealed, as well as finding the closure temperature for heavy ion tracks in dolomite. Natural defects and dislocations can be annealed too, but may require a different annealing temperature; annealed etched samples were checked for the presence of etched dislocations as well.

Annealing was performed with a Heraeus muffle furnace, as described in chapter 3.6. For every batch of annealing experiments, all dolomite samples used were cleaved heavy ion-irradiated crystals, picked from the same plate to ensure they all received the exact same fluence of Au ions. Etching of annealed samples was always done with 0.001 mol/l HCl at 20 °C, with an etching time of 60 min. All etching experiments were conducted on the same day on which the annealing process was finished. Etching was usually started within 30-60 min after annealing was complete. The etch pits (if present) were viewed with an Olympus microscope and their amount counted with Stream Enterprise software, and their shapes were investigated for any changes that may have resulted from annealing.

6.2 Constant time method – determining the closure temperature

The temperature at which heavy ion tracks on dolomite are annealed was determined with a set of experiments, using samples from BK0309Dol003-03 to -12. First, the average temperature range where ion tracks can no longer be etched was investigated by heating samples to 300, 350, 400, 450, and 500 °C respectively, with a constant annealing time of 100 hours. These samples were etched and checked for the presence of etched ion tracks. For etching temperatures of 300-450 °C, etch pits were found in the hexagonal areas not covered by the mask during irradiation. Their areal density matched the calculated fluence obtained from the etched reference foil, proving that ion tracks can still be successfully etched when the dolomite has been annealed to 450 °C (Fig. **6.1**). On the sample that was annealed to 500 °C though, no designated ion track etch pits appeared.

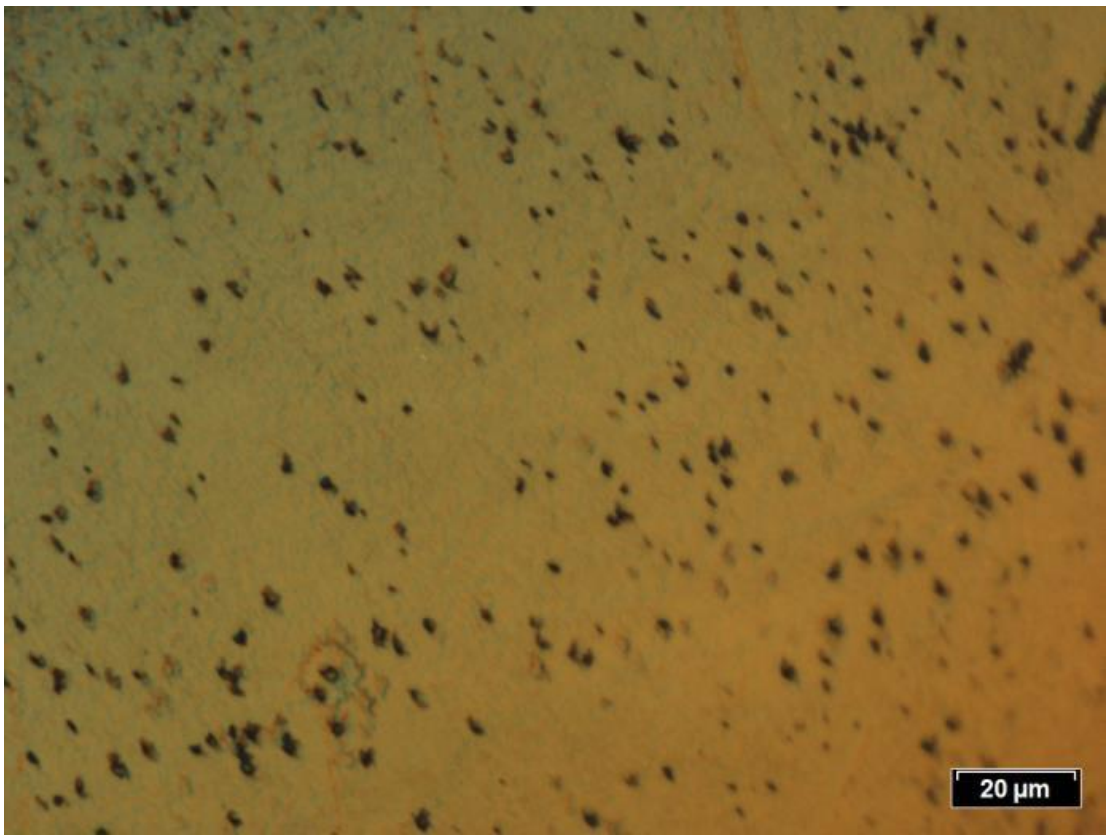

Fig. **6.1**: Heavy ion irradiated dolomite sample (BK0309Dol003-05) annealed for 100 hours at 450 °C, then etched with 0.001 mol/l HCl, 60 min, 20 °C. The surface is covered with dot-shaped etch pits of heavy ion tracks.

In order to determine the temperature at which tracks anneal, samples were heated to 470, 480, 490, 500 and 510 °C respectively, using an annealing time of 100 hours again. After etching, these were checked for ion track etch pits. On some of the samples that were heated to 490 °C or lower, ion tracks could still be etched, but the etch pits appear shallower and less well-defined than those observed on samples heated to 450 °C. No etched ion tracks were found on the samples that were heated to 500 or 510 °C. The counted areal density of the barely visible etch pits on a sample that had been annealed at 490 °C is, within error, in agreement with the calculated fluence, leading to the assumption that the closure temperature must be somewhere between 490 and 500 °C for ion tracks on dolomite. With the instruments at hand, it was not possible to determine the temperature more exactly due to the precision of the laboratory furnace being limited to ± 10 °C.

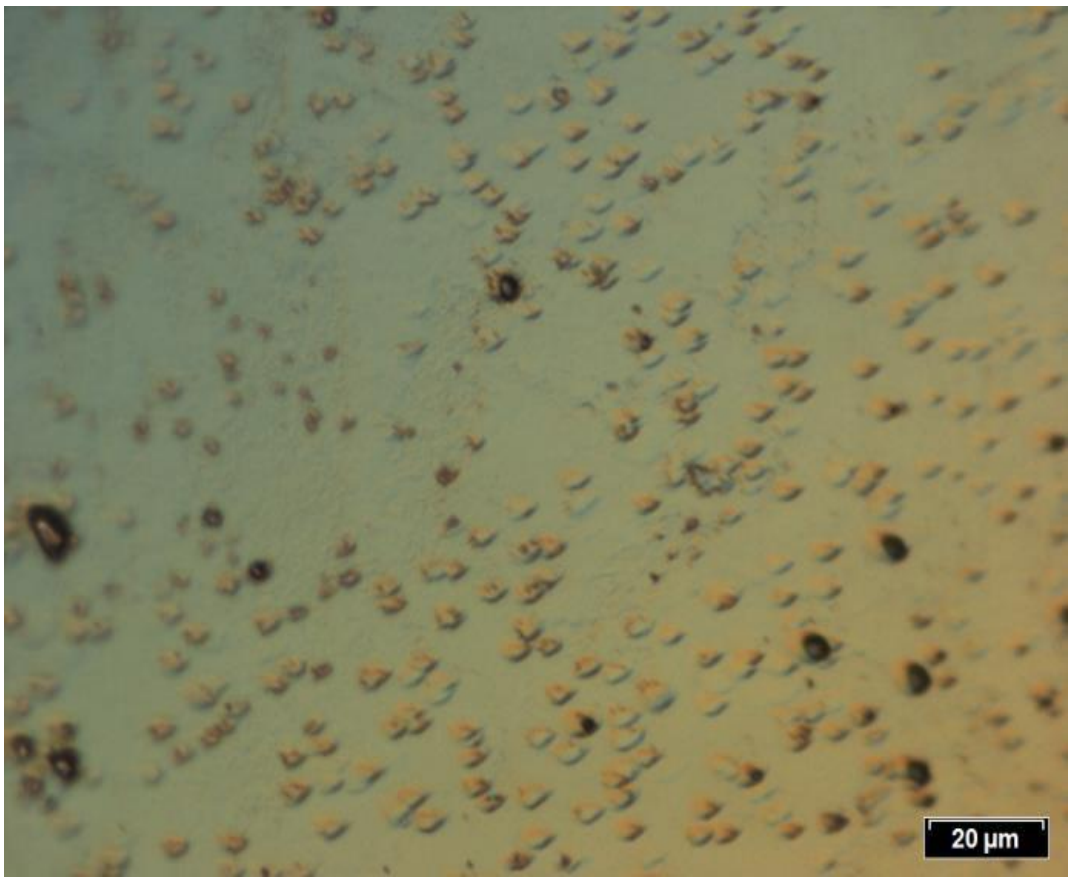

Fig. **6.2**: Heavy ion irradiated dolomite sample (BK0309Dol003-09) annealed for 100 hours at 490 °C, then etched with 0.001 mol/l HCl, 60 min, 20 °C. Etch pits of heavy ion tracks are visible, but they appear to be rather shallow and of low quality.

Generally, samples that were heated to temperatures close to 500 °C resulted in etch pits that are hard to distinguish against the background (Fig. **6.2**), making it unclear whether all of them are indeed etched ion tracks; for most samples, the etch pits were still of sufficient quality to be able to count them. Tab. **6.1** shows the statistics for etch pit density on dolomite samples that were annealed for 100 °C at various temperatures and then etched. The small sample size at higher temperatures results from the tendency of etch pits appearing too shallow for counting, or background features being enlarged to a degree that obscures the actual etched ion tracks. Not all microscope images showed etch pits of good enough quality to distinguish them against the background, due to some samples having very coarse surfaces; for the purpose of obtaining statistical data, all images with clearly visible etch pits were evaluated.

Tab. **6.1**: Etch pit density on etched (0.001 mol/l HCl, 60 min, 20 °C) heavy ion irradiated dolomite samples (BK0309Dol003-03 to -12) after annealing for 100 hours at various temperatures.

Dolomite, annealed at 350 °C			Dolomite, annealed at 450 °C			Dolomite, annealed at 490 °C			Reference foil		
Index no.	Areal density (22950 µm²)		Index no.	Areal density (22950 µm²)		Index no.	Areal density (22950 µm²)		Index no.	Areal density (22950 µm²)	
1	314		1	343		1	327		1	394	
2	300		2	355		2	351		2	381	
3	346		3	305		3	331		3	349	
4	362		4	377		4	394		4	411	
5	291		5	370		5	379		5	390	
6	343		6	287		6	277		6	380	
7	399		7	361					7	366	
8	332								8	385	
9	329								9	352	
10	359								10	358	
11	329								11	365	
									12	374	
									13	369	
									14	363	
									15	369	
									16	378	
									17	387	
									18	343	
									19	291	
									20	316	
	Area	Calc. Fluence (ions/cm²)	Area	Calc. Fluence (ions/cm²)		Area	Calc. Fluence (ions/cm²)		Area	Calc. Fluence (ions/cm²)	
Mean	337	1467121	343	1492584		343	1495177		366	1594880	
Std. deviation	30	132414	34	148092		42	181921		27	118468	

6.3 Constant temperature method – determining the annealing kinetics

With the closure temperature for heavy ion tracks on dolomite determined to be above 490 °C, experiments were done to study the effect of annealing time. A set of dolomite samples (BK0309Dol002-01 to -15) was annealed to 490 °C using various annealing times, with the goal of determining whether there's a certain annealing time after which the tracks can no longer be etched.

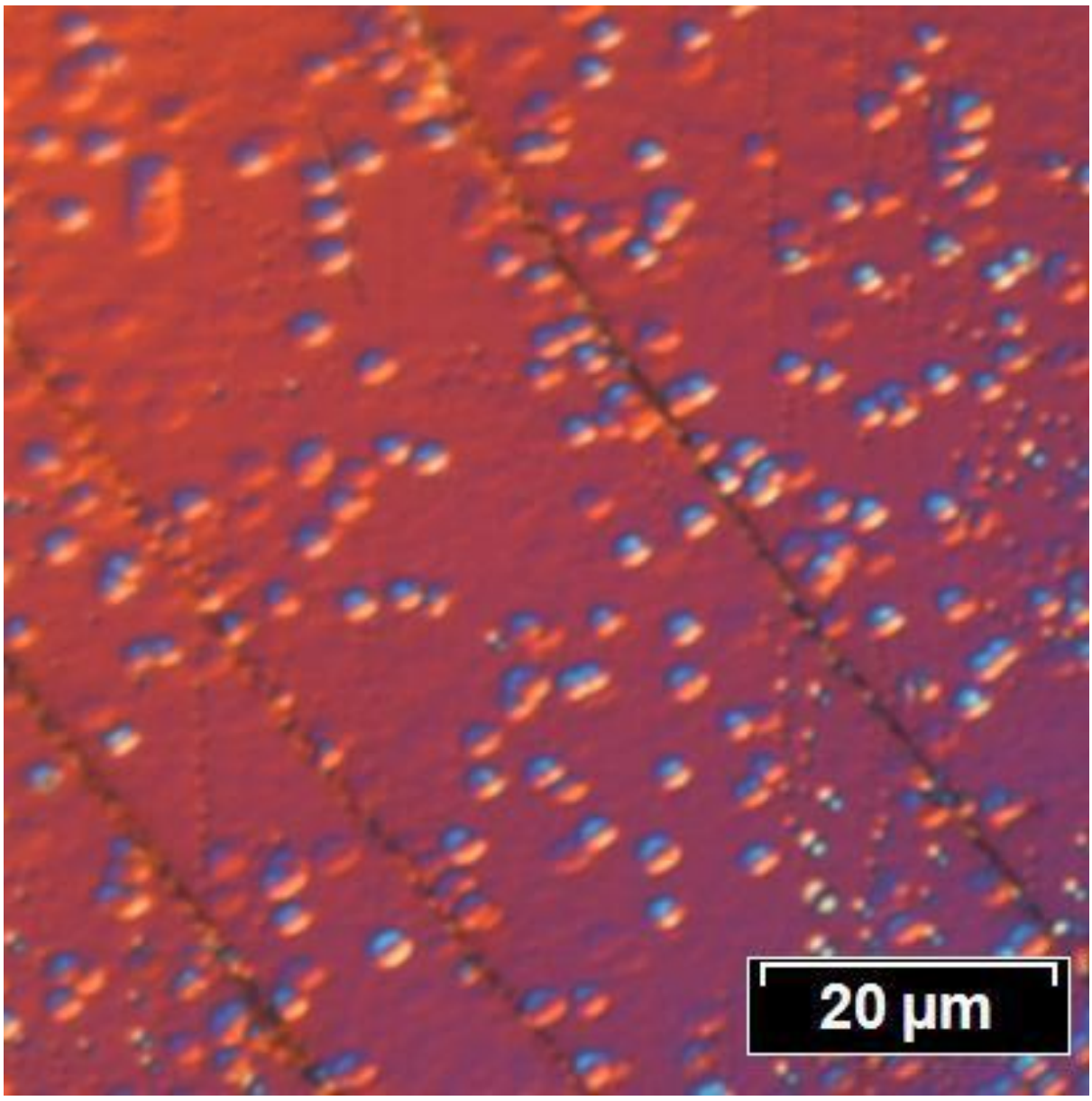

Fig. **6.3**: Heavy ion irradiated dolomite sample (BK0309Dol002-05) annealed for 20 hours at 490 °C, then etched with 0.001 mol/l HCl, 120 min, 20 °C. Well-defined etch pits of roughly circular shape are visible, displaying the etched heavy ion tracks.

When the sample was annealed for 20 h, etching produced well-defined ion track etch pits (Fig. **6.3**). Using an annealing time of 150 h resulted in shallow etch pits that are hard to distinguish against the background (Fig. **6.4**), and like the result of experiments done with the constant time method, it is uncertain whether all of these are the result of ion tracks or some are due to dislocations.

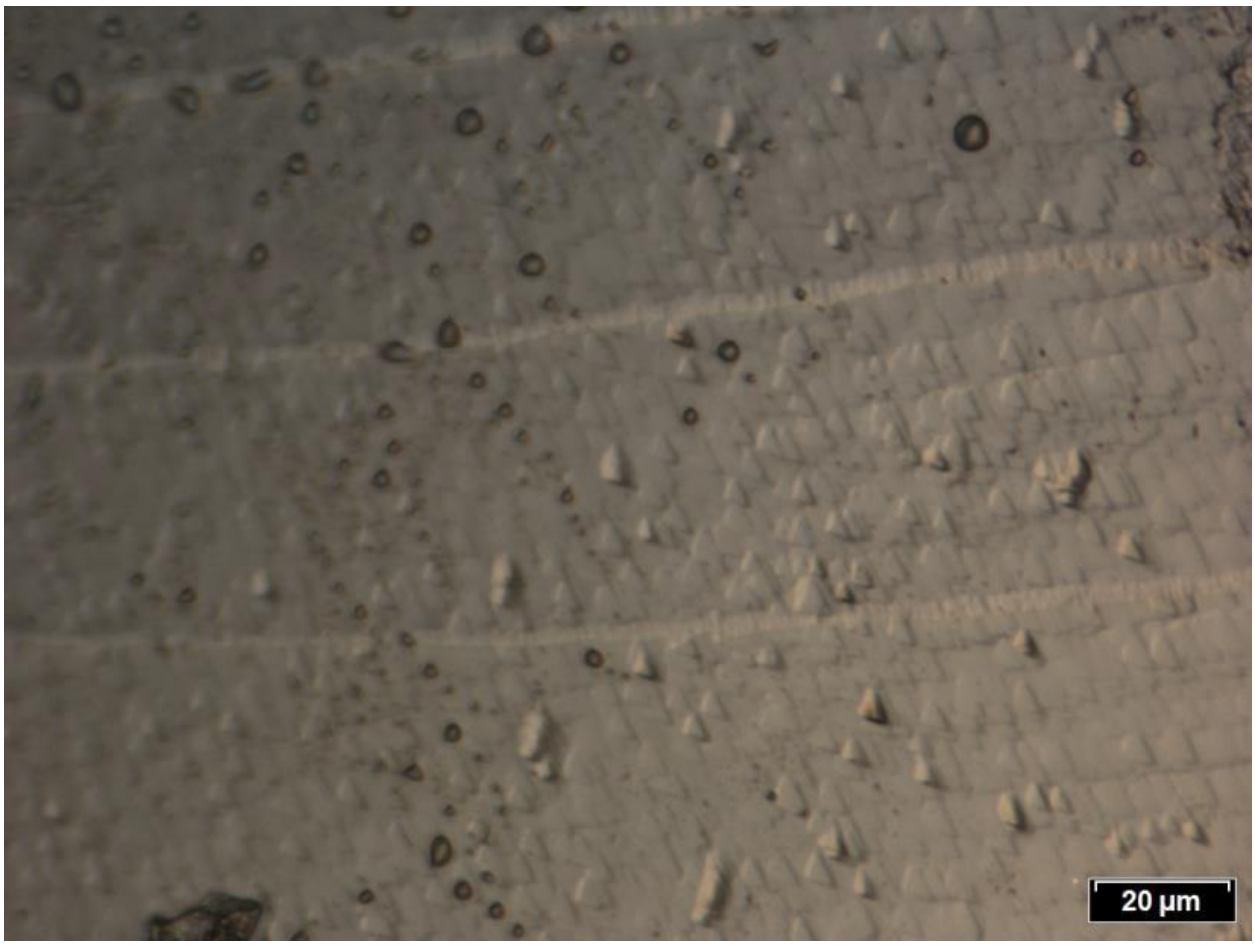

Fig. **6.4**: Heavy ion irradiated dolomite sample (BK0309Dol002-01) annealed for 150 hours at 490 °C, then etched with 0.001 mol/l HCl, 60 min, 20 °C. Many triangular-shaped etch pits are visible, however they appear very flat and are hard to distinguish against the background.

Unfortunately, the particular batch of samples used for this part of the annealing experiments proved to have surfaces of insufficient quality, and therefore, getting statistically significant information about the effect of annealing time wasn't possible. Fig. **6.5** shows an example of this phenomenon, with the surface of an annealed sample showing etch pits of heavy ion tracks but also features of the surface itself that have been enlarged by the etching process. This effect is present on the entire surface of this particular sample, making it impossible to find a zone that has only etched ion tracks and no other features overlapping with the etch pits. The etch pits didn't appear in clearly defined areas corresponding to the area that wasn't covered by the mask during irradiation, so it's unclear which etch pits are the result of etched ion tracks versus those that resulted from etched dislocations.

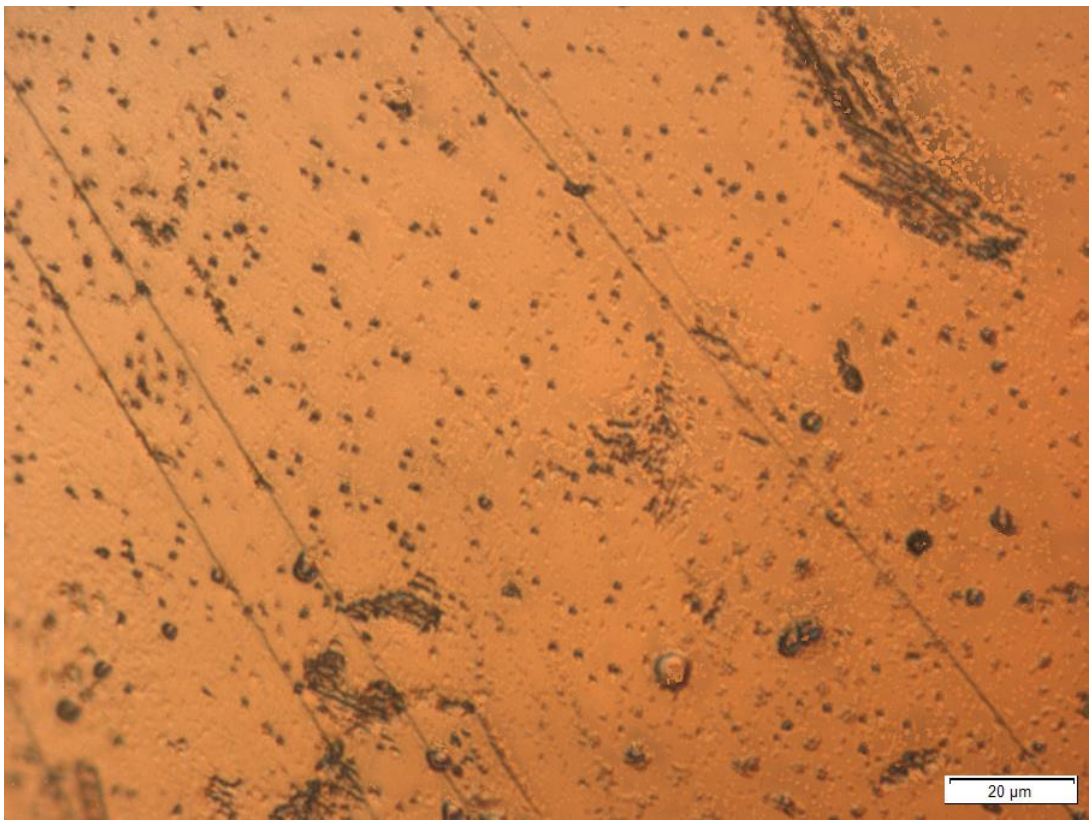

Fig. **6.5**: Heavy ion irradiated dolomite sample (BK0309Dol002-06) annealed for 51 hours at 490 °C, then etched with 0.001 mol/l HCl, 60 min, 20 °C. Some roughly circular-shaped etch pits are visible, but the background features on the sample surface have also been enlarged and make it impossible to perform exact counting of the number of etch pits.

With the data at hand, it is only possible to give a rough qualitative analysis of the results. For an annealing temperature of 490 °C, none of the various annealing times that were tested (from 20 to 150 h) resulted in the ion tracks disappearing, meaning that the ion tracks are stable at 490 °C and the closure temperature must be 500 °C or higher. Tab. **6.2** shows the etch pit density for an annealed dolomite sample compared to the reference foil, showing that within error, the density of etched ion tracks matches the fluence calculated from the etched foil. This result means that the ion tracks do not disappear when annealing dolomite to a temperature of 490 °C and the closure temperature must be higher.

Tab. **6.2**: Etch pit density on etched (0.001 mol/l HCl, 60 min, 20 °C) heavy ion irradiated dolomite sample (BK0309Dol002-05) after annealing for 20 hours at 490 °C.

Dolomite, annealed for 20h, 490 °C			Reference foil		
Index no.	Areal density (22950 µm²)		Index no.	Areal density (22950 µm²)	
1	833		1	583	
2	581		2	557	
3	768		3	629	
4	588		4	598	
			5	615	
			6	601	
			7	585	
			8	590	
			9	568	
			10	555	
			11	628	
			12	548	
			13	633	
			14	647	
			15	653	
			16	658	
			17	707	
			18	700	
			19	694	
			20	669	
	Area	Calc. Fluence (ions/cm²)		Area	Calc. Fluence (ions/cm²)
Mean	693	3017223		621	2705261
Std. deviation	128	555656		49	214037

In summary, it can be said that the closure temperature for dolomite has to be above 490 °C, although whether or not the heavy ion tracks disappear at temperatures slightly above 500 °C could not be determined with certainty due to the limited amount of available data. Samples that had been heated to 500 °C did not show any etch pits attributed to heavy ion tracks after etching, however it is not clear whether that is due to the small sample size or an indication of the closure temperature being indeed somewhere around 500 °C. More research is needed to find the exact temperature that causes tracks on dolomite to disappear. According to literature (Olszak-Humienik and Jablonski, 2015), dolomite decomposes at temperatures between 700 and 750 °C, so if a new set of experiments is conducted to determine the closure temperature for ion tracks, the focus should be on temperature ranges from 490 °C to about 650 °C to ensure that the sample remains intact.

7. Miscellaneous results

7.1 Raman spectroscopy analysis

Raman spectroscopy is an analytical method that can be used for determining the material composition of a sample, and which has been used in the past on calcite samples by Pabst et. al. (2010). The raw siderite samples from "Grube Pfannenberger Einigkeit" has a significant paragenesis of chalcopyrite, which had to be separated when cleaving samples for embedding. A bunch of siderite samples embedded in epoxy was examined with the Raman spectrometer available in the Thermochronology and Archaeometry research group of the Institute of Earth Sciences at Heidelberg University, in order to check for the presence of residual chalcopyrite. Other significant impurities may also show up in the Raman spectra.

For all examined siderite samples (Sid-001-01 to -15), Raman bands were observed at wavenumbers 180, 282 and 1084 cm^{-1}. These match the typical siderite Raman bands described in literature (Hanesch, Geophys. J. Int. (2009) 177, 941–948), with the symmetric stretching band of CO_3 appearing at 1090 cm^{-1} and translatory oscillations of CO_3 at 184 and 287 cm^{-1}. A weak band can be seen at 511-517 cm^{-1} that, according to literature, may be a Fe-O vibration mode. (Fig. **7.1**)

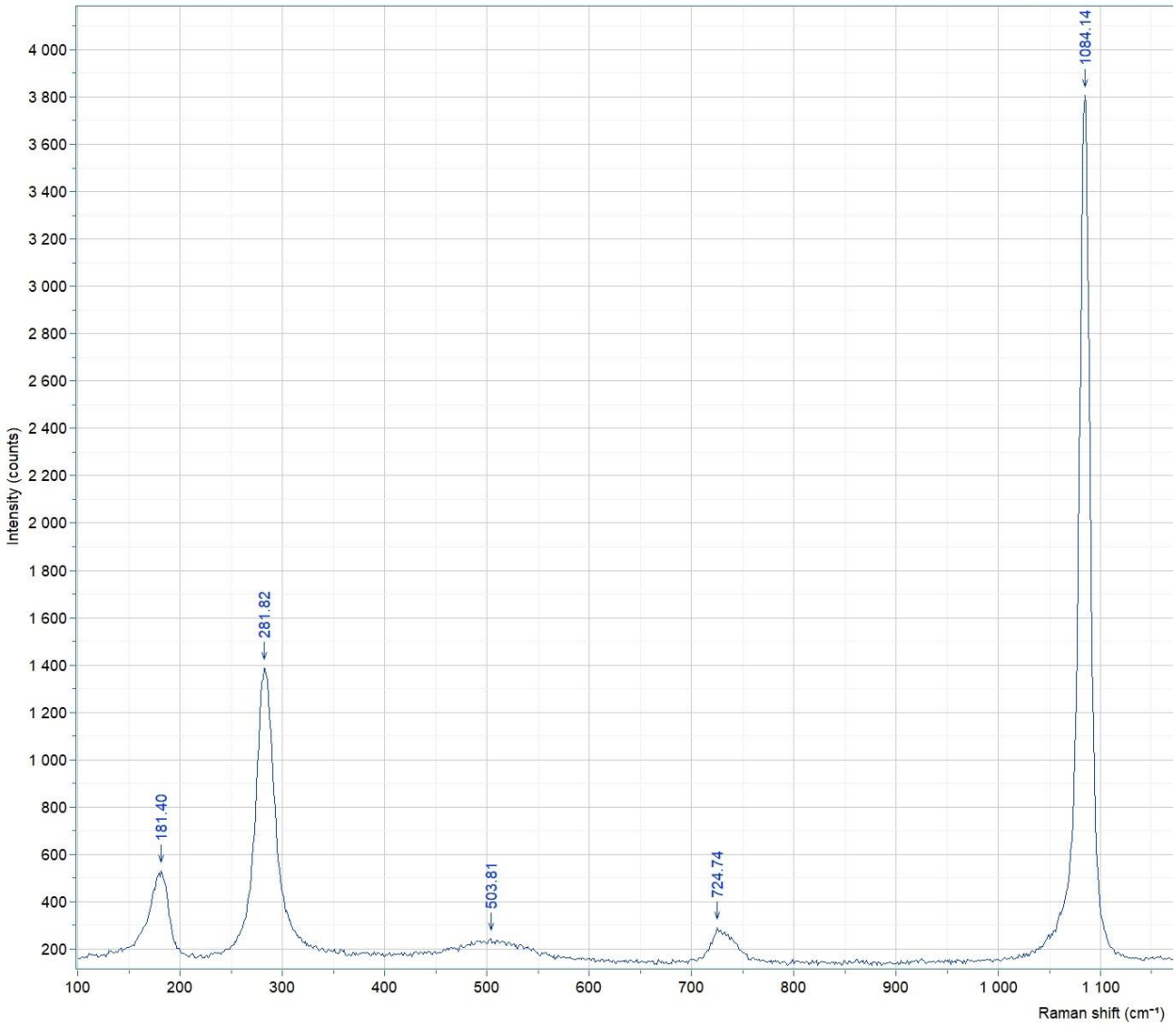

Fig. **7.1**: Siderite Raman spectrum (Sid-001-07) showing peaks at 180, 282 and 1084 cm^{-1}.

Additionally, Raman spectroscopy allows the analysis of the mineral's behaviour concerning irradiation. Several of the previously examined siderite samples were examined again after irradiation to see if any changes occur in the spectra. In all cases, the Raman bands were shifted to slightly higher wavenumbers (about 2-3 cm^{-1} higher) but this effect may be due to the fact that the Raman spectrometer has been deconstructed and rebuilt several times between the pre-irradiation and post-irradiation measurements. The fact that this effect was not observed in the online Raman measurements of siderite samples (detailed below) seems to support this explanation.

In order to study the effects of heavy ion beams on the composition of siderite, online Raman measurements have been performed. A system for performing online Raman measurements at the GSI in Darmstadt was designed by Dedera (2014) that allows one to perform Raman spectroscopy on samples in the irradiation chamber, gathering spectroscopic data before, during

and after irradiation for the same sample.

For this thesis, spectroscopic data was collected for siderite samples using ^{197}Au ions with an energy of 5.9 MeV/u and fluence ranges from $1*10^{10}$ up to $5*10^{12}$ ions/cm^2. By starting with a low fluence and gradually increasing it, and measuring the Raman spectra of the same spot on the sample every time, spectroscopic data was obtained that shows the intensity of all three siderite bands (180, 282 and 1084 cm^{-1}) decreasing as the fluence goes up, and basically disappearing entirely as soon as the sample is exposed to a fluence of $1*10^{12}$ or greater (Fig. **7.2**, Fig. **7.3**).

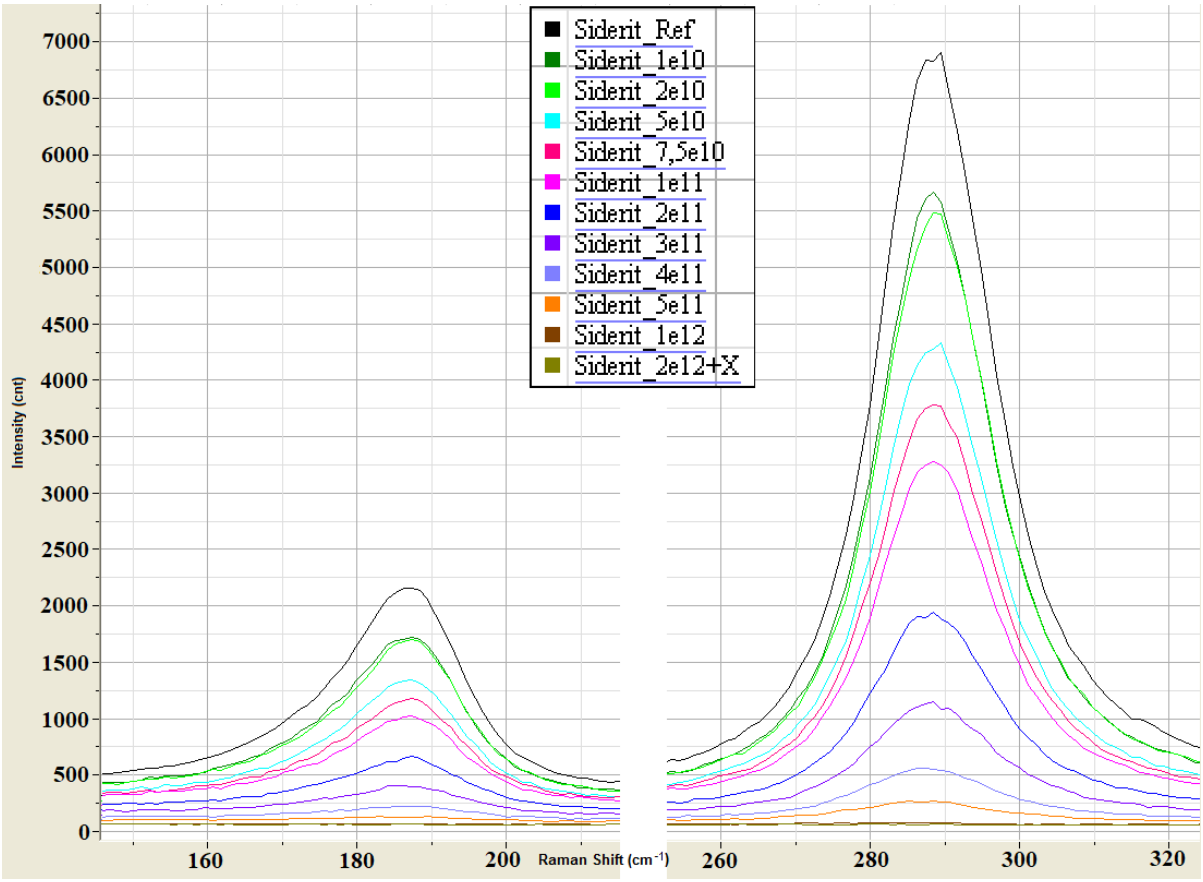

Fig. **7.2**: Siderite spectra sections showing the peaks at 180 and 282 cm^{-1} during online Raman measurement.

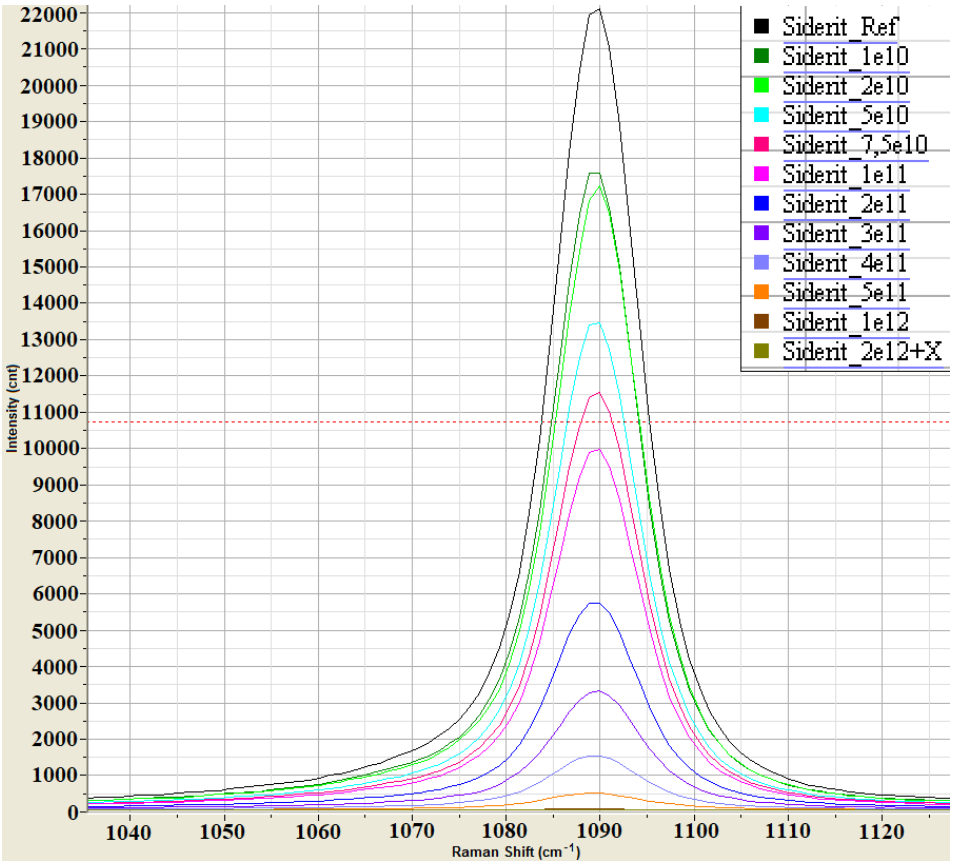

Fig. **7.3**: Siderite spectra sections showing the peak at 1084 cm^{-1} during online Raman measurement.

After the completion of the experiment, the siderite sample was found to have disappeared, with only a bit of black powdery residue left in the sample holder. This result shows that siderite is not stable when exposed to high fluences of heavy gold ions, which may be due to the sample being heated up when the ion beam hits. A similar result was observed in the annealing experiments for siderite, as seen in chapter 5.6, where heating the sample eventually caused it to disappear, again leaving only a bit of black powdery residue.

Generally, the intensity of all three siderite bands decreases with the fluence of gold ions applied, which is a sign of decomposition of the sample. Since each heavy ion pulse resulted in a significant decrease of intensity, it's likely that the heat generated inside the siderite sample by the heavy ion irradiation causes the decomposition temperature of siderite to be reached for a brief moment, resulting in some of the sample material potentially transforming into wuestite or graphite (which would explain the black residue that was found after the experiment was completed) or decomposing completely. No significant new peaks were observed on the irradiated samples; the characteristic wuestite peak at 586-596 cm^{-1} (Hanesch, Geophys. J. Int. (2009) 177, 941–948) was also absent after irradiation, meaning that the concentration of decomposition products was never very high at any specific point in time.

7.2 Geochemistry of siderite

The raw siderite used for obtaining cleaved samples was tested for the presence of traces of metals other than iron. For this purpose, large siderite chunks were crushed into smaller chunks with a weight of 10-30 g. These chunks were then ground into a fine powder using the grinding mill present in the cellar of Heidelberg University's Institute of Earth Sciences. It is important that when using a hammer to crush samples for this analysis, it has to be coated in plastic foil since otherwise contamination can occur, and the grinding mill also has to be cleaned before and after every use to ensure that no traces of other material mix with the powder. A total of four samples was prepared and sent to the Bureau Veritas Commodities laboratory in Vancouver, Canada for mineral analysis, using the ICP-MS method that was described in chapter 3.5.

Results of the ICP-MS analysis are shown in chapter 10.4; all analyzed siderite samples have Fe_2O_3 contents in the 50-55% range, with considerable amounts of manganese being present due to the fact that siderite forms a solid solution series with rhodochrosite ($MnCO_3$). Of the four siderite samples that were analyzed, three have noticeable copper contents; the Sid-HS04 sample in particular contains over 900 µg/g of Copper, which is a sign that chalcopyrite residues are probably present in the raw siderite rock. This analytical result is in agreement with the optical appearance of the siderite chunks; SidHS-04 in particular has visible black spots which are likely to be a result of the presence of chalcopyrite (Fig. **7.4**), while Sid-HS03, the sample that contains only 0.7 µg/g of Copper according to the analysis, is almost free of discolourations.

Fig. **7.4**: Raw siderite sample (SidHS-04). This particular sample has significant amounts of black spots, which according to the geochemical analysis may be the result of Cu (from chalcopyrite) in the sample.

The uranium content of these siderite samples is below 0.1 ppm according to the analysis, which means that the amount of natural radiation damage is most likely too low for fission track dating. The etch pits created by etching unirradiated samples are thus most likely the result of dislocations being enlarged into pits by the etchant.

8. Conclusion

A lot of etching experiments on carbonate minerals exist in literature, some very old, some recent. These were highly valuable for the development of etching recipes, giving examples of etching solutions that have worked in the past and which could be adapted for the goal of this particular work.

For the purpose of etching heavy ion irradiated dolomite samples, a useful etching solution was found to be 0.001 mol/l HCl at temperatures of 20 or 50 °C and etching times of 60-240 minutes. After 120 minutes of etching, the etch pits were found to have a length and width of about 8-10 µm, which is big enough for quantifying them but not so big as to cause overlapping.

For heavy ion irradiated siderite, two possibly useful etching solutions were found. The ion tracks could be successfully etched either by 10% H_2SO_4 or 10% HCl, using etching temperatures of 20 or 50 °C. It was found that the quality of etch pits produced by H_2SO_4 was generally better than those produced by HCl, with HCl failing to visualize all the ion tracks that should have been there and H_2SO_4-created etch pits also being more distinguishable against the background.

An important part of the experiments conducted on siderite was the development of a grinding and polishing procedure for samples. With this method, cracks and other elements of the natural mineral topology could be mostly eliminated and the sample surface's coarseness greatly reduced, which proved very valuable for getting higher quality etch pits. Since natural siderite samples can have a lot of features that would be enlarged by the etching process and therefore obscure the desired heavy ion track etch pits, it is advisable to prepare siderite samples with the new grinding and polishing method prior to irradiation and etching experiments. A similar method can be necessary for dolomite samples, if the grains are fine and coarse; the samples used in this study had smooth surfaces which didn't require any additional preparation. For future studies, if dolomite samples with coarse surfaces are used, the grinding and polishing method established for siderite can be used as a reference for creating a sample preparation method for dolomite, by using the same materials and methods but adjusting the specific parameters (grinding/polishing times, amount of grinding paste/lubricant used etc.) to find the optimal conditions.

For both dolomite and siderite, it was possible to successfully visualize neutron induced fission tracks by using the established etching methods. This result shows that dolomite and siderite are capable of being used for fission-track dating as long as the sample's uranium content is high enough. An important step necessary for such experiments was conducted in this work by determining the annealing kinetics of dolomite and siderite in an attempt to see whether there is a

closing temperature that causes tracks to disappear; for siderite, it was impossible to determine a closing temperature since the mineral decomposed at about 400 °C, while heavy ion tracks on dolomite seemed to disappear at temperatures above 500 °C but more analytical data is needed to verify this observation.

Online Raman measurements for siderite have shown the sensitivity of the mineral, with the three characteristic Raman bands of siderite gradually decreasing in intensity with increased heavy ion fluences. The fact that the sample had disappeared after completion of the measurement indicates that the ion beam must have caused the sample to be heated to a point above the decomposition temperature.

For future etching experiments on siderite, longer etching times may be necessary to produce larger etch pits that can be counted more easily. Due to the possibility of significant amounts of manganese or copper in siderite samples, which occur when rhodochrosite or chalcopyrite are present, the exact etching conditions for obtaining best results may vary from sample to sample.

In order to establish the use of dolomite and siderite for fission-track dating, further experiments will have to be conducted. More data for the annealing kinetics of these minerals is needed, and a method to identify and quantify spontaneous fission tracks has to be established. It is also important to have a reliable sample preparation method that results in sample surfaces of sufficient quality, so that the etching methods will visualize fission tracks as etch pits without them being obscured by background features; for that purpose, ways to further improve the grinding and polishing method presented in this thesis may have to be explored. These tasks could be the focus of a new project, e.g. a new doctoral thesis that focuses on creating a fission-track dating method for dolomite and/or siderite based on the results presented here.

As a final conclusion, the primary research objective of this study has been achieved, with the development of etching methods capable of visualizing heavy ion tracks and induced fission tracks in dolomite and siderite. The secondary objective revealed that the annealing kinetics of dolomite are significantly different from those of siderite, meaning that they need to be looked into in detail in a follow-up project. A reliable sample preparation method for siderite has also been developed that may prove useful for future experiments.

9. References

Afarideh, H., Faghih Habibi, M., Hashemi, F., Shokouhi, F., Uranium content and age determination of various minerals of Iran, Nuclear Tracks and Radiation Measurements 22 (1–4) (1993), 753–756.

Banerjee, A., Estimation of dolomite formation: Dolomite precipitation and dolomitization, Journal of the Geological Society of India 87 (2016) 561-572.

Baumhauer, H., 1894., Die Resultate der Aetzmethode in der krystallographischen Forschung, an einer Reihe von krystallisirten Körpern dargestellt. Verlag von Wilhelm Engelmann, Leipzig, 131 pp. (1894).

Bell, K.G., Uranium in carbonate rocks, Shorter contributions to general geology, 474-A (1963).

Bellemans, F., De Corte, F., Van D. Haute, P., Composition of SRM and CN U-doped glasses: Significance for their use as thermal neutron fluence monitors in fission track dating. Radiation Measurements 24 (1995), 153–160.

Beudant, F.S., Traité élementaire de Mineralogie (1832).

Boos, A., Ätzversuche an Calcit, Rhodochrosit und Siderit. Neues Jahrbuch für Mineralogie 78 (Abt. A) (1941), 89–130.

Bowen, O.E., Limestone and Dolomite Resources of California, California Division of Mines and Geology Bulletin 194 (1973), 18.

Cai, W.K., Liu, J. H., Zhou, H.C., Keeling, J., Glasmacher, U.A., 2021. Structure, genesis and resources efficiency of dolomite: New insights and remaining enigmas. Chem. Geol. doi.org/10.1016/j.chemgeo.2021.120191

Caminada, P., Das abenteuerliche Leben des Forschungsreisenden Déodat de Dolomieu, 2006.

Caruso, L., Simmons. G., Uranium and microcracks in a 1,000-meter core, Redstone, New Hampshire, Contrib Mineral Petrol 90 (1985) 1-17.

Chang, L., Deer, W.A., Howie, R.A., Zussman, J., Rock-forming Minerals: Non-Silicates, Volume 5B, Geological Society, 1998.

Copeland, P., Watson, E., Urizar, S., Alpha thermochronology of carbonates, Geochim. et.

Cosmochim. Acta 71 (2007) 4488-4511.

Daniell, F., Ueber einige Erscheinungen, die den Auflösungsprozess begleiten. Schweiggers Journal für Chemie und Physik 19 (1817) 38–53.

Dedera, S., Burchard, M., Glasmacher, U.A., Pabst, S. and Trautmann, C., Etching of Calcite for Fission-Track Dating. GSI Scientific Report 2010, PNI-MR-12.

Dedera, S., Glasmacher, U.A., Trautmann, C., Visualization of Ion-Induced Tracks in Carbonate Minerals (2015), PhD thesis.

Ditlov, V.A., Gatchegov, A.U. et. al., The radial etching velocity for tracks in polymer film, Radiation Measurements 28 (1997) 137-144.

Ebner, V.v., Die Lösungsflächen des Kalkspathes und des Aragonites: II. Die Ätzfiguren des Kalkspathes. III. Die Lösungsflächen des Aragonites. Sitzungsber. d. k. k. Akad. d.Wiss. Wien, Abtheilung 2, 91 (1885), 760–835.

Fleischer, R.L., Advances in Fission Track Dating, World Archeology Vol 7. No. 2 (1975) 136-150.

Gaubert, M.P., Sur les faces de dissolution de la calcite et sur les figures de corrosion des carbonates rhomboédriques, Bull. de la Soc. franc. de Min. 24 (1901) 326-351.

Gautelier, M., Oelkers, E.H., Schott, J., An experimental study of dolomite dissolution rates as a function of pH from -0.5 to 5 and temperature from 25 to 80 °C, Chem. Geol. 157 (1999) 13.

Gautelier, M., Oelkers, E.H., Schott, J., An experimental study of dolomite dissolution rates at 80 °C as a function of chemical affinity and solution composition, Chem. Geol. 242 (2007) 509-517.

Gotor, F.J., Macías, M., Ortega, A., Criado, J.M., Comparative study of the kinetics of the thermal decomposition of synthetic and natural siderite samples, Phys Chem Minerals 27 (2000), 495-503.

Grimmer, J.C. et al., Cretaceous-Cenozoic history of the southern Tan-Lu fault zone, Tectonophysics 359 (2002) 247-249.

Haidinger, W., Zweite Klasse: Geogenide. II. Ordnung. Baryte I. Parachrysobaryt. Siderit. In: Handbuch der Bestimmenden Mineralogie, Braumüller und Seidel, Wien (1845) 499-506.

Hanesch, M., Raman spectroscopy of iron oxides and (oxy)hydroxides at low laser power and possible applications in environmental magnetic studies, Geophys. J. Int. 177 (2009) 941-948.

Honess, A.P., Jones, J.R., Etch Figure Investigations with optically active solvents, Bull. Geol. Soc. Am. 48 (1937) 667.

Imbt, W.C., Ellison Jr, S.P., Porosity in Limestone and Dolomite Petroleum Reservoirs, Tulsa Geol. Society Digest 15 (1947) 39.

Keith, R.E., Gilman, J.J., Dislocation etch pits and plastic deformation in calcite. Acta Metallurgica 8 (1960) 1–10.

Kleber, W., Zum Mechanismus der Einkristallätzung mit optisch aktiven Substanzen. Zentralblatt der Mineralogie A (1938) 294–301.

Kleber, W., Zur Deutung der mit optisch-aktiven Säuren erzeugten Ätzerscheinungen. Mitteilung 429 aus dem Mineralogisch-Petrographischen Institut der Universität Bonn (1940) 455-461.

Krishnaswami, S., Lal, D., Prabhu, N., Characteristics of Fission Tracks in Zircon: Applications to Geochronology and Cosmology, Earth and Planetary Science Letters 22 (1974) 51-59.

Krylov, A., First discovery and formation process of authigenic siderite from gas hydrate–bearing mud volcanoes in fresh water: Lake Baikal, eastern Siberia, Geophysical Research Letters, vol. 35 (2008).

Leydolt, F., Neue Methode, die Structur und Zusammensetzung der Krystalle und organischen Naturproducte überhaupt zu untersuchen (1854).

Luo, Y.H., Zhu, D.Q., Pan, J., Zhou, X.L., Thermal decomposition behaviour and kinetics of Xinjiang siderite ore, Mineral Processing and Extractive Metallurgy 125 (2016), 17-25.

Lüttge, A., Winkler, U., Lasaga, A.C., Interferometric study of the dolomite dissolution: A new conceptual model for mineral dissolution, Geochim. et Cosmochim. Acta 67 (2003), 1099-1116.

Macdougall, D., Price, P.B., Attempt to Date Early South African Hominids by Using Fission Tracks in Calcite, Science 185 (1974) 943.

Nagpal, M.K., Nagpaul, K.K., Mehta, P.P., Uranium Contents in Minerals by Fission Track

Method, Pure and Applied Geophysics 102 (1972) 153-160.

Olszak-Humienik, M., Jablonski, M., Thermal behavior of natural dolomite, J. Therm. Anal. Calorim. 119 (2015) 2239-2248.

Orton, R., Unwin, P.R., Dolomite Dissolution Kinetics at Low pH: A Channel-flow Study. J. Chem. Soc. Faraday Trans. 89 (1993) 3947-3954.

Pabst, S., Burchard, M., Glasmacher, U.A., Miletich, R. et al., Radiation damage in heavy ion-irradiated carbonate minerals investigated by Raman and infrared spectroscopy, Scientific Report 2010, GSI Helmholtzzentrum für Schwerionenforschung, Darmstadt, 379.

Picht, O., Growth and characterization of bismuth telluride nanowires. Heidelberg, Univ., Diss. 2010.

Pokrovsky, O.S., Golubev, S.V., Schott, J., Dissolution kinetics of calcite, dolomite and magnesite at 25 °C and 0 to 50 atm pCO_2, Chem. Geol. 217 (2005) 239-255.

Pokrovsky, O.S., Golubev, S.V., Schott, J., Castillo, A., Calcite, dolomite and magnesite dissolution kinetics in aqueous solutions at acid to circumneutral pH, 25 to 150 °C and 1 to 55 atm pCO_2: New constraints on CO_2 sequestration in sedimentary basins, Chem. Geol. 265 (2009) 20-32.

Royer, M. L., Sur la décroissance du cristal dans un milieu isotrope actif, Bull. Soc. franc. de minéralogie 53 (1930) 350-374.

Schaller, W. T., Siderite and Barite from Maryland, Zeitschr. f. Krist. 42 (1906) 321-326.

Sippel, R.F., Glover, E.D., Fission Damage in Calcite and the Dating of Carbonates, Science 24 (1964) 409.

Stokes, G., On the change in Refrangibility of Light, Philosophical Transactions of the Royal Society of London 142 (1852) 463-562.

Tschermak, G., Lehrbuch der Mineralogie, Wien, Hölder (1894).

Tschermak, G., Min. u. petrogr. Mitth. 4 (1882), 99-121.

Wagner, G., Van den Haute, P., Fission track dating. Kluwer Academic Publishers (1992).

Ziegler, J.F., Ziegler, M.D., Biersack, J.P., SRIM – The stopping and range of ions in matter (2010). Nuclear Instruments and Methods in Physics Research Section B: Beam Interactions with Materials and Atoms 268 (2010), 1818–1823.

10. Appendix

10.1 List of Figures

10.2 List of Tables

10.3 List of samples used in this study

Appendix 10.3.1: Samples for etching experiments

Sample No.	Mineral	Results	Irradiation	Etching
DolSD01	Dolomite		^{197}Au 1*10^{6}, 11.1 meV/u	HCl 37% RT 20s
DolSD02	Dolomite		^{197}Au 1*10^{6}, 11.1 meV/u	conc. lactic acid 210 min RT + 30 min 50 °C + 30 min 80 °C
DolSD03	Dolomite		^{197}Au 1*10^{6}, 11.1 meV/u	HCl 0.001 mol/l 260 min RT + 150 min 50 °C
BK0309Dol001-02	Dolomite		^{197}Au 1*10^{6}, 11.1 meV/u	HCl 0.001 mol/l 225 min 50 °C
BK0309Dol001-01	Dolomite	overetched	^{197}Au 1*10^{6}, 11.1 meV/u	HCl 0.001 mol/l 240 min 50 °C
BK0309Dol001-10 to BK0309Dol001-15	Dolomite	Glued on specimen plate with nail polish	^{197}Au 1*10^{6}, 11.1 meV/u	HCl 0.001 mol/l 120 min 20 °C
BK0309Dol001-16	Dolomite		^{197}Au 1*10^{6}, 11.1 meV/u	HCl 0.001 mol/l 120 min 20 °C
BK0309Dol001-05 to BK0309Dol001-09	Dolomite	Glued on specimen plate with nail polish	^{197}Au 1*10^{6}, 11.1 meV/u	HCl 0.001 mol/l 150 min 20 °C
BK0309Dol001-04	Dolomite		^{197}Au 1*10^{6}, 11.1 meV/u	HCl 0.001 mol/l 240 min 20 °C
BK0309Dol001-03	Dolomite	Etch pits clearly visible	^{197}Au 1*10^{6}, 11.1 meV/u	HCl 0.001 mol/l 260 min 20 °C
BK0309Dol001-17	Dolomite		^{197}Au 1*10^{6}, 11.1 meV/u	HNO_3 0.91% 120 min 20 °C
DolB010-G	Dolomite, blue		1*10^{15} Neutrons on zircon	HCl 0.001 mol/l 60 min 25 °C
DolW04-G	Dolomite	Embedded, etched with sample holder	1*10^{15} Neutrons on zircon	HCl 0.001 mol/l 165 min 40 °C
DolW11-G	Dolomite		1*10^{15} Neutrons on zircon	HCl 0.001 mol/l 180 min 20 °C
DolW13-G	Dolomite	Etch pits distributed randomly on surface	1*10^{15} Neutrons on CN1	HCl 0.001 mol/l 240 min 20 °C + 150 min 40 °C + 30 min 50 °C
BK2705-01-Sid	Siderite		Not irradiated	HCl 0.001 mol/l 180 min 20 °C + HCl 0.01 mol/l 210 min 20 °C + HNO_3 0.91% 120 min 20 °C
Sid-1209-Ätztest 1	Siderite	Triangular etch pits	Not irradiated	HCl 10% 30 min 50 °C
Sid-1209-Ätztest 2	Siderite	Triangular etch pits	Not irradiated	HCl 10% 10 min 50 °C
Sid-1209-Ätztest 3	Siderite	Very small etch pits	Not irradiated	HCl 10% 30 min 20 °C
Sid-H_2SO_4-Ätztest	Siderite		Not irradiated	H_2SO_4 10% 30 min 20 °C + 60 min 50 °C
Sid-H_2SO_4-Ätztest b	Siderite	Irregular distribution of etch pits	Not irradiated	H_2SO_4 10% 30 min 50 °C
Sid-001-01-04	Siderite		^{197}Au 1*10^{6}, 5.9 meV/u	H_2SO_4 10% 30 min 50 °C
Sid-001-01-02	Siderite	Etch pits in hexagonal area	^{197}Au 1*10^{6}, 5.9 meV/u	H_2SO_4 10% 30 min 70 °C
Sid-001-01-05	Siderite		^{197}Au 1*10^{6}, 5.9 meV/u	H_2SO_4 10% 60 min 50 °C
Sid-001-02-01	Siderite	Etch pits well visible	^{197}Au 1*10^{6}, 5.9 meV/u	H_2SO_4 10% 60 min 50 °C
Sid-001-01-06	Siderite		^{197}Au 1*10^{6}, 5.9 meV/u	H_2SO_4 10% 60 min 50 °C
Sid-001-05	Siderite	Sample was polished for 15 min with OP-S suspension first, etch pits well visible	^{197}Au 1*10^{6}, 5.9 meV/u	H_2SO_4 10% 60 min 50 °C
Sid-001-06b	Siderite		^{197}Au 1*10^{6}, 5.9 meV/u	H_2SO_4 10% 60 min 50 °C

Appendix 10.3.1b: Samples for etching experiments (cont.)

Sample No.	Mineral	Results	Irradiation	Etching
Sid-001-12	Siderite	OP-S suspension used after etching to improve visibility of etch pits	^{197}Au 1*10^{6}, 5.9 meV/u	H_2SO_4 10% 60 min 50 °C
Sid-001-01-07	Siderite	Etch pits well visible	^{197}Au 1*10^{6}, 5.9 meV/u	H_2SO_4 10% 60 min 70 °C
Sid-001-06a	Siderite		^{197}Au 1*10^{6}, 5.9 meV/u	H_2SO_4 10% 75 min 50 °C
Sid-001-01-01	Siderite	Etch pits in hexagonal area (hard to see)	^{197}Au 1*10^{6}, 5.9 meV/u	H_2SO_4 10% 90 min 50 °C
Sid-001-01-03	Siderite	Etch pits well visible	^{197}Au 1*10^{6}, 5.9 meV/u	H_2SO_4 10% 120 min 50 °C
Sid-001-08	Siderite	Etch pits visible with transmitted light only (?)	^{197}Au 1*10^{6}, 5.9 meV/u	H_2SO_4 10% 240 min 50 °C
Sid-001-03-01	Siderite	Etch pits visible only after 10% HCl etching	^{197}Au 1*10^{6}, 5.9 meV/u	HCl 0.001 mol/l 300 min 20 °C + HNO_3 0.91 % 120 min 20 °C, 60 min 50 °C + HCl 10% 150 min 20 °C
Sid-001-03-02	Siderite	Many etch pits after etching at 50°C	^{197}Au 1*10^{6}, 5.9 meV/u	HCl 10% 90+90 min 20 °C + 60 min 50 °C
Sid-001-04-01	Siderite		^{197}Au 1*10^{6}, 5.9 meV/u	HCl 2% 480 min 20 °C + HCl 10% 60 min 20 °C
Sid-001-04-03	Siderite		^{197}Au 1*10^{6}, 5.9 meV/u	HCl 10% 30 min 50 °C
Sid-001-04-02	Siderite		^{197}Au 1*10^{6}, 5.9 meV/u	HCl 10% 60 min 50 °C
Sid-Disl01	Siderite		Not irradiated	H_2SO_4 10% 60 min 50 °C
Sid-Disl02	Siderite	Surface damaged (overetched)	Not irradiated	HCl 10% 30 min 50 °C
Sid-EB-Ätztest	Siderite	Embedded in epoxy	Not irradiated	H_2SO_4 10% 30 min 50 °C
SPT3	Siderite	For photos that document grinding and polishing	Not irradiated	H_2SO_4 10% 30 min 50 °C
Sid-AH-1	Siderite	Annealed at 250 °C for 14 d, then embedded, grinded and polished	Not irradiated	H_2SO_4 10% 60 min 50 °C
Sid-AH-2	Siderite	Annealed at 250 °C for 14 d, then embedded, grinded and polished	Not irradiated	H_2SO_4 10% 60 min 50 °C
Sid-Verheilungstest	Siderite	Annealed at 300 °C for 270 min, black residue on surface (maybe wuestite)	Not irradiated	H_2SO_4 10% 60 min 50 °C
1703-Sid-a	Siderite	Fission tracks visible with transmitted light	1*10^{16} Neutrons on CN5	H_2SO_4 10% 90 min 50 °C
1703-Sid-d	Siderite		1*10^{16} Neutrons on zircon	H_2SO_4 10% 210 min 50 °C
1703-Sid-e	Siderite		1*10^{16} Neutrons on zircon	H_2SO_4 10% 60 min 50 °C

Appendix 10.3.2: Samples for annealing experiments

Sample No.	Mineral	Conditions	Irradiation	Etching
BK0309Dol003-03	Dolomite	Annealed for 100 h at 300 °C	^{197}Au 1*10^{6}, 11.1 meV/u	HCl 0.001 mol/l 60 min 20 °C
BK0309Dol003-04	Dolomite	Annealed for 100 h at 350 °C	^{197}Au 1*10^{6}, 11.1 meV/u	HCl 0.001 mol/l 60 min 20 °C
BK0309Dol003-05	Dolomite	Annealed for 100 h at 450 °C	^{197}Au 1*10^{6}, 11.1 meV/u	HCl 0.001 mol/l 60 min 20 °C
BK0309Dol003-07	Dolomite	Annealed for 100 h at 470 °C	^{197}Au 1*10^{6}, 11.1 meV/u	HCl 0.001 mol/l 60 min 20 °C
BK0309Dol003-08	Dolomite	Annealed for 100 h at 480 °C	^{197}Au 1*10^{6}, 11.1 meV/u	HCl 0.001 mol/l 60 min 20 °C
BK0309Dol003-11	Dolomite	Annealed for 100 h at 480 °C	^{197}Au 1*10^{6}, 11.1 meV/u	HCl 0.001 mol/l 60 min 20 °C
BK0309Dol003-09	Dolomite	Annealed for 100 h at 490 °C	^{197}Au 1*10^{6}, 11.1 meV/u	HCl 0.001 mol/l 60 min 20 °C
BK0309Dol003-12	Dolomite	Annealed for 100 h at 490 °C	^{197}Au 1*10^{6}, 11.1 meV/u	HCl 0.001 mol/l 60 min 20 °C
BK0309Dol002-14	Dolomite	Annealed for 100 h at 490 °C	^{197}Au 1*10^{6}, 11.1 meV/u	HCl 0.001 mol/l 60 min 20 °C
BK0309Dol002-03	Dolomite	Annealed for 140 h at 490 °C	^{197}Au 1*10^{6}, 11.1 meV/u	HCl 0.001 mol/l 60 min 20 °C
BK0309Dol002-07	Dolomite	Annealed for 144 h at 490 °C	^{197}Au 1*10^{6}, 11.1 meV/u	HCl 0.001 mol/l 60 min 20 °C
BK0309Dol002-01	Dolomite	Annealed for 150 h at 490 °C	^{197}Au 1*10^{6}, 11.1 meV/u	HCl 0.001 mol/l 60 min 20 °C
BK0309Dol002-15	Dolomite	Annealed for 195 h at 490 °C	^{197}Au 1*10^{6}, 11.1 meV/u	HCl 0.001 mol/l 60 min 20 °C
BK0309Dol002-12	Dolomite	Annealed for 196 h at 490 °C (interrupted)	^{197}Au 1*10^{6}, 11.1 meV/u	HCl 0.001 mol/l 60 min 20 °C
BK0309Dol002-09	Dolomite	Annealed for 240 h at 490 °C	^{197}Au 1*10^{6}, 11.1 meV/u	HCl 0.001 mol/l 60 min 20 °C
BK0309Dol002-11	Dolomite	Annealed for 355 h at 490 °C (interrupted)	^{197}Au 1*10^{6}, 11.1 meV/u	HCl 0.001 mol/l 60 min 20 °C
BK0309Dol002-10	Dolomite	Annealed for 2100 h at 490 °C	^{197}Au 1*10^{6}, 11.1 meV/u	HCl 0.001 mol/l 60 min 20 °C
BK0309Dol003-06	Dolomite	Annealed for 100 h at 500 °C	^{197}Au 1*10^{6}, 11.1 meV/u	HCl 0.001 mol/l 60 min 20 °C
BK0309Dol003-13	Dolomite	Annealed for 100 h at 500 °C	^{197}Au 1*10^{6}, 11.1 meV/u	HCl 0.001 mol/l 60 min 20 °C
BK0309Dol003-14	Dolomite	Annealed for 100 h at 500 °C	^{197}Au 1*10^{6}, 11.1 meV/u	HCl 0.001 mol/l 60 min 20 °C
BK0309Dol003-10	Dolomite	Annealed for 100 h at 510 °C	^{197}Au 1*10^{6}, 11.1 meV/u	HCl 0.001 mol/l 60 min 20 °C
BK0309Dol002-05	Dolomite	Annealed for 20 h at 490 °C	^{197}Au 1*10^{6}, 11.1 meV/u	HCl 0.001 mol/l 120 min 20 °C
BK0309Dol002-06	Dolomite	Annealed for 51 h at 490 °C	^{197}Au 1*10^{6}, 11.1 meV/u	HCl 0.001 mol/l 120 min 20 °C
BK0309Dol002-04	Dolomite	Annealed for 70 h at 490 °C	^{197}Au 1*10^{6}, 11.1 meV/u	HCl 0.001 mol/l 120 min 20 °C
BK0309Dol002-02	Dolomite	Annealed for 120 h at 490 °C	^{197}Au 1*10^{6}, 11.1 meV/u	HCl 0.001 mol/l 120 min 20 °C
BK0309Dol002-08	Dolomite	Annealed for 140 h at 490 °C	^{197}Au 1*10^{6}, 11.1 meV/u	HCl 0.001 mol/l 120 min 20 °C
BK0309Dol002-13	Dolomite	Annealed for 147 h at 490 °C	^{197}Au 1*10^{6}, 11.1 meV/u	HCl 0.001 mol/l 120 min 20 °C

Appendix 10.3.3: Samples irradiated but not etched (for future use)

Sample No.	Mineral	Properties	Irradiation
BK1709-MalM01	Malachite, microcrystalline	2 samples (6 grains) embedded in epoxy	^{197}Au 1*10^{6}, 11.1 meV/u
BK1709-MalM02	Malachite, microcrystalline	2 samples (5 grains) embedded in epoxy	^{197}Au 1*10^{6}, 11.1 meV/u
BK1709-MalM03	Malachite, microcrystalline	2 samples (8 grains) embedded in epoxy	^{197}Au 1*10^{6}, 11.1 meV/u
BK1709-MalN01	Malachite, nanocrystalline	2 samples (6 grains) embedded in epoxy	^{197}Au 1*10^{6}, 11.1 meV/u
BK1709-MalN02	Malachite, nanocrystalline	2 samples (6 grains) embedded in epoxy	^{197}Au 1*10^{6}, 11.1 meV/u
BK0309-001-Dol	Dolomite	3 splinters	^{197}Au 1*10^{6}, 11.1 meV/u
BK0309-002-Dol	Dolomite	2 splinters + one very thin sample	^{197}Au 1*10^{6}, 11.1 meV/u
BK0309-003-Dol	Dolomite	1 splinter	^{197}Au 1*10^{6}, 11.1 meV/u
Sid-001-09	Siderite		^{197}Au 1*10^{6}, 5.9 meV/u
Sid-001-10	Siderite		^{197}Au 1*10^{6}, 5.9 meV/u
DolB01Gar	Dolomite, blue		1*10^{15} Neutrons on zircon
DolB02Gar	Dolomite, blue		1*10^{15} Neutrons on zircon
DolB03Gar	Dolomite, blue		1*10^{15} Neutrons on zircon
DolBW06Gar	Dolomite, top blue, bottom white		1*10^{15} Neutrons on zircon
DolW07Gar	Dolomite		1*10^{15} Neutrons on zircon
DolB08Gar	Dolomite, blue		1*10^{15} Neutrons on zircon
DolB09Gar	Dolomite, blue		1*10^{15} Neutrons on zircon
DolB12Gar	Dolomite, blue		1*10^{15} Neutrons on zircon
DolW14Gar	Dolomite		1*10^{15} Neutrons on zircon
DolB15Gar	Dolomite, blue		1*10^{15} Neutrons on zircon
DolW16Gar	Dolomite		1*10^{15} Neutrons on zircon
1703-Sid-b	Siderite		1*10^{16} Neutrons on zircon
1703-Sid-c	Siderite		1*10^{16} Neutrons on zircon

10.4 Geochemistry of siderite

The MDL (method detection level) is the minimum concentration of an analyte that can still be measured. It is a value that depends on the analyte and the method used to measure it, and is determined in the geochemistry laboratory by measuring several blanks and calculating the standard deviation of the results.

LOI stands for the loss of ignition, defined as the loss of mass when the sample is heated for analysis. This is done to get rid of volatile substances that may be present in the sample.

Analyte	Unit	MDL	Sid-HS01	Sid-HS02	Sid-HS03	Sid-HS04
SiO_2	wt. %	0.01	7.15	0.18	0.54	0.77
Al_2O_3	wt. %	0.01	0.02	<0.01	<0.01	<0.01
Fe_2O_3	wt. %	0.04	50.32	55.20	54.45	53.06
MgO	wt. %	0.01	3.07	2.81	2.65	2.58
CaO	wt. %	0.01	0.40	0.37	0.46	0.32
Na_2O	wt. %	0.01	0.02	0.02	0.03	0.01
K_2O	wt. %	0.01	<0.01	<0.01	<0.01	<0.01
TiO_2	wt. %	0.01	<0.01	<0.01	<0.01	<0.01
P_2O_5	wt. %	0.01	<0.01	<0.01	<0.01	<0.01
MnO	wt. %	0.01	8.35	8.90	9.11	10.48
Cr_2O_3	wt. %	0.002	<0.002	<0.002	<0.002	<0.002
Ba	µg/g	1	3	3	5	<1
Ni	µg/g	20	<20	<20	<20	<20
Sc	µg/g	1	1	<1	<1	2
LOI	wt. %	-5.1	30.6	32.5	32.7	32.6
Sum	wt. %	0.01	99.90	99.92	99.94	99.79
Be	µg/g	1	<1	<1	<1	1
Co	µg/g	0.2	7.0	8.5	7.5	20.5
Cs	µg/g	0.1	<0.1	<0.1	<0.1	<0.1
Ga	µg/g	0.5	6.2	6.9	7.5	7.2
Hf	µg/g	0.1	<0.1	<0.1	<0.1	<0.1
Nb	µg/g	0.1	<0.1	0.1	<0.1	<0.1

Analyte	Unit	MDL	Sid-HS01	Sid-HS02	Sid-HS03	Sid-HS04
Rb	µg/g	0.1	<0.1	<0.1	<0.1	<0.1
Sn	µg/g	1	<1	<1	<1	<1
Sr	µg/g	0.5	2.6	2.8	4.6	1.9
Ta	µg/g	0.1	<0.1	<0.1	<0.1	<0.1
Th	µg/g	0.2	<0.2	<0.2	<0.2	<0.2
U	µg/g	0.1	<0.1	<0.1	<0.1	<0.1
V	µg/g	8	<8	<8	<8	<8
W	µg/g	0.5	<0.5	<0.5	<0.5	<0.5
Zr	µg/g	0.1	0.5	0.3	0.7	1.7
Y	µg/g	0.1	13.6	24.7	22.7	21.9
La	µg/g	0.1	0.5	0.1	0.6	0.3
Ce	µg/g	0.1	0.2	<0.1	<0.1	0.3
Pr	µg/g	0.02	0.04	0.05	0.07	0.06
Nd	µg/g	0.3	0.3	0.6	0.5	0.6
Sm	µg/g	0.05	0.65	1.10	1.17	2.69
Eu	µg/g	0.02	0.31	0.63	0.55	1.14
Gd	µg/g	0.05	1.96	3.66	3.64	7.57
Tb	µg/g	0.01	0.45	0.84	0.80	1.35
Dy	µg/g	0.05	2.98	5.62	5.43	6.38
Ho	µg/g	0.02	0.61	1.03	0.97	0.90
Er	µg/g	0.03	1.79	2.95	2.81	1.92
Tm	µg/g	0.01	0.29	0.45	0.41	0.21

Analyte	Unit	MDL	Sid-HS01	Sid-HS02	Sid-HS03	Sid-HS04
Yb	µg/g	0.05	2.04	2.56	2.64	1.21
Lu	µg/g	0.01	0.29	0.31	0.31	0.14
TOT/C	wt. %	0.02	10.08	10.94	10.70	10.88
TOT/S	wt. %	0.02	0.03	<0.02	<0.02	0.11
Mo	µg/g	0.1	0.4	0.4	0.4	0.5
Cu	µg/g	0.1	200.6	119.6	0.7	904.2
Pb	µg/g	0.1	1.0	1.0	1.1	2.0
Zn	µg/g	1	23	19	20	16
Ni	µg/g	0.1	16.1	13.2	12.6	14.6
As	µg/g	0.5	<0.5	0.7	<0.5	18.4
Cd	µg/g	0.1	<0.1	<0.1	<0.1	<0.1
Sb	µg/g	0.1	<0.1	<0.1	<0.1	0.5
Bi	µg/g	0.1	<0.1	<0.1	<0.1	0.3
Ag	µg/g	0.1	<0.1	<0.1	<0.1	0.1
Au	ng/g	0.5	1.6	<0.5	<0.5	0.9
Hg	µg/g	0.01	0.23	0.07	0.02	0.02
Tl	µg/g	0.1	<0.1	<0.1	<0.1	<0.1
Se	µg/g	0.5	<0.5	0.5	<0.5	0.8

Eidesstattliche Versicherung gemäß § 8 der Promotionsordnung für die Gesamtfakultät für Mathematik, Ingenieur- und Naturwissenschaften der Universität Heidelberg / Sworn Affidavit according to § 8 of the doctoral degree regulations of the Combined Faculty of Mathematics, Engineering and Natural Sciences at the Heidelberg University

1. Bei der eingereichten Dissertation zu dem Thema / The thesis I have submitted entitled

   Siderite and Dolomite as a possible tool for thermochronological use

   handelt es sich um meine eigenständig erbrachte Leistung / is my own work.

2. Ich habe nur die angegebenen Quellen und Hilfsmittel benutzt und mich keiner unzulässigen Hilfe Dritter bedient. Insbesondere habe ich wörtlich oder sinngemäß aus anderen Werken übernommene Inhalte als solche kenntlich gemacht. / I have only used the sources indicated and have not made unauthorised use of services of a third party. Where the work of others has been quoted or reproduced, the source is always given.

3. Die Arbeit oder Teile davon habe ich wie folgt/bislang nicht[1)] an einer Hochschule des In- oder Auslands als Bestandteil einer Prüfungs- oder Qualifikationsleistung vorgelegt. / I have not yet/have already[1)] presented this thesis or parts thereof to a university as part of an examination or degree.

   Titel der Arbeit / Title of the thesis:.....

   Hochschule und Jahr / University and year:.....

   Art der Prüfungs- oder Qualifikationsleistung / Type of examination or degree:.....

4. Die Richtigkeit der vorstehenden Erklärungen bestätige ich. / I confirm that the declarations made above are correct.

5. Die Bedeutung der eidesstattlichen Versicherung und die strafrechtlichen Folgen einer unrichtigen oder unvollständigen eidesstattlichen Versicherung sind mir bekannt. / I am aware of the importance of a sworn affidavit and the criminal prosecution in case of a false or incomplete affidavit

Ich versichere an Eides statt, dass ich nach bestem Wissen die reine Wahrheit erklärt und nichts verschwiegen habe. / I affirm that the above is the absolute truth to the best of my knowledge and that I have not concealed anything.

Baldur Knörr